THE PHASE TRANSITIONS OF SEMIFLEXIBLE HARD SPHERE CHAIN LIQUIDS

A Thesis

Presented to

The Faculty of Graduate Studies

of

The University of Guelph

by

HANIF BAYAT MOVAHED

In partial fulfilment of requirements

for the degree of

Master of Science

August, 2005

ABSTRACT

THE PHASE TRANSITIONS OF SEMIFLEXIBLE HARD SPHERE CHAIN LIQUIDS

Hanif Bayat Movahed
University of Guelph, 2005

Advisor:
Professor Don Sullivan

We present a self-consistent theory for describing phase transitions in liquid crystals by using the Onsager second-virial approximation for the free energy. The key ingredients of this theory are the generation of semiflexible chains and calculation of the pair excluded volume and excluded area using Monte Carlo methods. In the first part, we solve the self-consistent equation for the single-chain probability density by an iteration method. From the probability density, we investigate the variation of thermodynamic variables such as the order parameter S_2 with volume fraction $\eta = \rho V_{mol}$ to find the isotropic-nematic phase transition. In the next part, the theory is extended to account for a smectic-A phase by assuming that a smectic-A solution for the probability density is a small perturbation around the nematic solution obtained previously. The perturbation is calculated using a lowest-order Fourier series representation. The coefficients of the Fourier series are found by solving two coupled self consistent equations.

ACKNOWLEDGEMENTS

I started my life in Canada by coming to the University of Guelph. At first it was not an easy experience, but by the great help and support of my dear friends, living at Guelph and studying at the University of Guelph became a really wonderful experience in my life. There are many people who deserve to have their names somewhere in this acknowledgement but unfortunately I do not have a chance to name them all.

First I should thank my honorable supervisor, Prof. Donald Sullivan, for giving me the chance to work in his group without ever having a chance to talk with me before coming here. A tremendous amount of gratitude goes out to him for all his support, guidance and patience over the past two years. During this project he provided me with his experience and his wide knowledge on liquid crystals. I should thank him for all the time he spent for me answering my numerous questions, writing numerous useful notes for me and explaining lots of different new concepts. I would like to extend very serious thanks to Dr. Raul Hidalgo who was my colleague for nearly three months. Sharing his knowledge and giving me great pieces of advice, beside his effort to make the program faster, were really useful in this project .Thanks also go to Prof. Bernie Nickel and Prof. Jeff Chen, the other members of my advisor committee for all their help. I am also grateful to Prof. Nickel for aiding us by allowing us to use his algorithms for different parts of this project and his guidance in different parts of our research. I should thank Roland Haas and Michael Arthur for helping me by proofreading my thesis materials and helping me in my English writing. I should specially thank Roland for all his other contributions such as teaching me LaTeX, sharing his innovative ideas for computational techniques, and sharing his computer knowledge with me.

Next, I should thank Fatemeh, my girlfriend, for all she did for me, both when she was far from me and when she was right beside me and helping me in all aspects of my life. Her support, encouragement and suggestions during writing my thesis were priceless. A special thanks to Sara, my great friend, for all her suggestions and help, she provided during the last year. I want to thank Roland Haas and Marc Bergevin for making my time at the department more enjoyable. I learned many things about the new culture by hanging out with Marc. I would like to thank all my other friends in Canada, specially Sina Valadkhan, Zahra Fakhraai, Majid Khadem Sameni, Viktor Vivcharyuk, Hassan Khassehkhan, Azardokht Hezarkhani, Geoff Lee-Dadswell, Peyman Heravi, Maryam Zahedi, Hamid Aliee, Hooman Homayounfar, Jeff Chizma, Ramtin Lotf Abadi and Pegah Valizadeh for all their support and help during the last two years. I should thank all other members of department and beyond, whom I forgot to mention here.

Finally, I should thank my parents for their tremendous support during all my life, both when I was close to them and while they were far away from me. Their emotional and financial support during the last two years have been continued to this moment. Beside this, great thanks go to my wonderful brothers Saeed and Saber for being amazing friends for me all of the time.

Thank you.

Dedicated to my mother and father for all they did

Contents

1 Introduction **1**

1.1 Liquid Crystals 1

1.2 Different Phases of Liquid Crystals 2

1.2.1 Isotropic 3

1.2.2 Nematic 3

1.2.3 Smectic-A 4

1.2.4 Other Phases 5

1.3 Overview of Different Liquid-Crystal Theories 5

1.3.1 About Onsager Theory 5

1.3.2 Different Models 6

1.4 Organization of this Thesis 8

1.4.1 Description of the Thesis 8

1.4.2 Chapters' Description 9

2 Semiflexible Hard Sphere Chains **11**

2.1 Definition and Representation 11

2.1.1 Shape Parameters 14

2.1.2 Thermodynamic Parameters 16

2.2 Free Energy Functional 18
2.2.1 Bond Bending Energy 19
2.2.2 Second Virial Expansion for the Multi-Chain Free Energy . . . 20
2.2.3 Minimization of the Free Energy Functional 25
2.3 Generation of the Chains 26
2.3.1 Including the Bending Energy in the Random Generation of Chains 29

3 Determining the Probability Density 31
3.1 Probability Distribution Function Equation 31
3.1.1 Excluded Volume 32
3.2 Simulation Techniques for Solving the Equation 33
3.2.1 Barrett's Algorithm [33] 33
3.2.2 Modifying the Probability Density Equation 35

4 Results for the Isotropic-Nematic Phase Transition 39
4.1 Introduction 39
4.1.1 Used Parameters 40
4.1.2 Limitations of the Calculation 41
4.2 $S_2 - \eta$ Graphs 43
4.2.1 Least Accurate Results 43
4.2.2 Accurate Results 48
4.3 Special Techniques 53
4.3.1 Histogram Technique 53
4.3.2 Mixing Method [35] 55
4.4 $P^* - \eta$ Graphs 57
4.5 Variation of $\langle \vec{r}_e{}^2 \rangle$ and $\langle \vec{r}_g{}^2 \rangle$ with η 58

4.5.1 Analytical Calculation of $\vec{r}_e^{\,2}$ 62
4.6 Distribution of the Probability Distribution Function 64
4.7 Discussion About Obtaining Different Results for Specific Number of Chains 66
4.7.1 Matrix Definition of S_2 70

5 Extension of theory to the Smectic-A Phase 75
5.1 Definition and Representation 75
5.1.1 Excluded Area 76
5.1.2 Barrett's Algorithm for Calculation of the Excluded Area . . . 78
5.1.3 Probability Density 79
5.2 Bifurcation Analysis 81
5.2.1 Fourier Series Representation 83
5.3 Solution for $\Delta f(z, \vec{\omega})$ 84
5.3.1 Final Equations 85

6 Results for the Nematic-Smectic-A Transition 88
6.1 Introduction 88
6.1.1 Problems 89
6.2 Initial Guesses and Techniques Used 90
6.2.1 Initial Guesses 90
6.2.2 Mixing Method [35] 94
6.2.3 Speed of the Program 94
6.2.4 Problem of Reaching Equilibrium 95
6.3 Range of Smectic-A Solutions 96
6.3.1 Table of Data 98

7 Summary and Conclusions **100**

7.1 Summary 100

7.2 Future Work 102

Bibliography **104**

List of Figures

1.1 Orientations and positions of molecules in the isotropic phase [5]. 3

1.2 molecules are in the same direction in the nematic phase 4

1.3 Molecules in smectic-A are ordered into layers. 4

1.4 In this kind of smectic phase, the molecules are tilted [5]. 5

2.1 b is the bond length between beads and D is the diameter of each bead 12

2.2 A chain cannot intersect itself or other chains 12

2.3 Maximum angle between bonds 14

2.4 Chain generation: Adding the second real bead of the chain 27

2.5 Coordinates after the first rotation 29

4.1 $S_2 - \eta$ graph for 500 chains 43

4.2 $S_2 - \eta$ graph for 1000 chains 44

4.3 $S_2 - \eta$ graph for 3500 chains 45

4.4 $S_2 - \eta$ graph for 5000 chains is compared with the Jaffer et al. result 46

4.5 $S_2 - \eta$ graph for 6500 chains is compared with the Jaffer et al. result 47

4.6 $S_2 - \eta$ graph for 7000 chains is compared with Jaffer et al. result 47

4.7 $S_2 - \eta$ graph for 10000 chains is compared with Jaffer et al. result 49

4.8 $S_2 - \eta$ graph for 11000 chains is compared with Jaffer et al. result 50

4.9 $S_2 - \eta$ graph for 12500 chains is compared with Jaffer et al. result 51

4.10 $S_2 - \eta$ graph for 14000 chains is compared with Jaffer et al. result 52

4.11 Histogram of $\cos\theta$ for 3000 chains 55

4.12 Histogram of $\cos\theta$ for 10000 chains 55

4.13 Histogram of $\cos\theta$ for 100000 chains 56

4.14 $S_2 - \eta$ graph for 6000 chains using mixing method 57

4.15 $P^* - \eta$ for 3500 chains 59

4.16 $P^* - \eta$ graph for 5000 chains 60

4.17 $P^* - \eta$ graph for 11000 chains 61

4.18 $\langle \vec{r_e}^{\,2} \rangle$ vs. η for 8000 chains 62

4.19 $\langle \vec{r_g}^{\,2} \rangle$ vs. η for 8000 chains 63

4.20 probability distribution for high probability chains 65

4.21 Different $S_2 - \eta$ graphs for 8000 chains are compared with Jaffer et al. 67

4.22 Different $S_2 - \eta$ graphs for 8000 chains 68

4.23 $\beta F/N - \eta$ graphs 69

4.24 $S_2 - \eta$ graphs for different definitions of S_2 for one set of chains 71

4.25 $S_2 - \eta$ graphs for different definitions of S_2 for another set of chains 72

4.26 $S_2 - \eta$ graphs for different sets of chains (different seeds) using the matrix definition 73

4.27 $S_2 - \eta$ graph for one one set of 8000 chains initialized in different orientations . . 74

5.1 Excluded area between chains 77

6.1 Smectic-A solutions for completely aligned limit 92

6.2 Range of volume fraction η vs. period d for smectic-A solutions 97

Chapter 1

Introduction

1.1 Liquid Crystals

Solid, liquid and gas materials are experienced in everyday life. Typically each type of matter has its own special phase under normal thermodynamic conditions. For example a chair is solid, water is liquid and the air is gas at room temperatures and atmospheric pressure. Phase transitions between these phases can be seen by changing the temperature and pressure. Liquid crystals are a kind of material which are not exactly liquid or solid while they have some characteristics of both. Just certain kinds of materials can exhibit this type of phase. These materials can be both natural and synthetic. As the name suggests these materials have the character of flowing like a liquid and light scattering like solid crystals. These kinds of complex characteristics make liquid crystals useful for many kinds of industrial purposes. The key parameter responsible for the characteristics of liquid crystals is the *shape of the particles*. Small molecules such as gases are often assumed to be spherical molecules and the interaction between them is spherically symmetric. But many organic materials can be pictured as long rods, flat plates or chains. For example, liquid crystals are usually

formed by long, thin, rod-shaped molecules. [1]

Liquid crystal materials were discovered for the first time in 1888 by an Austrian botanist, F. Renitzer. At that time those liquid crystals were not useful for any kind of commercial applications, but just only 25 years ago for the first time they became used for electronically driven displays. [2], [3]

Nowadays, liquid crystals are used in everyday life. Liquid Crystal Displays (LCD) have numerous advantages over traditional cathode-ray tube displays. For example, LCDs are easier to read and work with for long periods of time than most other video monitors. However, they have some disadvantages such as limited view angle, brightness, contrast, and high manufacturing costs. However, as research continues, many of these disadvantages are becoming less significant. [2], [3], [4]

Liquid crystals' unique characteristics make them really suitable for using in displays. Most of these properties stem from the fact that liquid crystals have different characteristics depending on the direction in which they are measured. Liquid crystals behave differently depending on the direction in which electric or magnetic fields are applied. Since light is an electromagnetic wave, its properties depend on the direction of its propagation and polarization with respect to the direction of the molecules in the liquid crystal. [3], [4]

1.2 Different Phases of Liquid Crystals

As mentioned, in everyday life, matter exists in three main phases. Each one of these phases can exist within special temperature and pressure ranges, and the phase transitions between them occur at special thermodynamic points (pressure and temperature).

For liquid crystals, three main different kinds of phases exist depending on the

order and positions of the molecules in the system. Some other phases of liquid crystals, which are not discussed in our project, will be named later.

1.2.1 Isotropic

In the isotropic phase the probability density function does not depend on the orientation or position of the molecules. This means that there are similar numbers of molecules (chains) in different orientations or positions. In this phase the molecules' positions and orientations are random and no long-range order is exhibited.

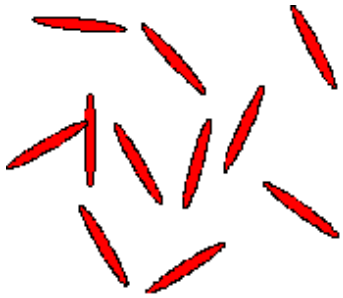

Figure 1.1: Orientations and positions of molecules in the isotropic phase [5].

1.2.2 Nematic

By cooling or compressing, the isotropic phase may undergo a transition to the nematic phase. In the nematic phase, which is the simplest type of liquid crystalline phase, the long axes of the molecules are aligned. This means that the molecules in the nematic phase are pointed on average along the same direction, known as the director $\hat{n}$ (unit vector) . [1]

This phase is used in many liquid crystal devices (e.g., the "twisted nematic" cell), because the average orientation may be manipulated with an electric field. As molecular orientation changes through a cell, the polarization of light will change in

Figure 1.2: Most of the molecules are nearly in the same direction in the nematic phase [5].

response to the molecular reorientation in time scales of milliseconds. [5]

1.2.3 Smectic-A

Further cooling and compressing may drive the system into a *smectic phase*. In the smectic-A phase, the molecules are ordered in layers and the layers' normals are parallel to the average orientation of the molecules. While the smectic-A is orientationally ordered, it is ordered positionally in only one direction normal to the layers and is disordered in other two directions (parallel to the layers). Because of this fact, the smectic-A is considered as a two-dimensional liquid and a one-dimensional solid. [1] [5]

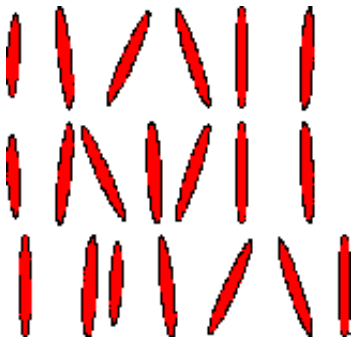

Figure 1.3: Molecules in smectic-A are ordered into layers and most of the molecules nearly have the same direction [5].

1.2.4 Other Phases

Other than the three main phases discussed before, there are other liquid-crystalline phases such as smectic-C, chiral smectic-C, etc, which are not considered here. For example, smectic-C is a smectic phase in which the molecules are tilted with respect to the layer normal.

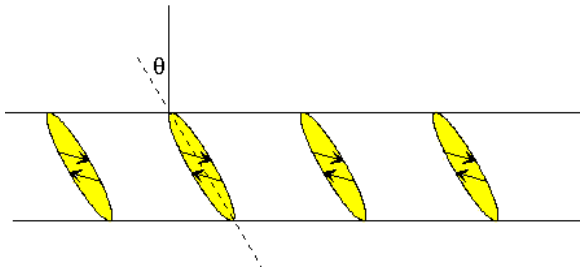

Figure 1.4: In this kind of smectic phase, the molecules are tilted [5].

1.3 Overview of Different Liquid-Crystal Theories

1.3.1 About Onsager Theory

After introducing the different phases of liquid crystals, the molecular interactions should be considered, which are responsible for forming these phases. At first glance it looks like an impossible task to find these forces, since a wide variety of different molecules are involved in forming liquid crystal phases and it is hard to find the common characteristics between all these different molecules. But many non-spherical molecules like rod shaped particles repel each other at short distances and attract each other at larger distances, like spherical ones. [1]

Lars Onsager, the Nobel prize winner of 1968 in chemistry, opened the field of microscopic theories of liquid crystals by showing that phase transitions between isotropic and nematic phases can be induced just by considering the short range

purely repulsive forces between rigid rod-shaped molecules. His theory is based on a second-order virial approximation to the free energy of the molecules. He was able to show that the nematic phase formed in weakly concentrated solution [6]. Then in the 1980's, this conclusion was confirmed by Monte Carlo simulation studies led mainly by Frenkel [7], [8].

While real liquid-crystal molecules interact by more complicated forces (such as van der Waals attractions and repulsions, multipolar forces), it is widely believed that the main statistical structure of liquid crystals is determined by the "hard-core" interactions [8], as in the case of simple monatomic liquids. Studies of hard-core models are also of practical relevance to, for example, colloidal materials such as solutions of virus particles [9]. To a first approximation, cylindrical hard rods provide a good model for colloidal particles with short-ranged repulsive interactions.

This project is based on the Onsager theory. The details of this theory are given in the next chapters (2, 3).

1.3.2 Different Models

Molecules that form liquid-crystal phases rarely consist solely of a rigid core. Flexibility in the particles can be introduced by several models, for example by considering chain molecules composed of linked hard spheres [10], [11], [12], [13], [14]. Related models consider chains formed from linked spherocylinders [15], or molecules modelled by "persistent" wormlike chains [16], [17], [18]. In this work, we will focus on the model of linked hard spheres.

Most studies of liquid crystalline ordering in semiflexible chains of linked hard spheres have been based on computer simulations [12], [13], [14], [19], [20], [21]. Despite great advances in simulation techniques and computational speed, simulations

are still limited by their time consumption, specially for studying phase transitions under a range of thermodynamic state conditions and molecular parameters. Somewhat less work has been done using approximate theories such as density-functional theory [8], under which we can include Onsager's pioneering study [6]. Studies closely related to the present one have been described by Fynewever and Yethiraj [13] and by Jaffer et al. [10], [11]. These works extend the approach used by Onsager, which is based on a second-virial approximation to the free energy, to account for higher-virial corrections, either by means of a "Parson-Lee" [22], [23] approximation or by using scaled particle theory [10], [11]. (Similar "corrected" approaches have been applied to fluids of rigid spherocylinders [24] as well as to the wormlike chain model [16], [25].) In the case of semiflexible hard sphere chains, however, these works have been limited to studies of phase transitions involving spatially uniform phases, i.e., isotropic and nematic phases. One goal of the present work is to extend the theory to the smectic-A phase, in which the probability density varies periodically in space.

Another issue concerns the coupling between molecular chain conformations and thermodynamics. In most theories of macromolecular systems, these effects are decoupled, i.e., the theories assume that the chains exhibit the same conformation (e.g. "ideal" or "Gaussian") in the reference state of a single isolated molecule and in a condensed many body system [26]. It is well known, however, that this is incorrect [27]. Actually some of the theories for liquid-crystalline phases of semi-flexible molecules mentioned earlier [10], [11], [13], [16], [17], do account for this "thermodynamics-conformation" coupling in the case of the orientionally-ordered nematic phase. Again such studies have yet to be extended to positionally-ordered phases such as smectic-A.

1.4 Organization of this Thesis

1.4.1 Description of the Thesis

Like in the Onsager theory, here we study the phase transitions in semiflexible hard sphere chains by using just the second virial approximation to the Helmholtz free energy. As mentioned in Section 1.3.1, in this theory only the shape of the hard sphere chains is involved in the interactions between chains. This interaction is a repulsive force between the chains, which results in the fact that the chains cannot overlap with each other and each individual chain is "self avoiding" or "non-intersecting".

In this work each molecule is represented by a chain consisting of a series of hard spheres. Overlap can only occur between adjacent spheres of one chain, and any other kind of overlap is forbidden. Beside this kind of interaction, a simple form of bending energy is added for each chain. We used just weak flexibility by using a fixed high value for the stiffness coefficient. By minimizing the Helmholtz free energy of the system, a self consistent equation for the molecular probability density is derived.

After producing a few thousand chains using Monte Carlo method and by considering the above constraints, the excluded volume between each pair of chains is calculated. Since excluded volume is a key function in the interaction between chains, it has a main role in solving the equation. Since the probability density appears in both sides of that equation, it is called a "self-consistent" equation. The goal for solving these equations is to find the probability density which minimizes the Helmholtz free energy function. For calculating the excluded volume between pairs of chains we used a Monte Carlo computational method. It is obvious that by using a Monte Carlo method, an approximate value for the excluded volume of one pair of chains is calculated. After calculating the excluded volume between chains, by solving the self

consistent equation the probability density function for a single chain is determined. By using the final probability density of the chains and calculating specific thermodynamic parameters such as the order parameter (S_2), the phase transition between the uniform nematic and isotropic phases is determined. Since in this case, it is assumed that the probability density function is translationally invariant, for describing the smectic phase the theory should be extended.

For considering the smectic phase, it is assumed that the smectic-A solution is a small perturbation around the nematic solution obtained previously. The perturbation is represented using a lowest-order Fourier series representation. The coefficients of the Fourier series are found by solving two coupled self consistent equations. To solve these equations the excluded areas between each pair of chains must be evaluated. After solving the two self consistent equations, the lowest volume fraction(η) which yields a non-trivial solution represents the phase transition point between smectic-A and nematic.

1.4.2 Chapters' Description

This thesis has two main parts. The first part is focused on *isotropic and nematic* phases and in the second part, the *smectic phase* is considered in addition to the other two phases. In the first three chapters, we focus on the isotropic-nematic phase transition and in the last two chapters we focus on adding the smectic-A phase to the previous phases and determining the smectic-nematic phase transition. The theory for the last part differs slightly from the first part, since in the first part it is assumed that the probability density of each molecular configuration depends only on the set of bond orientations and does not depend on the positions of the chains.

The first chapter (this chapter) describes the fundamental concepts of this project,

such as the different phases in liquid crystals, and gives an overview of this project. The second chapter first describes the details of the hard sphere chain model studied. Then it goes on to describe the Helmholtz free energy functional in the liquid crystal system by keeping just the second viral coefficient expansion of the free energy. Then we will show how the probability density is found by minimization of the Helmholtz free energy, and in the last part of this chapter we will describe the chain generation method used in the programs by considering the bond bending energy.

The third chapter describes the numerical solution of the probability density equation. We will explain Barrett's algorithm for calculation of the excluded volume between semiflexible chains. Then we will describe how the main self-consistent equation of chapter two was analyzed for computational purposes. Chapter four contains different graphs of $S_2-\eta$ and $P^*-\eta$ (where these quantities are defined in Chapter 2) for different numbers of chains. The main goals of these graphs is to determine the phase transition point between isotropic and nematic phases. Beside those results, we will describe most of the computational problems we faced in this part of the project and we will explain most of the computational techniques used for solving the problems and improving the results.

The fifth chapter explains the theoretical extension of chapters two and three to the smectic-A phase. In this chapter, one can find the new definitions and representations for finding the probability density function for the smectic-A phase. Beside this, the bifurcation analysis and the mathematical analysis which led us to two coupled self-consistent equations are described. In chapter six, the results of our studies of the smectic-A phase are gathered as a few charts and graphs. In addition, we will describe some of the computational techniques used for this part of our work. And in the last chapter, we give a summary and conclusions of this project.

Chapter 2

Semiflexible Hard Sphere Chains

2.1 Definition and Representation

This chapter will explain the properties of semiflexible hard sphere chains. Then the Helmholtz energy function of this model and the assumptions in the theory will be described. In the last part, the algorithm and simulation method used for chain generation can be found.

We modelled the polymer chain as a "pearl necklace" of fused hard spheres. As can be seen in Figure 2.1, we assumed that b, the distance between two adjacent beads, has a fixed value and denote D as the diameter of each sphere. In most of the cases it is assumed that $b < D$ since this is chemically realistic. While b has a fixed value, D is a variable which can take any value between zero and $2b$. This is because b cannot be less than the radius of a sphere for semiflexible chains, as shown later.

Since it is hard sphere chain model, the chain spheres must be "self avoiding" or "non-intersecting". This means that overlap can only occur between adjacent spheres and, as can be seen in Figure 2.2, any overlap between non-adjacent spheres is forbidden. The non-adjacent spheres can "touch" but not "penetrate" each other.

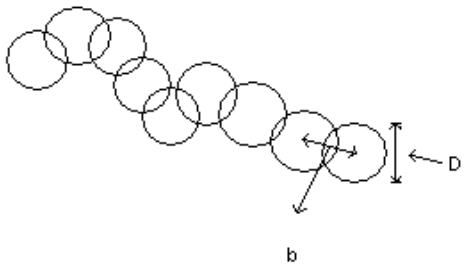

Figure 2.1: b is the bond length between beads and D is the diameter of each bead

If $b/D = 1$, the spheres are tangent to each other. It is clear that there is a maximum value for the angle between two adjacent bonds since non-adjacent spheres cannot penetrate each other, as shown below.

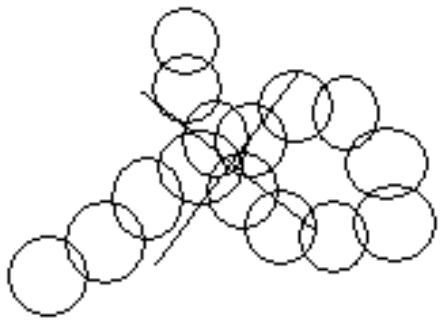

Figure 2.2: A chain cannot intersect itself or other chains

We label the spheres sequentially, starting from one end of chain, by index i:

$$i = 1, 2, 3..., N_c$$

where N_c is the number of spheres in the chain. The number of bonds for N_c spheres is $N_c - 1$ so the bonds between adjacent spheres can be labelled by an index as follows:

$$i = 1, 2, 3..., N_c - 1$$

Bond n represents the bond between spheres number n and $n + 1$.

The angle between bond n and $n+1$ is denoted by $\theta_{n,n+1}$. As mentioned, there is a maximum value for the angle between two adjacent bonds, θ_{max}, which can be found by using the cosine rule. According to the following Figure 2.3, $\theta = \theta_{max}$ happens when sphere n and sphere $n + 2$ are tangent to each other. In this case, there is a triangle with two sides of length b and one side of length D. Therefore we can use the cosine rule to find the maximum angle between bonds:

$$D^2 = 2b^2 + 2b^2 cos\theta_{max}$$

$$\therefore\ cos\theta_{max} = \frac{D^2}{(2b^2)} - 1 \tag{2.1}$$

Notice that θ_{max} must satisfy $\cos\theta_{max} \leq 1$, hence D and b must satisfy $D/2 < b$. (If $b < D/2$, no bending of the chain would be allowed and it would be perfectly rigid.)

The conformation of a chain molecule is described by the positions $\vec{r}_1$, $\vec{r}_2$, .., $\vec{r}_{N_c}$ of its N_c spheres, which is denoted $\vec{R}$ for simplicity. We denote the orientation of bonds in the chain by ω_1, ω_2, .. ω_{N_c-1}. Since there are $N_c - 1$ bonds, $N_c - 1$ orientations should be defined, where $\omega_n = (\theta_n, \phi_n)$ and θ_n and ϕ_n stand for the

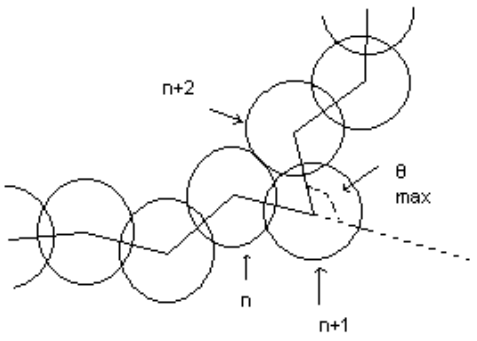

Figure 2.3: The maximum angle (θ_{max})between bonds between spheres n, $n+1$ and $n+1$, $n+2$

polar and azimuthal angles of the n_{th} bond with respect to a space fixed coordinate frame. Since the bond length b is fixed, if the position of just one sphere ($\vec{r_i}$) and the orientations of $N_c - 1$ bonds are known, we can find the positions of the rest of the spheres. This means that we need $2N_c + 1$ degrees of freedom to specify the conformation of a chain.

2.1.1 Shape Parameters

2.1.1.1 Mean-Square End-to-End Distance ($\langle \vec{r_e}^{\,2} \rangle$)

The vector $\vec{r_e}$ connecting the two ends of the chain is defined by

$$\vec{r_e} = \sum_{i=1}^{N_c-1} \vec{b_i} = \vec{r}_{N_c} - \vec{r}_1. \tag{2.2}$$

where $\vec{b}_i$ is the i^{th} bond-vector, $\vec{b}_i = \vec{r}_{i+1} - \vec{r}_i$. The mean value of $\vec{r}_e{}^2$ is

$$\langle \vec{r}_e{}^2 \rangle = \frac{1}{N} \int d\vec{R}\, \rho(\vec{R})\, \vec{r}_e{}^2. \tag{2.3}$$

where N is the number of chains and $\rho(\vec{R})$ is the probability density of configuration $\vec{R}$ which is normalized such that $\int d\vec{R}\rho(\vec{R}) = N$. To find the approximate value of $< \vec{r}_e{}^2 >$ (mean square of $\vec{r}_e$), the square value of Eq. (2.2) can be calculated:

$$\vec{r}_e{}^2 = \sum_{i=1}^{N_c-1} \vec{b}_i{}^2 + 2 \sum_{i<j} \vec{b}_i.\vec{b}_j, \tag{2.4}$$

then by considering Eq. 2.3 we get

$$\langle \vec{r}_e{}^2 \rangle = \sum_{i=1}^{N_c-1} \langle \vec{b}_i{}^2 \rangle + 2 \sum_{i<j} \langle \vec{b}_i.\vec{b}_j \rangle = (N_c - 1)b^2 + 2 \sum_{i<j} \langle \vec{b}_i.\vec{b}_j \rangle. \tag{2.5}$$

For a single isolated "random-flight" chain the beads are added in random orientations which can have any values (in the neglect of self-avoidance)and the average of $\vec{b}_i.\vec{b}_j$ is zero [28]. Then:

$$\langle \vec{r}_e{}^2 \rangle \equiv (N_c - 1)b^2, \tag{2.6}$$

where b is the length of $\vec{b}$.

2.1.1.2 Square Radius of Gyration ($\langle \vec{r_g}{}^2 \rangle$)

The radius of gyration r_g is defined as the square root of the mean square distance between the center of mass of the chain and the atoms. This definition can be presented as follows:

$$\vec{r}_g{}^2 = \frac{1}{N_c} \sum_{i=1}^{N_c} [\vec{r}_i - \vec{r}_{cm}]^2, \tag{2.7}$$

where

$$\vec{r}_{cm} = \frac{1}{N_c} \sum_{i=1}^{N_c} \vec{r}_i.$$

For finding the average value of $\vec{r}_g{}^2$

$$\langle \vec{r}_g{}^2 \rangle = \frac{1}{N} \int d\vec{R}\, \rho(\vec{R})\, \vec{r}_g{}^2. \tag{2.8}$$

It can be proved that for the random-flight or Gaussian chain, the radius of gyration is equal to [28]

$$\langle \vec{r}_g{}^2 \rangle \approx \frac{\langle \vec{r}_e{}^{\,2} \rangle}{6} \quad (N_c \to \infty)\,. \tag{2.9}$$

2.1.2 Thermodynamic Parameters

2.1.2.1 Volume Fraction (η)

Since in this project temperature is constant (the bending energy coefficient is fixed), phase transitions are induced merely by changing the density of the whole system (expanding or compressing). The volume fraction η variation is the reason for phase transitions in the model, and typically all other thermodynamic variables depend on this quantity. The volume fraction η is defined as the product of the number density of the system ρ and the molecular volume V_{mol}, where $\rho = N/V$ and N is the number of molecules and V is the system volume. Here V_{mol} is the volume of each chain, which is given as follows [10], [29]:

$$V_{mol} = \frac{\pi D^3}{6} \left[1 + \frac{1}{2}(N_c - 1) \left(3\Big(\frac{b}{D}\Big) - \Big(\frac{b}{D}\Big)^3 \right) \right], \tag{2.10}$$

where b is the bond length between the beads and D is the diameter of the beads.

At small η, only isotropic phases are expected to be found. With increasing η, nematic and smectic phases may occur. Note that for a system of pure hard spheres, there is a maximum physically allowed η ($\eta_{max} < 1$) due to closest-packing of the spheres. Due to the approximation used in this work, values of $\eta > \eta_{max}$ may occur. In this project, except a few graphs, almost all the η values are smaller or equal to one.

2.1.2.2 Order Parameter (S_2):

As mentioned in the previous chapter S_2, the order parameter, is the key parameter for detecting the isotropic-nematic phase transition. S_2 is defined as follows:

$$S_2 = \frac{1}{2}\langle 3cos^2\theta - 1\rangle, \tag{2.11}$$

where θ is the angle between the molecular axis and the direction of alignment. For this work, it is assumed that $\vec{r}_e$ is the molecular axis and the direction of alignment is the z axis. Then, in Eq. (2.11), $\cos\theta = z_e/|r_e|$ where $z_e = z_{N_c} - z_1$.

In the isotropic phase, where the orientation of molecules is completely random, the value of S_2 is zero. This happens since

$$\frac{1}{2}\int_0^{2\pi}\int_0^{\pi} d\phi\, sin\theta\, d\theta\, [3cos^2\theta - 1] = \frac{2\pi}{2}[-cos^3\theta + cos\theta]_0^{\pi} = 0. \tag{2.12}$$

For the nematic and smectic phases, S_2 is obviously greater than zero since most values of θ are near zero. In the completely aligned limit for nematic or smectic-A phases, where all the molecules are aligned in the direction of $\vec{z}$, the S_2 value is 1,

since $cos^2\theta = 1$, and

$$\frac{1}{2}\langle[3cos^2\theta - 1]\rangle = \frac{1}{2}[2] = 1. \tag{2.13}$$

2.1.2.3 Pressure and the reduced pressure

By using thermodynamic relations, the pressure (force per area) of the system is given by

$$P = \frac{1}{N}\,\rho^2\Big(\frac{\partial F}{\partial \rho}\Big)_{N,T}, \tag{2.14}$$

where F is the Helmholtz free energy of the system. For most of our calculations the reduced pressure is used, which is defined as

$$P^* \equiv \frac{PV_{mol}}{kT}, \tag{2.15}$$

where k, T and V_{mol} are the Boltzmann constant, temperature and volume per molecule, respectively. Pressure and volume per molecule are given by Eqs. (2.14) and (2.10), respectively. It should be mentioned that T is constant in this model.

2.2 Free Energy Functional

In 1873 van der Waals discovered that the distinction between liquid and gas can be explained by assuming an intermolecular attraction at large distances and repulsion at short distances. Van der Waals' assumption was proved in the early decades of the 20th century by the development of quantum mechanics. The short range repulsion is related to Pauli's exclusion principle and mutual electrostatic repulsion of the electrons in the outer shells of atoms. The long range attraction, which is known as a van der Waals force, is caused by dipole-induced-dipole interactions. [1]

The details of these forces are different for different materials. Until the 1950's it was believed that both attractions and repulsions were necessary for freezing and melting. It was thought that at low temperature the particles can neither move too far because of the attractive force, nor become closer to each other. Alder's computer simulation in 1957 showed a freezing process in a system of spheres just by considering *repulsive* intermolecular forces [30]. Therefore it was shown that the repulsive forces alone can be responsible for freezing. However both forces are necessary for evaporation and condensation processes. [1]

As mentioned in Section 1.3.1, in the 1940's, Onsagar showed that the isotropic-nematic phase transition for hard rod-like particles can be produced by considering only short range repulsive forces associated with the shape of the particles. Later Frenkel showed that the smectic phase occurs in a system of hard rods [7], [8]. We have used the Onsager theory for evaluating the Helmholtz free energy in the system. [1]

2.2.1 Bond Bending Energy

In our work, besides the repulsive forces between chains related to the shape of the particles (**hard-sphere** interaction), we assumed a simple **bond bending** energy for each chain. The bond bending energy controls the flexibility of the chains themselves. In one of the simplest forms, the bond bending energy can be modelled as

$$u_{n,n+1} = -\epsilon \, cos\theta_{n,n+1} \ (\epsilon > 0) \tag{2.16}$$

For minimization of the Helmholtz free energy, we are looking for the minimization of the internal energy, while we seek to maximize the entropy. For positive ϵ, the

energy is minimized when $\cos\theta_{n,n+1}$ is maximized. This happens when $\theta_{n,n+1} \longrightarrow 0$, the bond angle is zero and the chain is stretched out in a straight line. It is clear that this is in competition with maximization of the entropy, since maximization of entropy favors disordering of the chain, leading to a random distribution of bond angles. The above energy is just for one individual chain, however the main task for this part is to calculate the interaction between different chains. For all of the results of this thesis we used $\kappa = \beta\epsilon = 50$, where $\beta = 1/kT$, T is temperature and k is the Boltzmann constant.

2.2.2 Second Virial Expansion for the Multi-Chain Free Energy

In a system containing N chains (molecules), $\rho(\vec{R})$ can be defined as the probability density of finding a molecule with configuration $\vec{R}$. The normalization condition for the density function is as follows:

$$\int d\vec{R}\,\rho(\vec{R}) \equiv \int d\vec{r_i}\,d\omega_1 d\omega_2 .. d\omega_{N_c-1}\,\rho(\vec{R}) = N \tag{2.17}$$

From statistical mechanics, it is known that

$$\beta F(N,V,T) = -\ln Z(N,V,T), \tag{2.18}$$

where $Z(N,V,T)$ is the canonical partition function, given by

$$Z(N,V,T) = \frac{1}{N!}\int d\tau \exp[-\beta H_N(\tau)] \tag{2.19}$$

$$d\tau = \prod_{i=1}^{N} \left(\frac{d\vec{R}_i d\vec{p}_i}{h^{(2N_c+1)}} \right). \tag{2.20}$$

where $\vec{R}_i$ and $\vec{p}_i$ denote the position and momentum of molecule i, respectively. In Eq. (2.20), we have used the fact that each molecule has $(2N_c+1)$ degrees of freedom. By considering the above equations and defining H (Hamiltonian) as in the following equation:

$$H_N(\vec{R}^N, \vec{p}^{\,N}) = U_N(\vec{R}^N) + K_N(\vec{p}^{\,N}), \tag{2.21}$$

where $\vec{R}^N = (\vec{R}_1, \vec{R}_2, ..., \vec{R}_N)$ and $\vec{p}^{\,N} = (\vec{p}_1, \vec{p}_2, ..., \vec{p}_N)$ represent the positions and momenta of the chains, respectively, we reach the following equation for $Z(N, V, T)$

$$Z(N, V, T) = \frac{Q(N, V, T)}{N! \lambda^{N(2N_c+1)}}, \tag{2.22}$$

where λ and $Q(N, V, T)$ represent the "De Broglie wavelength" and "configurational integral", which are defined as follows:

$$\lambda = \frac{h}{(2\pi m k_B T)^{1/2}} \tag{2.23}$$

$$Q(N, V, T) = \int d\vec{R}^N \exp[-\beta U_N(\vec{R}^N)]. \tag{2.24}$$

By using Eqs. (2.18) and (2.22) we get

$$\beta F(N, V, T) = -\Big(\ln Q(N, V, T) - \ln N! - \ln \lambda^{N(2N_c+1)} \Big). \tag{2.25}$$

By using the Stirling formula ($\ln N! \approx N \ln N - N$):

$$\beta F(N, V, T) \approx -\ln Q(N, V, T) + (N \ln N - N) + N \ln \lambda^{2N_c+1}$$

$$\Longrightarrow \beta F(N,V,T) \approx -\ln Q(N,V,T) + N\ln N + N(\ln \lambda^{2N_c+1} - 1). \tag{2.26}$$

To obtain a more explicit form for the Helmholtz free energy, the configuration integral (Q) should be expanded. We represent

$$U_N(\vec{R}^N) = \sum_{i<j}^{N} u_2(\vec{R}_i, \vec{R}_j) + \sum_{i=1}^{N} u_1(\vec{R}_i), \tag{2.27}$$

where u_2 and u_1 are two-body and one-body potentials, respectively. For our hard-sphere chains, $u_1(\vec{R})$ includes the intrachain hard-sphere repulsions (self-avoidance), the bending energies (2.16), as well as any possible external fields (which are not considered in this work). Therefore

$$Q(N,V,T) = \int d\vec{R}^N \exp[-\beta U_N(\vec{R}^N)]$$

$$= \int d\vec{R}^N \exp\Big[-\sum_{i<j}^{N} \beta u_2(\vec{R}_i, \vec{R}_j)\Big] \exp\Big[-\sum_{i=1}^{N} \beta u_1(\vec{R}_i)\Big]. \tag{2.28}$$

We use the Mayer function f_M to expand this equation, which is defined as

$$f_M(\vec{R}_i, \vec{R}_j) = \exp[-\beta u_2(\vec{R}_i, \vec{R}_j)] - 1. \tag{2.29}$$

By using the Mayer function, Eq. (2.28) can be written as

$$\int d\vec{R}^N \exp\Big[-\sum_{i<j}^{N} \beta u_2(\vec{R}_i, \vec{R}_j)\Big] \exp\Big[-\sum_{i=1}^{N} \beta u_1(\vec{R}_i)\Big]$$

$$= \int d\vec{R}^N \prod_{i<j}^{N} (1 + f_M(\vec{R}_i, \vec{R}_j)) \exp[-\sum_{i=1}^{N} \beta u_1(\vec{R}_i)]$$

$$= \int d\vec{R}^N (1 + \sum_{i<j}^{N} f_M(\vec{R}_i, \vec{R}_j) + ...) \exp[-\sum_{i=1}^{N} \beta u_1(\vec{R}_i)]. \tag{2.30}$$

which is obtained by linearizing in $f_M(\vec{R}_i, \vec{R}_j)$.

The last equation can be rewritten as

$$Q(N,V,T) = Q_{id}\left(1 + \sum_{i<j}^{N} \frac{1}{Q_{id}} \int d\vec{R}^N f_M(\vec{R}_i, \vec{R}_j) \exp[-\beta \sum_{i=1}^{N} u_1(\vec{R}_i)] + ...\right),$$

$$= Q_{id}\left(1 + \frac{N(N-1)}{2} \frac{\int d\vec{R}_1 d\vec{R}_2 f_M(\vec{R}_1, \vec{R}_2) \exp -\beta[u_1(\vec{R}_1) + u_1(\vec{R}_2)]}{\int d\vec{R}_1 d\vec{R}_2 \exp -\beta[u_1(\vec{R}_1) + u_1(\vec{R}_2)]} + ...\right), \tag{2.31}$$

where

$$Q_{id} = \int d\vec{R}^N \exp[-\beta \sum_{i=1}^{N} u_1(\vec{R}_i)] = Q_1^N, \tag{2.32}$$

and

$$Q_1 = \int d\vec{R} \exp[-\beta u_1(\vec{R})]. \tag{2.33}$$

For $N \gg 1$, and defining the unperturbed probability density as

$$\rho_0(\vec{R}) = \frac{N}{Q_1} \exp[-\beta u_1(\vec{R})], \tag{2.34}$$

Eq. (2.31) becomes

$$Q(N,V,T) = Q_{id}\left(1 + \frac{1}{2} \int d\vec{R}_1 d\vec{R}_2 f_M(\vec{R}_1, \vec{R}_2) \rho_0(\vec{R}_1) \rho_0(\vec{R}_2) + ...\right) \tag{2.35}$$

For short-range repulsive interactions, the Mayer function $f_M(\vec{R}_1, \vec{R}_2)$ has a microscopic range. It can then be shown that the integral in Eq. (2.35) has a magnitude of order Na, where a is a dimensionless parameter proportional to the number density

$\rho = N/V$. The present expansion is limited to low density, so we may assume formally that $|a| \ll 1$. Then using (by Taylor-series expansion for small $|a|$)

$$(1+a)^N \approx 1 + Na \tag{2.36}$$

we find that the logarithm of $Q(N,V,T)$ is given by

$$\ln Q(N,V,T) = \ln Q_{id} + \frac{1}{2}\int d\vec{R}_1 d\vec{R}_2 f_M(\vec{R}_1,\vec{R}_2)\rho_0(\vec{R}_1)\rho_0(\vec{R}_2) + ... \tag{2.37}$$

Substituting Eq. (2.37) into Eq. (2.26) as well as using Eq. (2.32), we obtain for the Helmholtz free energy,

$$\beta F = N\big[\ln N + \ln \lambda^{2N_c+1} - 1 - \ln Q_1\big] - \frac{1}{2}\int d\vec{R}_1 d\vec{R}_2 f_M(\vec{R}_1,\vec{R}_2)\rho_0(\vec{R}_1)\rho_0(\vec{R}_2) + ... \tag{2.38}$$

Finally, using Eq. (2.34) as well as the normalization condition Eq. (2.17), Eq. (2.38) can be written as

$$\beta F = \int d\vec{R}\rho_0(\vec{R})\big[\ln \rho_0(\vec{R})\lambda^{2N_c+1} - 1 + \beta u_1(\vec{R})\big] - \frac{1}{2}\int d\vec{R}_1 d\vec{R}_2 \rho_0(\vec{R}_1)\rho_0(\vec{R}_2) f_M(\vec{R}_1,\vec{R}_2) + ... \tag{2.39}$$

The De Broglie wavelength λ is an unimportant parameter. As mentioned, $u_1(\vec{R})$ represents intramolecular potential energies and possible effects of external fields on the configuration $\vec{R}$. The last integral of Eq. (2.39) is related to interactions between chains. As was defined in Eq. (2.29)

$$f_M(\vec{R}_i,\vec{R}_j) = \exp[-\beta u_2(\vec{R}_i,\vec{R}_j)] - 1, \tag{2.40}$$

where $u_2(\vec{R}_i,\vec{R}_j)$ is the intermolecular potential energy. For the hard sphere model,

the interaction is a very simple function; $u_2(\vec{R}_i, \vec{R}_j)$ is infinity when there is any overlap between two chains and is zero otherwise. This definition indicates that overlap between chains cannot occur. This is represented by the Mayer function as follows:

$$f_M(\vec{R}_i, \vec{R}_j) = 0, \text{ if no overlap}$$

$$f_M(\vec{R}_i, \vec{R}_j) = -1, \text{ if there is an overlap} \tag{2.41}$$

Eq. (2.39) is the standard form of the Onsager or second-virial approximation to the free energy [8], [24], which represents F as a functional of the probability density. Although, in the above derivation, the probability density is given by the "unperturbed" expression Eq. (2.34) (i.e., independent of intermolecular interactions), from now on we replace $\rho_0(\vec{R})$ in Eq. (2.39), by the full probability density $\rho(\vec{R})$. The latter is an arbitrary, unknown function that may depend on intermolecular interactions, and which will be determined by functional minimization of F. The justification for replacing ρ_0 by ρ can be established more clearly using the grand canonical ensemble [31].

2.2.3 Minimization of the Free Energy Functional

In order to find the minimum of the free energy Eq. (2.39) after being truncated to the second virial term, we must include the constraint equation Eq. (2.17). For this purpose the Lagrange method is used, defining

$$\beta\hat{F} \equiv \beta F - \nu \int d\vec{R}\rho(\vec{R}), \tag{2.42}$$

where ν is a Lagrange multiplier. By using the relation

$$\frac{\delta\ \rho(\vec{R}_i)}{\delta\ \rho(\vec{R}_1)} = \delta(\vec{R}_i - \vec{R}_1) \tag{2.43}$$

we find

$$\frac{\delta\ \beta F}{\delta\ \rho(\vec{R}_1)} = (\ln \rho(\vec{R}_1)\lambda^{2N_c+1} + \beta u_1(\vec{R}_1)) - \int d\vec{R}_2 f_M(\vec{R}_1, \vec{R}_2)\rho(\vec{R}_2) \tag{2.44}$$

Minimizing $\beta\hat{F}$ and therefore setting $\frac{\delta\ \beta\hat{F}}{\delta\ \rho(\vec{R})} = 0$ gives the final equation:

$$\rho(\vec{R}_1) = c\ \exp[-\beta u_1(\vec{R}_1) + \int d\vec{R}_2\ f_M(\vec{R}_1, \vec{R}_2)\rho(\vec{R}_2)], \tag{2.45}$$

where c is a normalization constant, determined by Eq. (2.17). The probability density $\rho(\vec{R}_1)$ appears in both sides of the above equation, therefore it is a "self-consistent" equation for $\rho(\vec{R}_1)$. It should be mentioned that $\vec{R}_1$ and $\vec{R}_2$ are "multi-dimensional" variables and each of them represents a set of vectors. These conformations are generated by a Monte Carlo method, which is discussed in the next section.

2.3 Generation of the Chains

At first we do not consider the bond bending potential energy and we give an algorithm for chain generation just by considering their hard-core interactions. But in the next step we will add the bond bending energy to the algorithm for chain generation.

In order to generate semiflexible hard sphere chains, we first place the initial bead at the origin $(0, 0, 0)$, then the chains are grown by adding subsequent beads to an existing chain. Each subsequent bond will be rotated by random angles with respect

to the previous bond, i.e., each bond is generated using random values for $\cos\theta$ and ϕ relative to the previous bond. We must be careful that $\cos\theta$ has a range between 0 and $D^2/2b^2 - 1$. It should be mentioned that for calculating the first real bond we assume that there is a "virtual bond" between $(0, 0, -1)$ and $(0, 0, 0)$ (using units in which the bond-length $b = 1$) which is not considered in the actual generated chain and does not have any effect in choosing the ϕ and θ of the first actual bond ($\theta_{max} = \pi$). This helps the generated chains to have a random orientation in space. As you will see, this virtual bond is just used to help the calculation of the first bond.

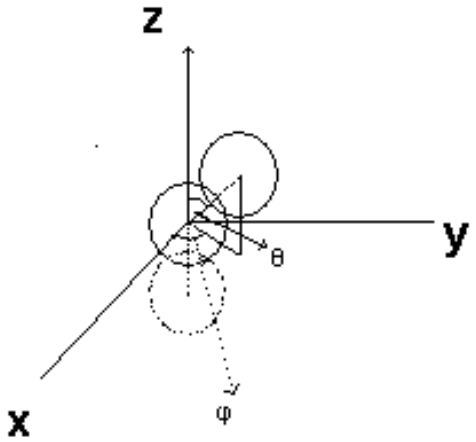

Figure 2.4: Chain generation: Adding the second real bead of the chain

As can be seen in Figure 2.4, the second real bead is added by selecting random values of $\cos\theta$ and ϕ relative to the previous two beads.

After each bead addition, for example adding the bead i, it should be checked that there is no overlap with the previous beads $1 .. (i - 2)$. If an overlap is found,

the process should stop and generation of that chain should *start over again*, since the process should be completely random.

For adding the next bead we used a special technique created by Prof. B. G. Nickel. Three vectors $\vec{p}$, $\vec{q}$ and $\vec{b}$ are defined as the current coordinate axis of the system, where $\vec{b}$ is the last bond between beads i and $i+1$. The task is to find the components of $\vec{b'}$ (new bond) in the coordinates x, y and z. Since the random variables of ϕ and $\cos\theta$ are given with respect to the previous coordinates $\vec{p}, \vec{q}$ and $\vec{b}$, the new components of these vectors should be calculated in the initial system. For this purpose the initial $\vec{b}$, $\vec{p}$ and $\vec{q}$ are defined as follows for the first bond (using units in which the bond-length $b = 1$):

$$\vec{b} = (0, 0, 1), \vec{p} = (0, 1, 0) \text{ and } \vec{q} = (1, 0, 0) \tag{2.46}$$

which are perpendicular to each other, and $\vec{q} = \vec{p} \times \vec{b}$. As mentioned, this first bond is virtual and there is no actual bead at $(0, 0, -1)$

Then on the next step, after generating random values of $\cos\theta$ and ϕ, the coordinates of $\vec{q}$ and $\vec{p}$ should be rotated first by an angle of ϕ around $\vec{b}$ and then rotated by an angle of θ around the new $\vec{p}$ axis. This is the final $\vec{b}$ for the next bond.

The final $\vec{q}$ is calculated by $\vec{p} \times \vec{b}$. The equations for the functions are as follows:

$$\vec{p'} = \vec{p}\, cos\phi - \vec{q}\, sin\phi \ , \ \vec{q_1} = \vec{q}\, cos\phi + \vec{p}\, sin\phi \tag{2.47}$$

$$\vec{b'} = \vec{b}\, cos\theta + \vec{q_1}\, sin\theta \ , \ \vec{q'} = \vec{p'} \times \vec{b'}.$$

It should be mentioned that always $|\vec{p}|$ and $|\vec{q}|$ have one unit of length, where the units are defined in which the bond-length $b = 1$. The torsion angle ϕ as defined here is the IUPAC-IUB convention [32].

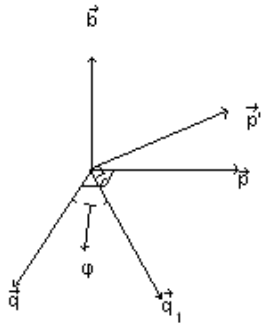

Figure 2.5: The first rotation is around $\vec{b}$. $\vec{q}_1$ is the coordinate of $\vec{q}$ after the first rotation.

2.3.1 Including the Bending Energy in the Random Generation of Chains

To add the bond bending energy function to the chain Monte Carlo generation, different probability weights should be given to the different configurations. This probability should be proportional to $e^{-\beta u_1(\theta)} = e^{\kappa\, cos\theta}$, where $\kappa = \beta\epsilon$ is a dimensionless bending-energy parameter, see Eq. (2.16). It is clear that the probability is maximized when $\cos\theta = 1$ and the chain is straight. To find a simulation technique for adding the bond bending energy term, we define a function x which satisfies

$$0 \leq x \leq 1 \text{ and } |dx| \propto d\, cos\theta\, e^{-\beta u_1(\theta)}.$$

Hence we can define

$$x = \frac{\int_{cos\theta}^{1} dcos\theta\, e^{-\beta u_1(\theta)}}{\int_{-1+\frac{D^2}{2}}^{1} dcos\theta\, e^{-\beta u_1(\theta)}}. \tag{2.48}$$

Using

$$u_1(\theta) = \frac{-\kappa\, cos\theta}{\beta}, \tag{2.49}$$

x will be given by

$$x = \frac{\int_{cos\theta}^{1} d\, cos\theta\, e^{\kappa\, cos\theta}}{\int_{-1+\frac{D^2}{2}}^{1} d\, cos\theta\, e^{\kappa\, cos\theta}} = \frac{(e^{\kappa} - e^{\kappa\, cos\theta})}{(e^{\kappa} - e^{\kappa(D^2/2-1)})}. \tag{2.50}$$

Therefore, $\cos\theta$ will be given by

$$\cos(\theta) = \frac{1}{\kappa} \ln((1-x)e^{\kappa} + xe^{\kappa(D^2/2-1)}), \tag{2.51}$$

where as mentioned $0 \leq x \leq 1$.

By using the above equation, a random value of $\cos\theta$ can be found by selecting a random value of x between one and zero. In the absence of a bending energy, hence $\kappa \longrightarrow 0$, the above equation becomes

$$\cos\theta \approx \frac{1}{\kappa} \ln[1 + \kappa(1 - x + x(\frac{D^2}{2} - 1))] \approx 1 - x + x(\frac{D^2}{2} - 1) = 1 - x(2 - \frac{D^2}{2}). \tag{2.52}$$

The function $1 - x(2 - D^2/2)$ yields the probability distribution for $\cos\theta$ uniformly between 1 and $D^2/2 - 1$, so this result agrees with the behavior for the non-bonding energy case.

Chapter 3

Determining the Probability Density

3.1 Probability Distribution Function Equation

The probability density equation (Eq. (2.45)) is a self-consistent equation, which will be solved iteratively. For solving the density function by an iteration method, the first step is to make an *initial guess* for $\rho(\vec{R})$. This initial guess is inserted in the right side of the equation and the result of the left side will be the input for the right side of the equation in the next step. This process is continued until the point in which the changes between input and output become very small. When there is no noticeable change in the probability density, this value is assumed to be the solution of the self consistent equation.

The main step in solving Eq. (2.45) is to evaluate the following integral:

$$I(\vec{R_1}) \equiv \int d\vec{R_2}\, f_M(\vec{R_1}, \vec{R_2})\, \rho(\vec{R_2}), \tag{3.1}$$

where $\vec{R}_1$ is a given arbitrary chain configuration and the integral $\mathrm{d}\vec{R}_2$ stands for all possible chain configurations in the system. Due to its multi-dimensional nature, the Monte Carlo method is one of the best options to evaluate the above integral.

One simplified case is the spatially uniform system, which applies to isotropic and nematic phases. In this case, it can be assumed that $\rho(\vec{R}_i)$ is translationally invariant and only depends on the set of bond orientations $\vec{\omega}_i \equiv (\omega_{i,1} .. \omega_{i,Nc-1})$ and not on the positions of the spheres ($\rho(\vec{R}_i) = \rho(\vec{\omega}_i)$).

3.1.1 Excluded Volume

The excluded volume $V_{ex}(\vec{\omega_1}, \vec{\omega_2})$ between two chains with configuration $\vec{\omega_1}$ and $\vec{\omega_2}$ is defined as a volume of space surrounding and including the chain with configuration $\vec{\omega_1}$ which is excluded (forbidden) to the other chain with configuration $\vec{\omega}_2$ due to the presence of the first chain. For calculating the excluded volume, we used a Monte-Carlo method, which is an approximate computational method for calculating the excluded volume. We used the Barrett algorithm [33] for this purpose. The excluded volume between a pair of rigid or non-rigid molecules is calculated as follows:

$$V_{ex}(\vec{\omega}_1, \vec{\omega}_2) = -\int d\vec{r}_{12} f_M(12), \tag{3.2}$$

where $f_M(12)$ is the Mayer function between two chains and $\vec{r}_{12} = \vec{r}_2 - \vec{r}_1$, where $\vec{r}_1$, $\vec{r}_2$ denote the positions of particular reference beads on chains one and two. According to Eq. (2.41), $f_M(12) = -1$ if there is any overlap, and $f_M(12) = 0$ if there is no overlap.

Now by using $\rho(\vec{R}_i) = \rho(\vec{\omega}_i)$ and Eq. (3.2), Eq. (3.1) becomes

$$I(\vec{R}_1) \equiv I(\vec{\omega_1}) = -\int d\vec{\omega_2}\, V_{ex}(\vec{\omega_1}, \vec{\omega_2})\rho(\vec{\omega_2}). \tag{3.3}$$

3.2 Simulation Techniques for Solving the Equation

3.2.1 Barrett's Algorithm [33]

As mentioned, the calculation of the excluded volume between a pair of rigid or non-rigid molecules is done by using the following formula:

$$V_{ex}(\vec{\omega}_1, \vec{\omega}_2) = -\int d\vec{r}_{12} f_M(12),$$

As mentioned in Eq. (2.40)

$$f_M(12) = e^{-\beta\, u_2(12)} - 1$$

and the hard-sphere potential between the two chains is defined by

$$u_2(12) = \sum_{i=1}^{N_c}\sum_{j=1}^{N_c} u_{HS}(|\vec{r}_i - \vec{r}_j|). \tag{3.4}$$

Hence $f_M(12)$ can be written as a function of $f_M(r_{ij})$:

$$f_M(12) = \prod_{i,j}^{N_c}(1 + f_M(r_{ij})) - 1, \tag{3.5}$$

where $f_M(r_{ij})$ is the Mayer-function for spherical monomers i and j ($f_M(r_{ij}) = e^{-\beta\, u_{HS}(r_{ij})} - 1$).

It is clear that, if any pair of beads (for example m and n) between two chains has an overlap $f_M(r_{mn}) = -1$, then $f_M(12) = -1$, and if there is no overlap between any beads of two chains, all $f_M(r_{ij}) = 0$ and then $f_M(12) = 0$.

The last equation can be written alternatively as

$$f_M(12) = \frac{1}{n_{overlap}} \sum_{i,j}^{N_c} f_M(r_{ij}), \tag{3.6}$$

where $n_{overlap}$ is the number of bead overlaps between chains one and two. The above equation is valid when $n_{overlap}$ is not zero. When there is no overlap ($n_{overlap} = 0$) $f_M(12) = 0$. Therefore

$$V_{ex}(\vec{\omega}_1, \vec{\omega}_2) = -\int_{overlap} d\vec{r}_{12}\, f_M(12) = -\sum_{i,j}^{N_c} \int_{overlap} d\vec{r}_{12}\, \frac{1}{n_{overlap}} f_M(r_{ij}). \tag{3.7}$$

Since $f_M(r_{ij}) = 0$ unless monomers i and j overlap with each other, the above equation can be written as

$$V_{ex}(\vec{\omega}_1, \vec{\omega}_2) = -\sum_{i,j}^{N_c} \int_{overlap} d\vec{r}_{12}\, \frac{1}{n_{overlap}} f_M(r_{i,j}) = \sum_{i,j}^{N_c} \int_{overlap\,(i,j)} d\vec{r}_{ij} \frac{1}{n_{overlap}}, \tag{3.8}$$

where $overlap(i,j)$ means the overlap domain of beads i (in chain 1) and j (in chain 2). To calculate $\int d\vec{r}_{ij}$, the Monte-Carlo technique is used. We note that

$$\int_{overlap(i,j)} d\vec{r}_{ij} = \int_0^D r_{ij}^2 dr_{ij} \int_0^\pi sin\theta_{ij}\, d\theta_{ij} \int_0^{2\pi} d\phi_{ij}, \tag{3.9}$$

where all above variables are relative to the center of monomer i. The above equation

can be written as

$$\int_{overlap(i,j)} d\vec{r}_{ij} = \frac{4\pi D^3}{3} \int_0^1 d\upsilon_1 \int_0^1 d\upsilon_2 \int_0^1 d\upsilon_3, \tag{3.10}$$

where $\upsilon_1 \equiv r_{ij}^3/D^3$, $\upsilon_2 \equiv (cos\theta_{ij} + 1)/2$ and $\upsilon_3 \equiv \phi_{ij}/2\pi$.

In practice three random numbers between zero and one are generated for υ_1, υ_2 and υ_3. By using Eqs. (3.10), (3.8) is given approximately by

$$V_{ex}(\vec{\omega}_1, \vec{\omega}_2) = \sum_{i,j}^{N_c} \int_{overlap(i,j)} d\vec{r}_{ij} \frac{1}{n_{overlap}} \approx \sum_{i,j}^{N_c} \frac{1}{N_B} \frac{4\pi D^3}{3} \sum_{k=1}^{N_B} \frac{1}{n_{overlap}}, \tag{3.11}$$

where N_B is the number of random "Barrett" points generated by the program and $n_{overlap}$ is the total number of bead overlaps for each "Barrett" point in the overlap domain of i (in chain one) and j (in chain two).

In our program, we stored the excluded volume for all the pairs of chains in the RAM memory. While this method uses lots of computer memory, it is an useful way to save calculation time.

3.2.2 Modifying the Probability Density Equation

First we will consider only uniform systems (isotropic and nematic), for which $\rho(\vec{R}) = \rho(\vec{\omega})$, since the probability density function does not depend on the position of the chain. It is useful to insert the average number density, $\rho = N/V$, into $\rho(\vec{\omega})$ to define the conformation probability distribution function as follows:

$$\rho(\vec{\omega}) = \rho f(\vec{\omega}). \tag{3.12}$$

By using Eq. (2.17) we have

$$\int d\vec{\omega} f(\vec{\omega}) = 1. \tag{3.13}$$

In the absence of intermolecular interactions, ($f_M(\vec{R}_1, \vec{R}_2) = 0$), Eq. (2.45) becomes

$$\rho(\vec{R}_1) \rightarrow \rho_0(\vec{R}_1) = c_0 \, e^{-\beta u_1(\vec{R}_1)}. \tag{3.14}$$

By using all the three last equations, the unperturbed distribution function $f_0(\vec{\omega}_1)$ can be defined as :

$$f_0(\vec{\omega}_1) = c_0' \, e^{-\beta u_1(\vec{\omega}_1)}, \tag{3.15}$$

where

$$c_0' = \frac{1}{\int d\vec{\omega}_1 e^{-\beta u_1(\vec{\omega}_1)}}. \tag{3.16}$$

Then the full *"perturbed"* distribution function $f(\vec{\omega}_1)$, from Eq. (2.45), satisfies the equation

$$f(\vec{\omega}_1) = c' f_0(\vec{\omega}_1) e^{I(\vec{\omega}_1)}, \tag{3.17}$$

where $I(\vec{\omega}_1)$ is given by Eq. (3.3) and c' is

$$c' = \frac{1}{\int d\vec{\omega}_1 f_0(\vec{\omega}_1) e^{I(\vec{\omega}_1)}}. \tag{3.18}$$

The average value of any function $g(\vec{\omega}_1)$ with respect to the unperturbed distribution function can be defined as

$$\int d\vec{\omega}_1 \; f_0(\vec{\omega}_1) \, g(\vec{\omega}_1) \equiv \langle \, g \, \rangle_{(0)}. \tag{3.19}$$

In the Monte Carlo method used in this work, a large number N of chain conformations with probability proportional to $f_0(\vec{\omega})$ is generated, so the above equation

becomes

$$\langle g \rangle_{(0)} \approx \frac{1}{N} \sum_{i=1}^{N} g(\vec{\omega}_i). \tag{3.20}$$

The main goal in this section is to describe the computational method to solve Eq. (3.17). As mentioned, the computational method to solve this equation is an iteration method or mixing method. The iteration method should be started from an initial guess for $I(\vec{\omega})$, and then it should be continued until successive iterates for $I(\vec{\omega})$ converge to unchanging values. Let $I_m(\vec{\omega})$ denote the m^{th} iterate of the integral $I(\vec{\omega})$. In this method I_{m+1} is calculated using I_m. By considering Eqs. (3.3), (3.12), (3.17), (3.18) and (3.19), $I_{m+1}(\vec{\omega}_1)$ is given by

$$I_{m+1}(\vec{\omega}_1) = -\rho \; \frac{\int d\vec{\omega}_2 V_{ex}(\vec{\omega}_1, \vec{\omega}_2) \; f_0(\vec{\omega}_2) \; e^{I_m(\vec{\omega}_2)}}{\int d\vec{\omega}_2 \; f_0(\vec{\omega}_2) \; e^{I_m(\vec{\omega}_2)}}, \tag{3.21}$$

which can be expressed as

$$I_{m+1}(\vec{\omega}_1) = -\rho \; \frac{\left\langle \; V_{ex}(\vec{\omega}_1, \vec{\omega}_2) \; e^{I_m(\vec{\omega}_2)} \right\rangle_{(0)}}{\left\langle e^{I_m(\vec{\omega}_2)} \right\rangle_{(0)}}. \tag{3.22}$$

By applying Eq. (3.20) for chains generated with probability proportional to $f_0(\vec{\omega}_2)$, the last equation can be expressed as

$$I_{m+1}(\vec{\omega}_1) = -\rho \; \frac{\sum_{i=1}^{N} V_{ex}(\vec{\omega}_1, \vec{\omega}_i) \; e^{I_m(\vec{\omega}_i)}}{\sum_{i=1}^{N} e^{I_m(\vec{\omega}_i)}}. \tag{3.23}$$

Equilibrium of the iteration method is obtained by repeating the above calculation until successive iterates $I_{m+1}(\vec{\omega}_1)$ and $I_m(\vec{\omega}_1)$ are "equal" to each other, within some tolerance, for each of the chain configurations $\vec{\omega}_1$ generated by the Monte Carlo method described in Section 2.3. This equation may have different solutions, each of which is a local minimum of the Helmholtz free energy and only one of which is that which

gives the global minimum F.

A suitable initial guess $I_1(\vec{\omega}_1)$ can be found by replacing $I_0(\vec{\omega}_i)$ in the right-hand-side of Eq. (3.23) by zero, hence

$$I_1(\vec{\omega}_1) = -\rho \ \frac{\sum_{i=1}^{N} V_{ex}(\vec{\omega}_1, \vec{\omega}_i)}{N}. \tag{3.24}$$

In this method, $I_m(\vec{\omega})$ is used as an input to calculate $I_{m+1}(\vec{\omega})$, which is the main method used for this part of our work. Later on, in the next chapter and for studying the smectic phase, we will describe an alternative "mixing" method for performing iterations.

Chapter 4

Results for the Isotropic-Nematic Phase Transition

4.1 Introduction

In this chapter I will discuss the results we obtained from solving Eq. (3.23). The main goal is to find the isotropic-nematic phase transition point.

The phase transition point has several characteristics, but the main one that we focused on is the jump on the graphs of $S_2 - \eta$ and $P^* - \eta$. It should be mentioned that the phase transition point has several other criterion such as sudden increases in the number of needed iterations before reaching equilibrium.

Most of the results were compared with those obtained by Jaffer et al. [39], [10]. Their work was based on an approximate analytical evaluation of the excluded volume for semiflexible hard sphere chains which should give nearly the same results as ours in the high bending stiffness coefficient (κ) regime.

As a first step for checking the produced configurations as well as our calculation of

the excluded volume, we compared the program results for different numbers of beads, b (bond length) and D (bead diameter) with the "Stick-bead model program" of Prof. B. G. Nickel. We compared some of the variables defined in Section 2.1.1, such as the mean-square radius of gyration $\langle \vec{r_g}^{\,2} \rangle$ and mean-square end-to-end distance $\langle \vec{r_e}^{\,2} \rangle$. Beside these, to check the excluded volumes, we compared the unperturbed second virial coefficient B_2 with the results of the " Stick-bead model" program. By referring to Eq. (2.39), the second virial coefficient is given by

$$B_2 = \frac{1}{2} \int d\vec{\omega_1} d\vec{\omega_2} f_0(\vec{\omega_1}) f_0(\vec{\omega_2}) V_{ex}(\vec{\omega_1}, \vec{\omega_2}). \tag{4.1}$$

where $f_0(\vec{\omega})$ is "unperturbed" probability density function. After these checks, we used mostly constant values for b, D, N_B, κ and N_c. For $N_c = 8$, $D/b = 1$ and $\kappa = 50$ the mean-square radius of gyration $\langle \vec{r_g^2} \rangle$ and mean-square end-to-end distance $\langle \vec{r_e}^{\,2} \rangle$ for 6000 chains are as follows: 5.09 , 46.82. It is obvious that the value of $\langle \vec{r_e}^{\,2} \rangle$ is far from the approximation of $\langle \vec{r_e}^{\,2} \rangle$ in Section 2.1.1 $\langle \vec{r_e}^{\,2} \rangle \approx (N_c - 1)b^2 = N_c - 1$. That approximation is valid for the case that $\theta_{max} = \pi$ and there is no restriction on the bond orientations, while in our model the bonds are restricted to avoid any intersection of the chain by itself. On the other hand, the value obtained for $\langle \vec{r_e}^{\,2} \rangle$ is close to that for a perfectly rigid 8-bead chain, namely $\langle \vec{r_e}^{\,2} \rangle = 7^2 = 49$.

4.1.1 Used Parameters

As was said in the previous section, since we wanted to compare our results with the previous work of Jaffer et al. [10], all of the results of this thesis were calculated in a high stiffness case, $\kappa = 50$.

The number of beads in each chain is 8 in all the following results. We used 8,

a relatively small number of beads in each chain, since we wanted to avoid adding another time consuming part to the program. By referring to the Barrett Algorithm section in the previous chapter (3.2.1), one can see that the time needed to run the Barrett algorithm to calculate the excluded volume is of the order of N_c^2, where N_c is the number of beads in each chain.

N_B is the variable which represents the number of random "Barrett" points generated by the program. According to the Barrett algorithm, the program running time is of the order of N_B. Therefore our purpose was to find the minimum value of N_B which gives an accurate result for the excluded volume. We choose $N_B = 5$ for our work as a compromise between accuracy and time needed. We would have preferred larger N_B to obtain more precise results. As mentioned before, we assumed the bond length, b, as our unit of length. While in these units the sphere diameter D could be between 0 and 2, it was set to 1 for all of the final calculations of this thesis ($D/b = 1$).

4.1.2 Limitations of the Calculation

It is preferable to use a large number N of chains in the Monte Carlo calculation. While at first glance it looks like the program requires a time of order N^2, actually the program runs nearly in the time of order N^3 (N represents the number of chains generated). The calculation time of the excluded volumes is of the order of N^2, but the iteration part of computation is of the order of N^3, since the number of required iterations for reaching convergence is of the order of N. Besides that, the problem of memory consumption to save the excluded volumes and other memory consuming parts of the programs were other limitations to increasing the number of chains. However this problem could be solved much easier than the first problem. We could

use the HDD (Hard Drive Disk) for this purpose instead of using RAM memory. It should be mentioned, however, that reading data from HDD is significantly slower than using RAM. Besides this, we used some techniques to avoid consuming memory. For example, we saved just half of the excluded volume information between chains. Since there is a symmetry in the excluded volume between chains, it can be assumed that $V_{ex}(\vec{\omega}_1, \vec{\omega}_2) = V_{ex}(\vec{\omega}_2, \vec{\omega}_1)$ and therefore just half of the information could be saved.

Besides all of the above problems, we must make proper guesses for the initial weight of the different configurations in order for the solutions to converge towards the nematic solution and not towards the trivial isotropic solution at high η or some other local minima of the Helmholtz free energy.

Eq. (3.21) at high η has at least two solutions. The first is related to the isotropic phase and the other one is related to the nematic phase. We should use a proper weight for the initial configuration to force the equations to converge to the nematic solution. It seems that this equation may have other solutions which are local minima of the Helmholtz free energy.

Since we are limited in the number of chains that can be used, we have tried different methods to improve sampling in our chain generation. Some special techniques for this purpose will be discussed later in this chapter.

Since we used many random variables in this program, we had to be careful about the kind of random number generator which we employed. We used different random generators at first and then we selected the best one for our work. We used Ran2, the random generator from Numerical Recipes in $c++$ [34], which is one of the most well known random number generators.

4.2 $S_2 - \eta$ Graphs

4.2.1 Least Accurate Results

According to Sections 2.1.2 and 1.2.2, the main parameter for observing the phase transition in a liquid crystal from the isotropic to the nematic phase is the value of the order parameter S_2 in the system. When S_2 drops to nearly zero while η is decreasing, it signals the phase transition point from nematic to isotropic. The main goal in this part is to find a smooth and continuous graph similar to the results of Jaffer et al. [10]. As it can be seen in Figure 4.1, the graph for 500 chains is not smooth enough, but one can nearly find the phase transition point as a jump in the graph near $\eta = 0.45$.

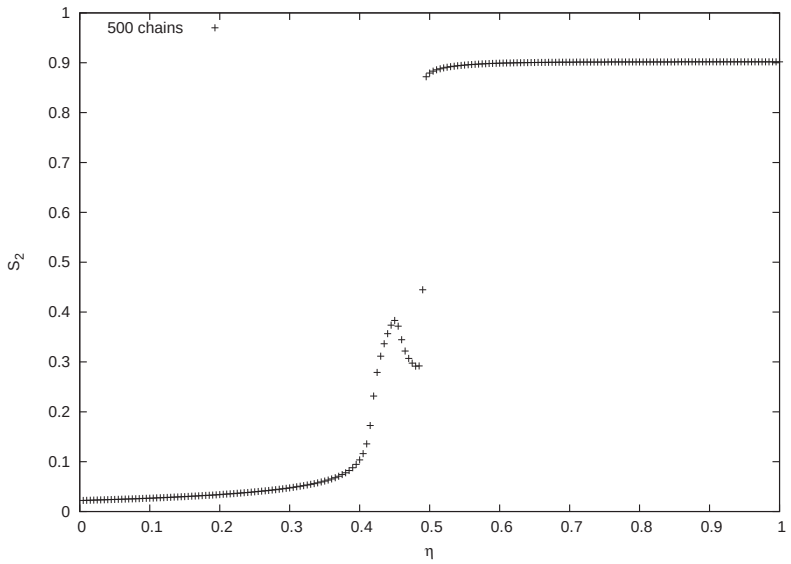

Figure 4.1: $S_2 - \eta$ graph for 500 chains. The graph is not sufficiently smooth and continuous.

To force the system to converge to the nematic solution, different initial weights should be given to different chain configurations depending on $\cos\theta$, where θ is the angle between the end-to-end vector of a molecule and the z direction. For the results

of Figure 4.1, the following initial weight has been used:

$$if(0 \leq \cos^2\theta_i \leq 0.2) \rightarrow (f_0[\vec{\omega}_i] = \frac{1}{fS}) \text{ and } if(0.2 < \cos^2\theta_i \leq 0.7) \rightarrow (f_0[\vec{\omega}_i] = \frac{5}{fS}) \text{ and}$$

$$if(0.7 < \cos^2\theta_i \leq 0.9) \rightarrow (f_0[\vec{\omega}_i] = \frac{20}{fS}) \text{ and } if(0.9 < \cos^2\theta_i) \rightarrow (f_0[\vec{\omega}_i] = \frac{120}{fS}) \tag{4.2}$$

The number fS is a normalization constant chosen so that $\sum_{i=1}^{N} f_0[\vec{\omega}_i] = 1$, where $f_0[\vec{\omega}_i]$ is the initial weight of the chain configuration i, Eqs. (3.15), (3.16), which normally is $1/N$ for all the chains in our Monte Carlo generation method, and θ_i is the angle between the end-to-end vector and the z direction. Choosing the initial probability density $f_0[\vec{\omega}_i]$ as in Eq. (4.2) can be interpreted as choosing an initial value of $I(\vec{\omega}_i)$ different from that in Eq. (3.24). It is possible to give equal weight at first to different configurations but typically giving different initial weights to different configurations can be helpful in obtaining proper results.

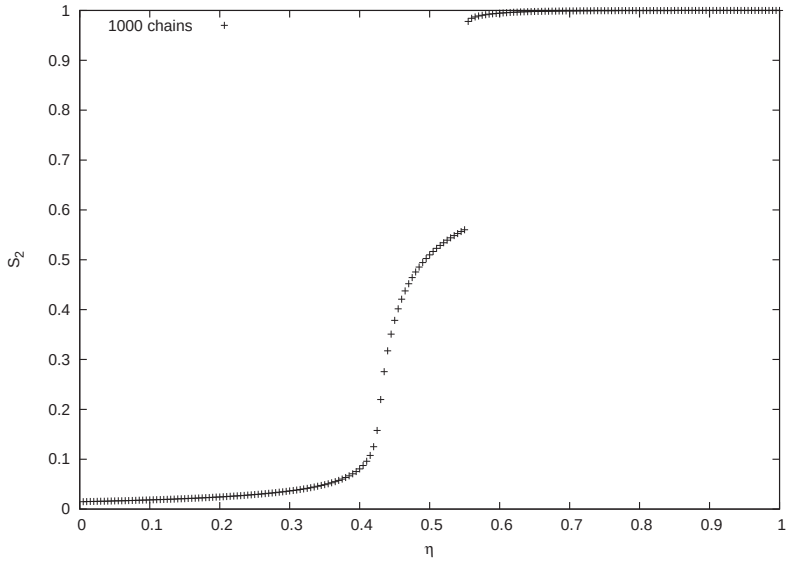

Figure 4.2: $S_2 - \eta$ graph for 1000 chains. The graph is smoother than for 500 chains, but it is still not smooth enough, especially due to the jump in S_2 between two non-zero values for $\eta \approx 0.55$.

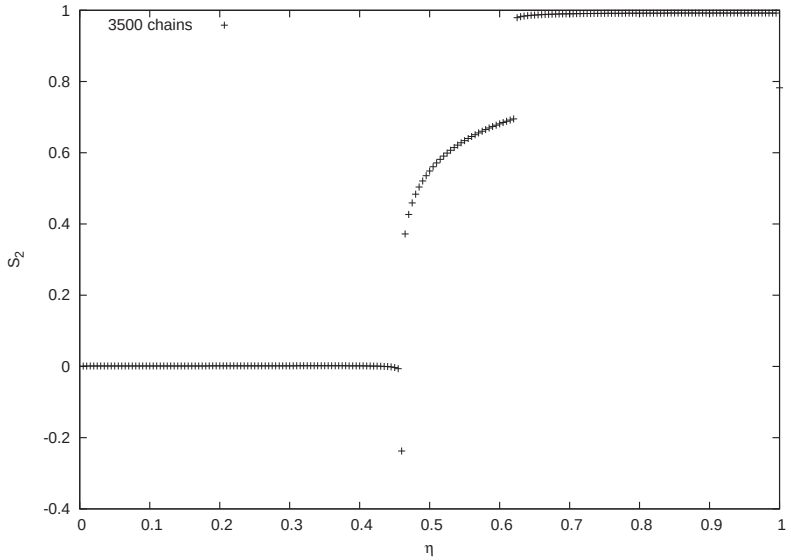

Figure 4.3: $S_2 - \eta$ graph for 3500 chains; the special initial weight described in Section 4.2.1.1 is used for this calculation.

The graph shown in Figure 4.2 is for 1000 chains. This graph was obtained from different initial weights (similar to Eq. (4.2)) for different configurations, and since it involves more chains it looks smoother. However, as in Figure 4.1, the phase transition point indicated by the initial rise in S_2 occurs for $\eta \approx 0.40$, which is inaccurate in comparison with Jaffer et al. [10]. This is because the number of chains was not sufficiently high.

The next graph is for 3500 chains, shown in Figure 4.3. As one can see, by increasing the number of chains, the graph becomes much smoother and the phase transition occurs near the expected point [10], which is near $\eta = 0.49$ for this system. Beside the jump in S_2 for the phase transition between zero and non-zero values, Figures 4.1, 4.2, 4.3 show discontinuities in S_2 between two non-zero values. These discontinuities are not seen in later graphs, and just one jump indicating the phase transition point can be seen in those graphs.

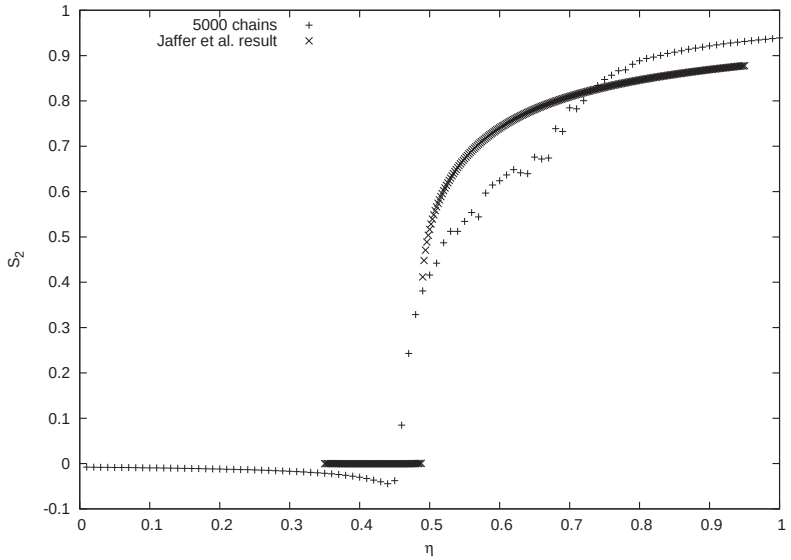

Figure 4.4: $S_2 - \eta$ graph for 5000 chains (+); the other smooth graph (x) represents the expected result from Jaffer et al. [10].

4.2.1.1 Special Initial Weight

For Figure 4.3 and almost all the following graphs, a special initial weight has been used [6]

$$f_0[\vec{\omega}_i] = \frac{\alpha cosh(\alpha|cos(\theta_i)|)}{C(4\pi sinh(\alpha))} \tag{4.3}$$

$$\alpha = \frac{\pi}{4}\left(\rho D((N_c - 1) + D)^2\right)^2,$$

The number C is a normalization constant chosen so that $\sum_{i=1}^{N} f_0[\vec{\omega}_i] = 1$, where $f_0[\vec{\omega}_i]$ is the initial weight of the chain configuration i, Eqs. (3.15), (3.16). This initial weight has a tendency to give larger probability to the chains aligned nearly along the z direction. By using this initial configuration the result converges better to the nematic solution. Choosing the initial probability density $f_0[\vec{\omega}_i]$ can be interpreted as choosing an initial value of $I(\vec{\omega}_i)$.

In Figure 4.4 one can see the result for 5000 chains. While the graph is not sufficiently smooth, the phase transition is near the expected one [10]. As can be seen

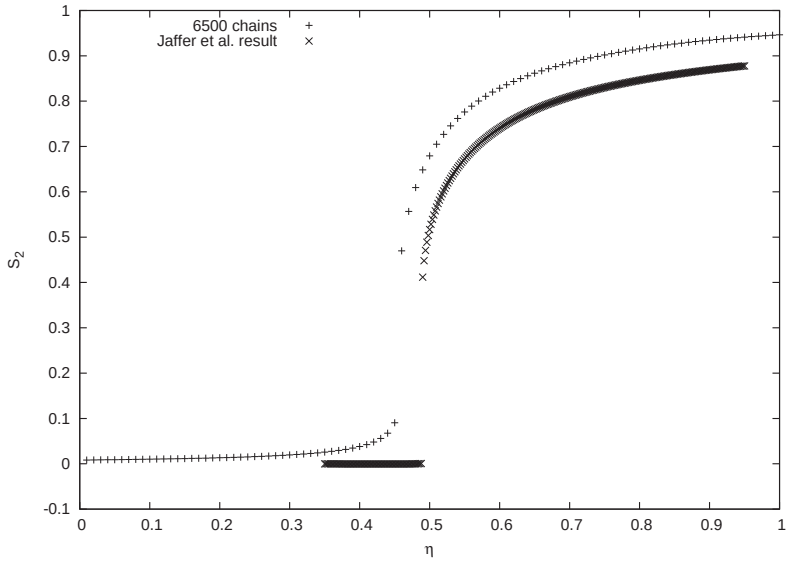

Figure 4.5: $S_2 - \eta$ graph for 6500 chains (+); the other smooth graph (x) represents the expected result from Jaffer et al. [10].

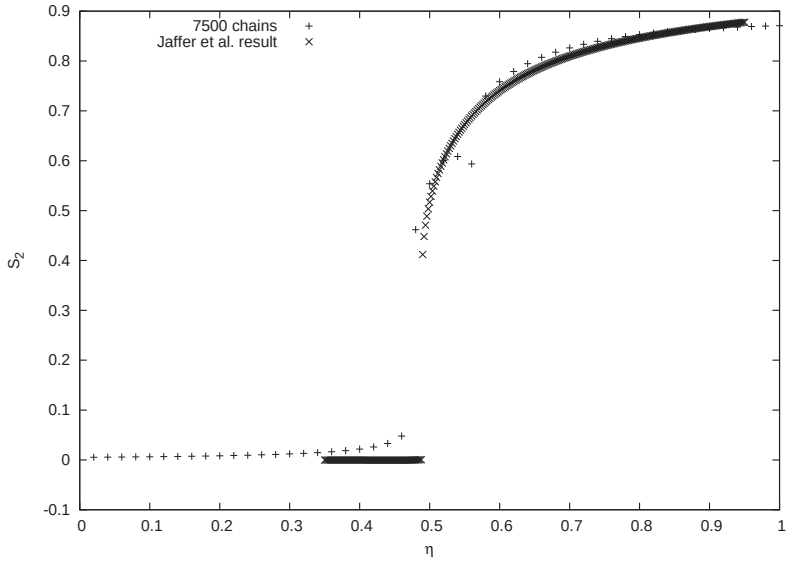

Figure 4.6: $S_2 - \eta$ graph for 7000 chains (+); the other smooth graph (x) represents the expected result from Jaffer et al. [10].

in Figures 4.5 and 4.6, similar results were not obtained for nearly the same number of chains (6500 and 7000 chains) because many parameters in the program are random and if the program is run again with a slight change in the number of chains or using a different seed value, one may not get the exactly the same result. This problem is reduced by increasing the number of chains, but it does not completely vanish in the range of chain numbers which we are working with.

4.2.2 Accurate Results

After increasing the number of chains to 10000 or more, the results became more trustworthy. As can be seen in Figure 4.7, the graph is nearly the same as that of Jaffer et al. [10] near the phase transition point.

The next graphs are for 11000 and 12500 chains (Figures 4.8, 4.9). These are among the best results which we obtained by using the iteration method. For calculations with these numbers of chains, we used some of the best computers available for more than a week. For saving the excluded volume of 12500 chain configurations, we need nearly one gigabyte of computer memory. This is because we need to fill in half of the places of the two dimensional matrix (12500$\times$ 12500) with double precision variables, where each double precision variable needs 8 bytes of memory, hence requiring

$$\frac{12500 \times 12500}{2} \times 8 \text{ Bytes } = 625 \ \times 10^6 \text{ Bytes.} \tag{4.4}$$

While we used double precision variables for saving the excluded volumes, it is possible to use floating point variables and use just half the amount of the mentioned memory. This is possible because the excluded volume between chains is calculated with the Monte Carlo computational method, which is an approximate method whose precision depends on the number of used "Barrett" points. The number of "Barrett" points

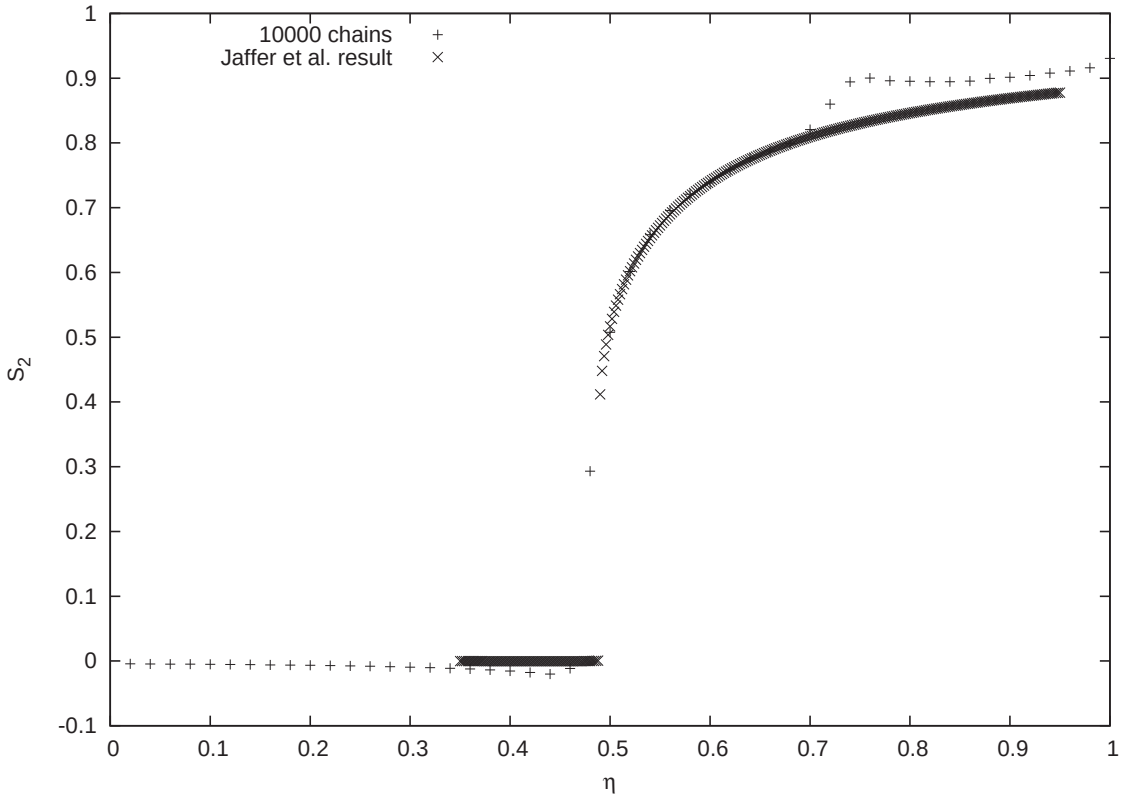

Figure 4.7: $S_2 - \eta$ graph for 10000 chains (+); the other smooth graph (x) represents the expected result from Jaffer et al. [10].

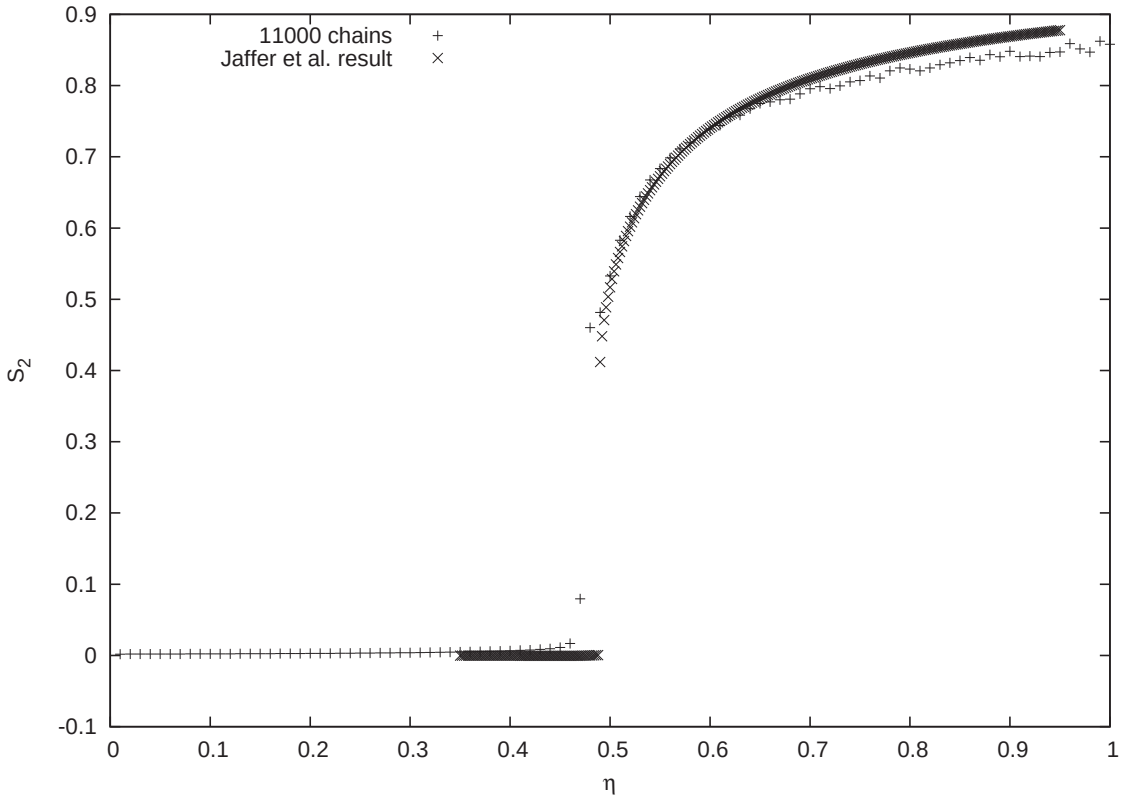

Figure 4.8: $S_2 - \eta$ graph for 11000 chains (+); the other smooth graph (x) represents the expected result from Jaffer et al. [10].

for all of our results is 5, which is a small number. The results in Figures 4.8 and 4.9 also employed the histogram technique described in the next Section 4.3.1.

Figure 4.10 is the graph for 14000 chains, which is the largest number of chains that we used. For this result we used a similar technique to the histogram technique (Section 4.3.1). While we expect to obtain similar results to Jaffer et al. [10], it should be mentioned that their work is "approximate", and therefore we cannot be sure if the small differences between our results and those of Jaffer et al. are due to approximations or numerical effects.

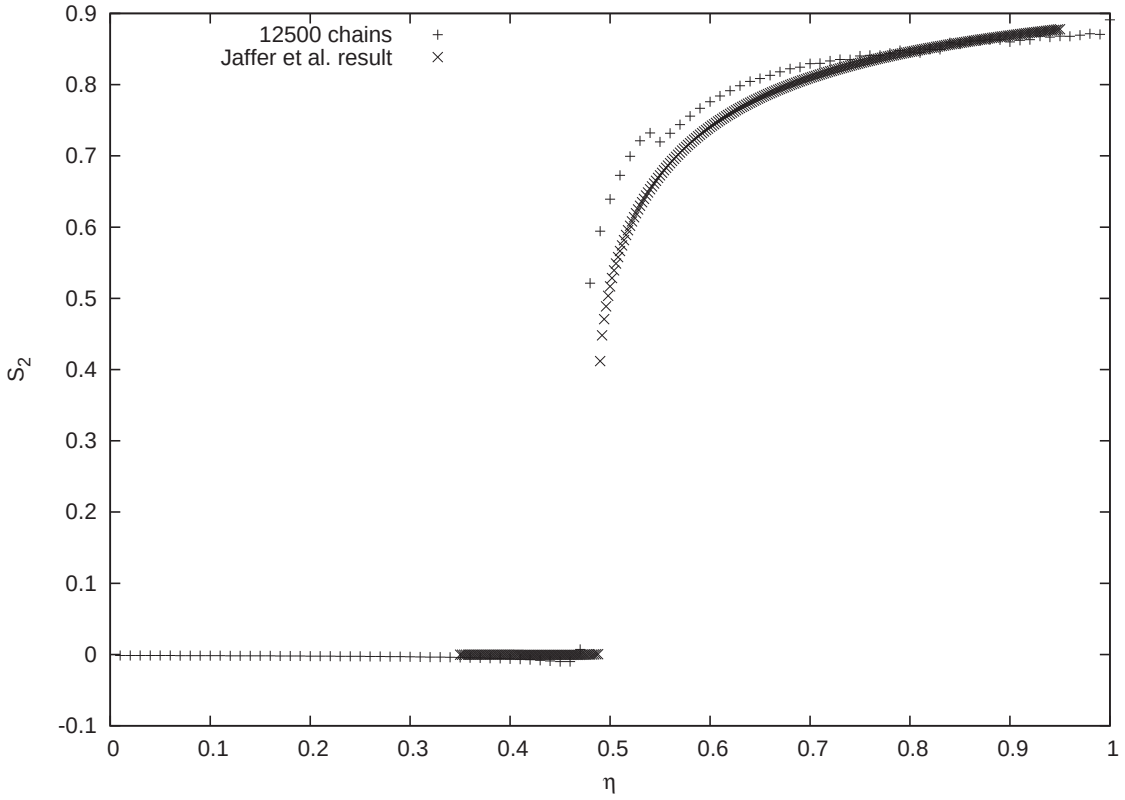

Figure 4.9: $S_2 - \eta$ graph for 12500 chains (+); the other smooth graph (x) represents the expected result from Jaffer et al. [10].

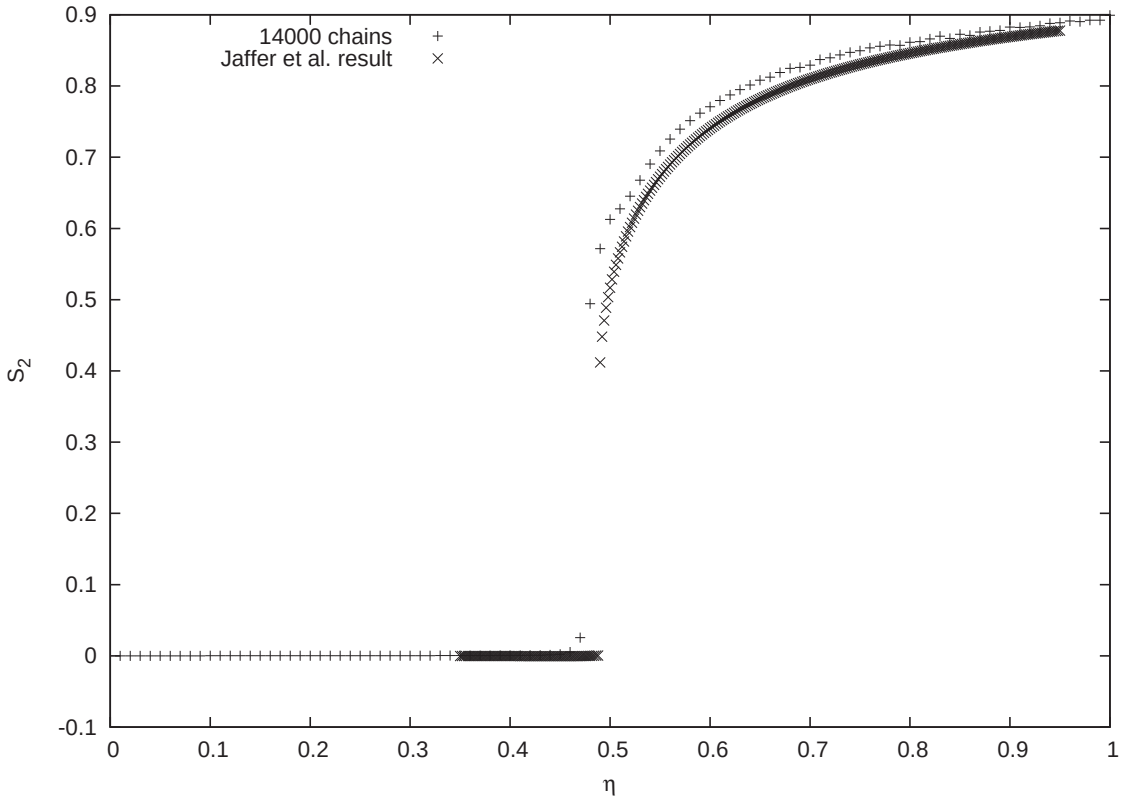

Figure 4.10: $S_2 - \eta$ graph for 14000 chains (+), the other smooth graph (x) represents the expected result from Jaffer et al. work

4.3 Special Techniques

4.3.1 Histogram Technique

As mentioned in Section 4.1.2 we used special techniques to obtain a better sample of chains which has smaller fluctuations in the number of chains in each interval of $\cos\theta$. The main technique used for this purpose is the histogram technique.

In the histogram technique, the best set of chains is selected among all sets of generated chains. This means that instead of making one set of chains, M chain sets are generated and after calculating the histograms of $\cos\theta$ for all the chains in each set (i.e., finding the concentration of chains in each $\cos\theta$ interval), the set of chains with the least variant histogram is selected. Here θ represents the angle between the end-to-end vector and the z axis and $M = 400$ in our work. It should be mentioned that generating chains is a fast computational process, therefore generating 400 sets of chains is not a time consuming process. To calculate the histogram of $\cos\theta$ for each set of chains, the range between -1 and 1 is divided into N_θ intervals. If those intervals have a width of Δ, $N_\theta \times \Delta$ should be 2. In our work N_θ is equal to 200.

In this procedure, we select the set of chains that has most nearly the same number of chains in each interval of $\cos\theta$. Each interval holds the number of chains whose values of $\cos\theta$ is in that range. It is clear that when the chains are generated completely randomly, their histogram should have a similar number of chains in each interval. For N chains, we expect fluctuations of order $\sqrt{N_\theta/N}$ in their histogram and we are trying to reduce these fluctuations.

To understand the above explanation, refer to Figures 4.11, 4.12 and 4.13. As can be seen in the graphs, by increasing the number of chains the points concentrate more in the area near 0.005 and they have nearly the same number of chains in each

interval. Since there are 200 intervals in each graph, the average ratio of the number of chains in each interval to the total number of chains (concentration) is $1/200 = 0.005$. The data is consistent with the fluctuation formula $0.005(1 \pm \sqrt{N_\theta/N})$.

In our work we produce two sets of chains at first separately and save the configuration of the better one in the RAM memory. Then in the $M-2$ other steps we produce one set of chains in each step and we compare that one with the saved one. The configuration of the better set of the chains (between the stored configuration and the newly generated configuration) is stored in the RAM memory. At the end, we have the best set of chains. To compare two sets of chains with each other, the variance of the number in each $\cos\theta$ intervals of each of them should be calculated. The variance for one set is calculated as follows:

$$\sigma^2 = \frac{\sum_{i=1}^{200}(x_i - \bar{x})^2}{199}, \tag{4.5}$$

where x_i represents the number of chains in interval i and $\bar{x}$ represents the average number of chains in each interval. The best set of chains has the least variance. For example, the results of Figures 4.8, 4.9 are obtained by using exactly the above technique.

As mentioned in connection with Figure 4.10 we used a similar technique to the histogram technique. This technique was suggested by Prof. B. G. Nickel and is based on modifying the histogram technique by artificially making the set of chains have a histogram variance of zero. It means that instead of finding the least variant set of chains between M different sets, we artificially make one set of chains have a histogram variance of zero. For this purpose, we fill each histogram interval with the same number of chains. For example, for 14000 chains, each interval should have 70 chains. To do this, as each chain is generated its $\cos\theta$ value is registered in the

histogram. When the number of chains in a given histogram interval reaches its prescribed value, any additional chains falling in that interval are rejected.

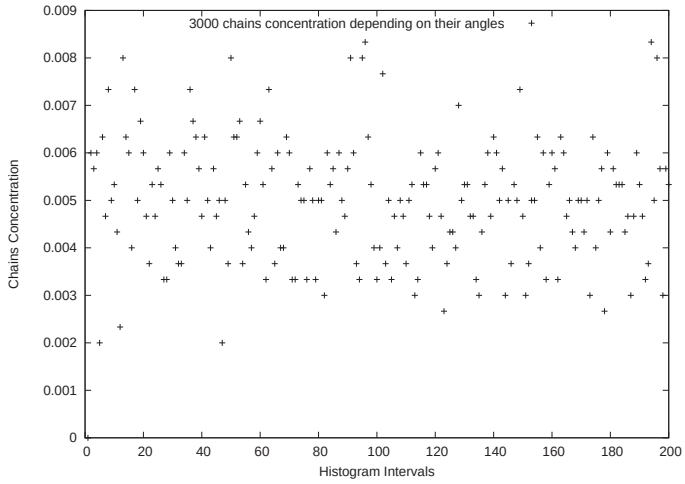

Figure 4.11: Histogram of $\cos\theta$ for 3000 chains

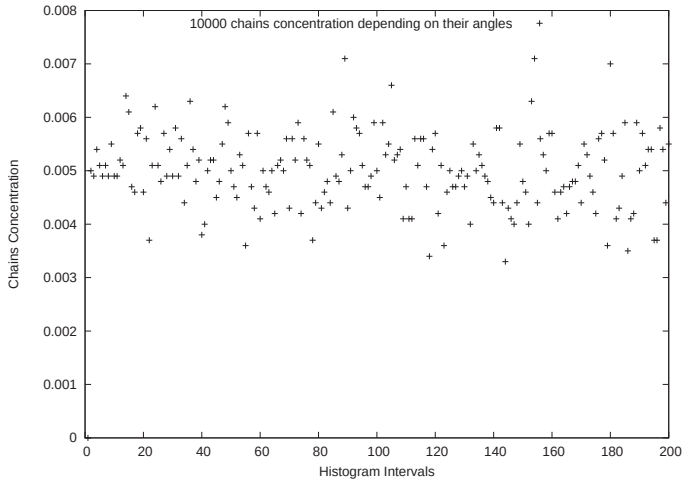

Figure 4.12: Histogram of $\cos\theta$ for 10000 chains

4.3.2 Mixing Method [35]

In all graphs of Section. 4.2, we used the exact value from the last iteration output as input for the next iteration. This means that $I_m(\vec{\omega})$ is the input for calculating

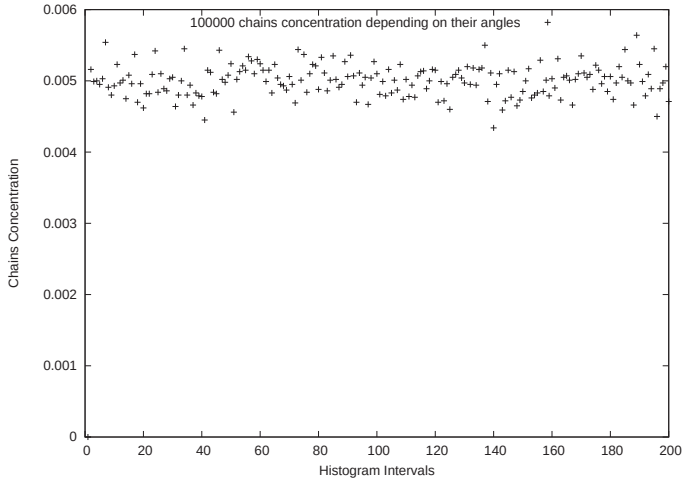

Figure 4.13: Histogram of $\cos\theta$ for 100000 chains

$I_{m+1}(\vec{\omega})$. But while we were working on the second part of this project, the nematic-smectic phase transition, we utilized the mixing method as a better technique for solving the self consistent equations.

In the mixing method, $I_m(\vec{\omega})$ is not used as the only input to the next iteration, but the mixture of previous iterations is used as an input to find $I_{m+1}(\vec{\omega})$. Mathematically, in the mixing method

$$I_{in}^{(n+1)} = \alpha\, I_{in}^{(n)} + (1-\alpha)\, I_{out}^{(n)}, \tag{4.6}$$

where $I_{in}^{(n)}$ is the "input" for the calculation of the n_{th} iteration and $I_{out}^{(n)}$ is the corresponding output. Then from the above equation we get

$$I_{in}^{(n+1)} - I_{in}^{(n)} = (\alpha-1)\, I_{in}^{(n)} + (1-\alpha)\, I_{out}^{(n)} = (1-\alpha)\,(I_{out}^{(n)} - I_{in}^{(n)}) \tag{4.7}$$

where $(1-\alpha)$ is a factor between zero and one. When $\alpha = 0$, the previous "unmixed" iteration method is recovered, while $\alpha = 1$ would result in no changes of $I(\vec{\omega})$ during iteration.

By choosing the proper α, the results of this technique can be made more accurate

than the previous results. For example, using $\alpha = 0.15$, we can reduce the number of chains to 6000 while still achieving better results. Typically, the ranges of all the

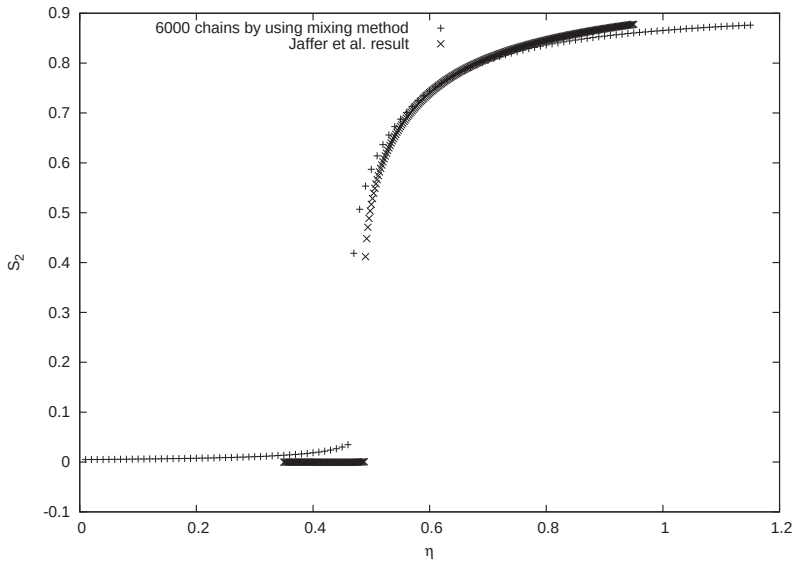

Figure 4.14: One of the best results obtained by using the mixing method for 6000 chains.

previous graphs were $\eta = 0.0 \ldots 1.0$, while in the next graph (Figure 4.14) the range is between 0 and 1.2. It should be mentioned again that any η larger than η_{max} (which is smaller than 1) does not have any physical meaning. However, it can be helpful to reach smectic or nematic phases in some cases such as in the next part of this project.

4.4 $P^* - \eta$ Graphs

This section is similar to Section 4.2 except for the fact that the graphs show reduced pressure P^* instead of S_2 as a function of η.

As can be seen in Figures 4.15, 4.16 and 4.17, by comparing these graphs with the expected ones [10], these graphs are typically smoother than the $S_2 - \eta$ graphs. The phase transition can be located between the local maximum (as a sharp feature) and local minimum (after the sharp feature) of the graphs. Actually in the area between

the local maximum and minimum, the system separates into two phases with different ratios of volumes. At a first order transition, the true location of the transition is where the pressure on the two branches is equal and satisfies equal values of the chemical potential μ. That is, we should find the values of η in the coexisting phases which satisfy the following equations:

$$P^*(\eta_{iso}) = P^*(\eta_{nem}) \text{ and } \mu(\eta_{iso}) = \mu(\eta_{nem}), \tag{4.8}$$

In principle, the chemical potential μ can be obtained by integrating the Gibbs-Duhem equation ($\rho = N/V$)

$$\frac{\partial \mu}{\partial \rho} = \frac{1}{\rho} \frac{\partial P}{\partial \rho}, \tag{4.9}$$

although this was not investigated in this work.

4.5 Variation of $\langle \vec{r}_e{}^2 \rangle$ and $\langle \vec{r}_g{}^2 \rangle$ with η

Figures 4.18 and 4.19 plot the mean-square end-to-end distance $\langle \vec{r_e}^{\,2} \rangle$ and mean square radius of gyration $\langle \vec{r_g}^{\,2} \rangle$ vs. η for a system of 8000 chains. The isotropic-nematic phase transition is clearly indicated by the break in the curves. In the isotropic phase these seems to be a extremely weak decrease in both $\langle \vec{r_e}^{\,2} \rangle$ and $\langle \vec{r_g}^{\,2} \rangle$ with increasing η. In the nematic phase, in contrast, $\langle \vec{r_e}^{\,2} \rangle$ and $\langle \vec{r_g}^{\,2} \rangle$ increase clearly with η, i.e., the chains become more extended when they are aligned. The value of $\langle \vec{r_e}^{\,2} \rangle$ is far from what was calculated for a system of "random-flight" chains in Section 2.1.1 and is close to the value for rigid chains. This is because in our case, $\kappa = 50$, which is near the completely rigid case. The value of $\langle \vec{r_e}^{\,2} \rangle$ for a system of

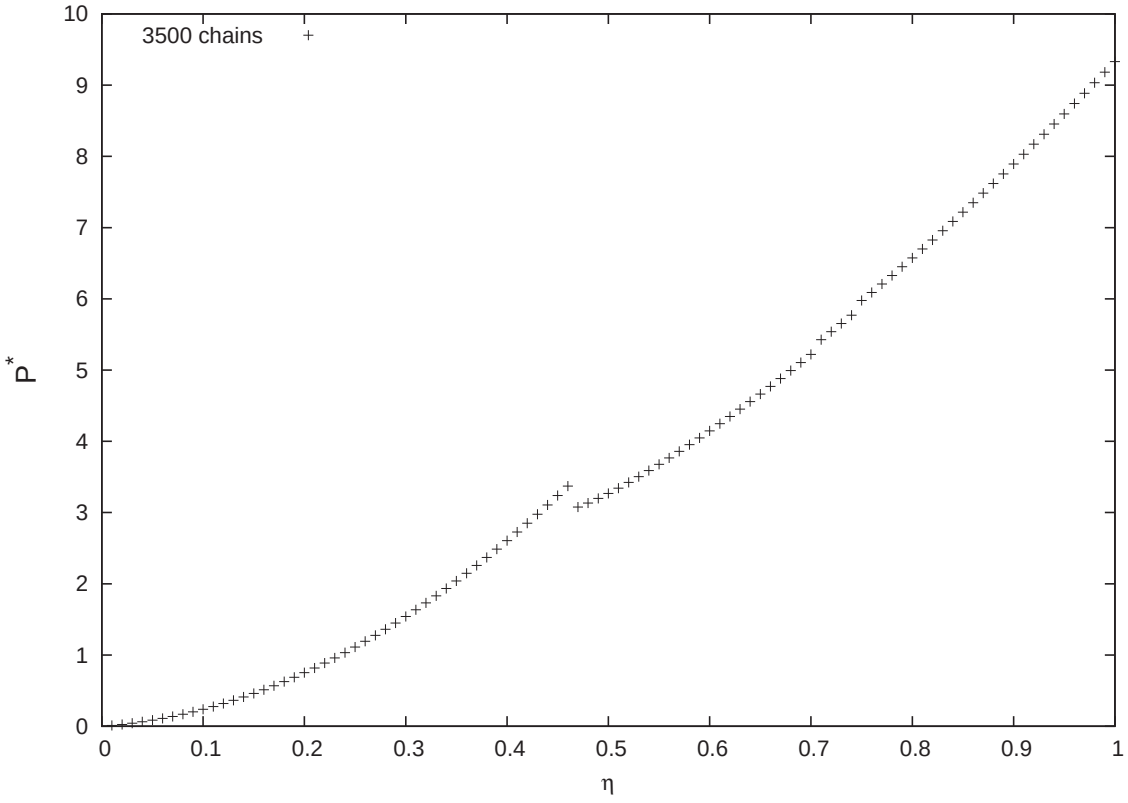

Figure 4.15: $P^* - \eta$ for 3500 chains

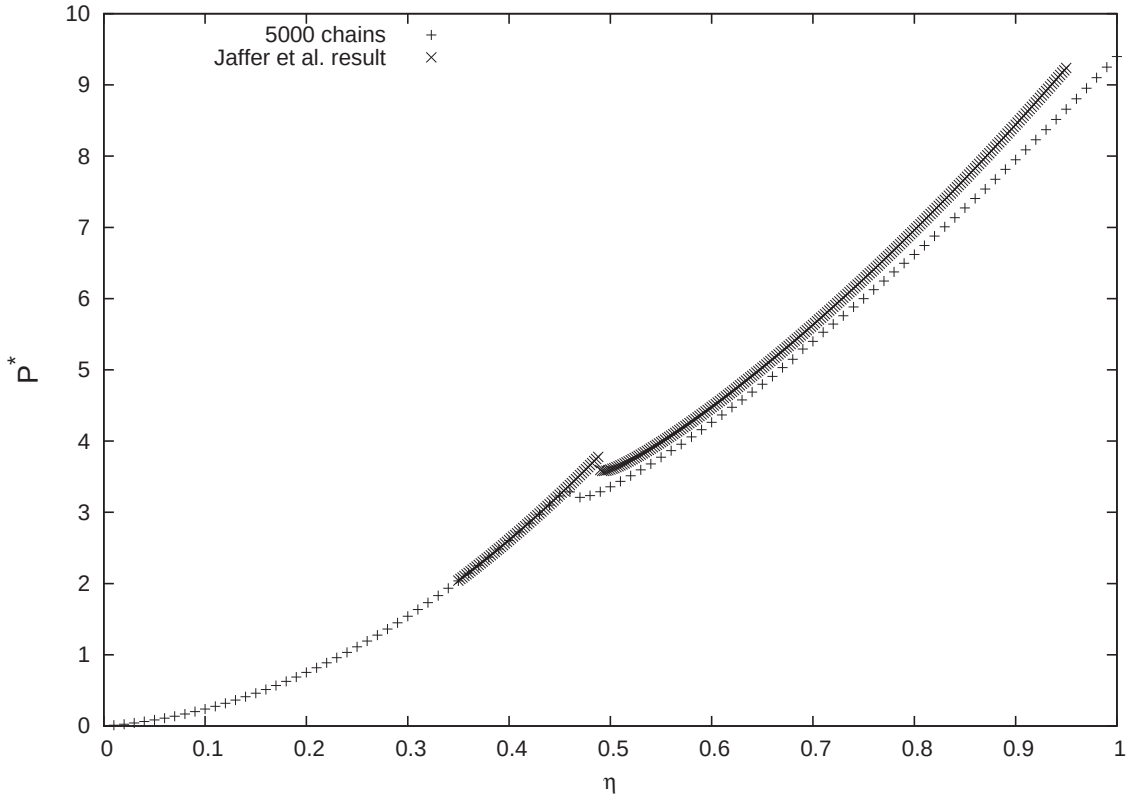

Figure 4.16: Comparison between $P^* - \eta$ graph (+) for 5000 chains and the expected (x) result [10].

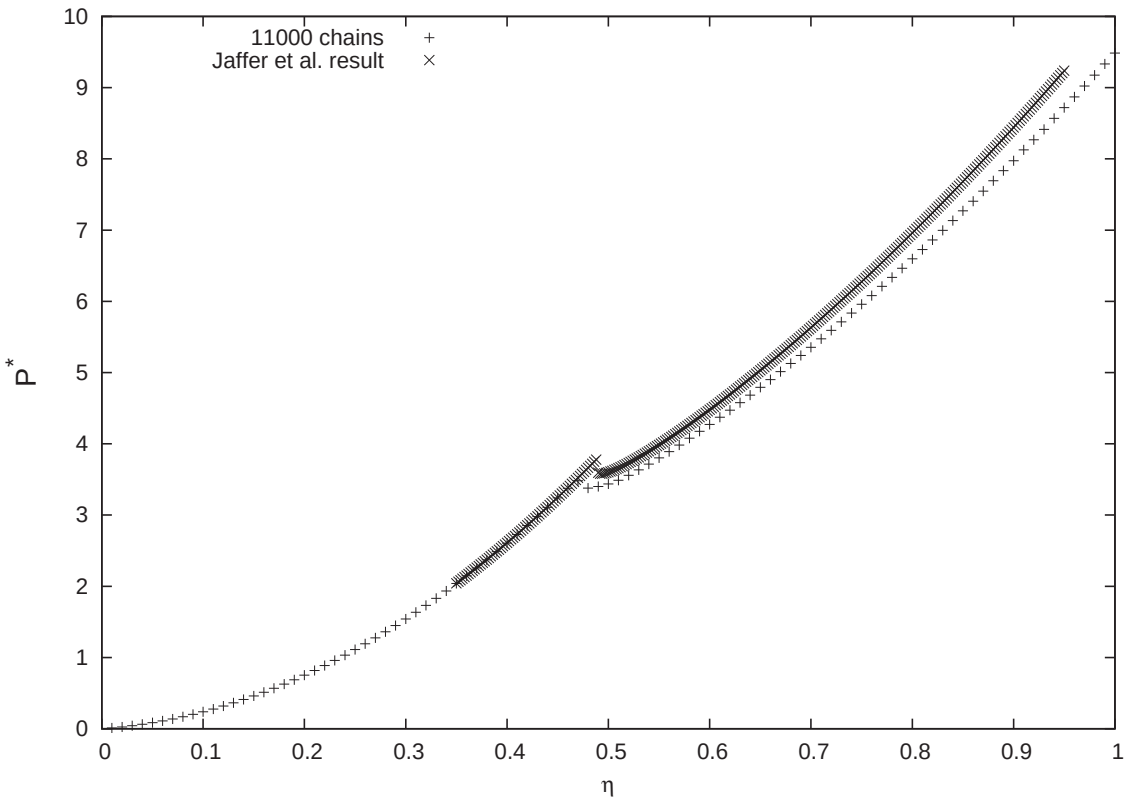

Figure 4.17: Comparison between $P^* - \eta$ graph (+) for 11000 chains and the expected (x) result [10].

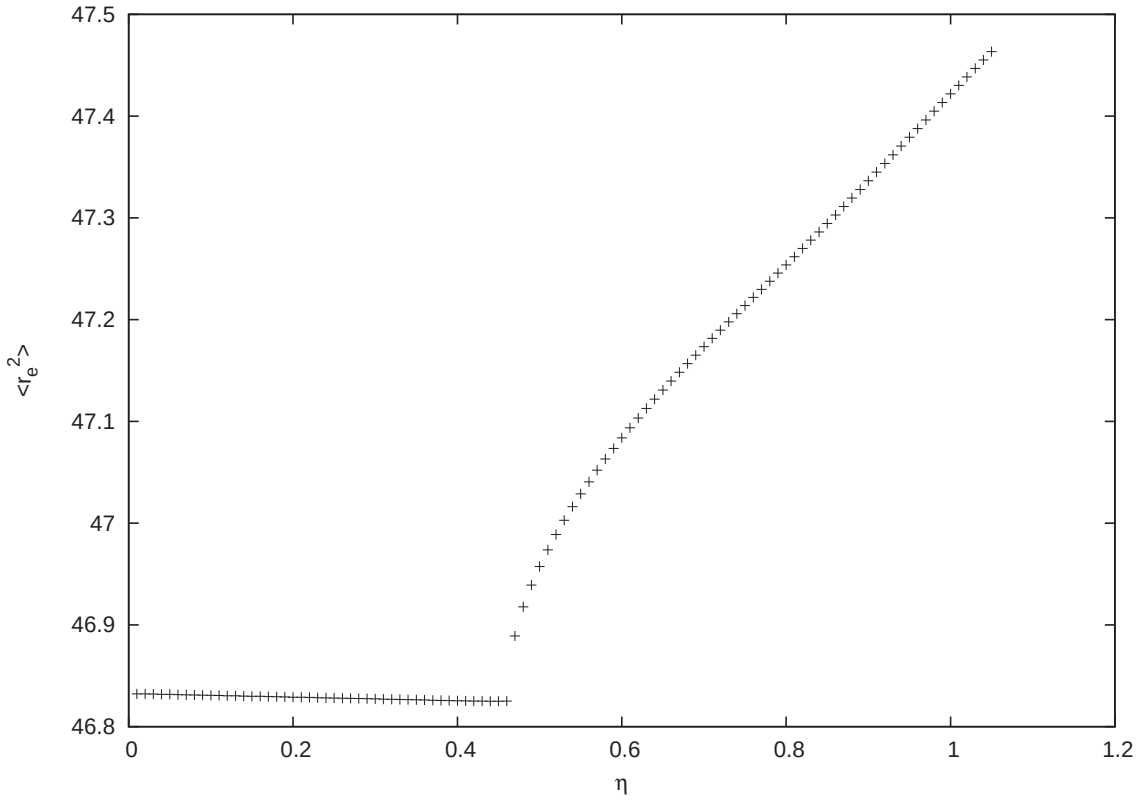

Figure 4.18: $\langle \vec{r_e}^{\,2} \rangle$ vs. η for 8000 chains

"random-flight" chains with no restriction on the angles is $N_c - 1 = 7$ and for the completely rigid case the value of $\langle \vec{r_e}^{\,2} \rangle$ is $(N_c - 1)^2 = 49$.

4.5.1 Analytical Calculation of $\vec{r_e}^{\,2}$

To calculate the expected value of $\vec{r_e}^{\,2}$ for the isotropic case where all the chains have nearly the same probability distribution value we should find the average value of $\cos\theta$.

By considering the Section 2.3.1, we can calculate the average of $\cos\theta$ as

$$\langle \cos\theta \rangle = \frac{\int_{-1+\frac{D^2}{2}}^{1} \exp(50cos\theta)\cos\theta \, d\cos\theta}{\int_{-1+\frac{D^2}{2}}^{1} \exp(50cos\theta) \, d\cos\theta}, \tag{4.10}$$

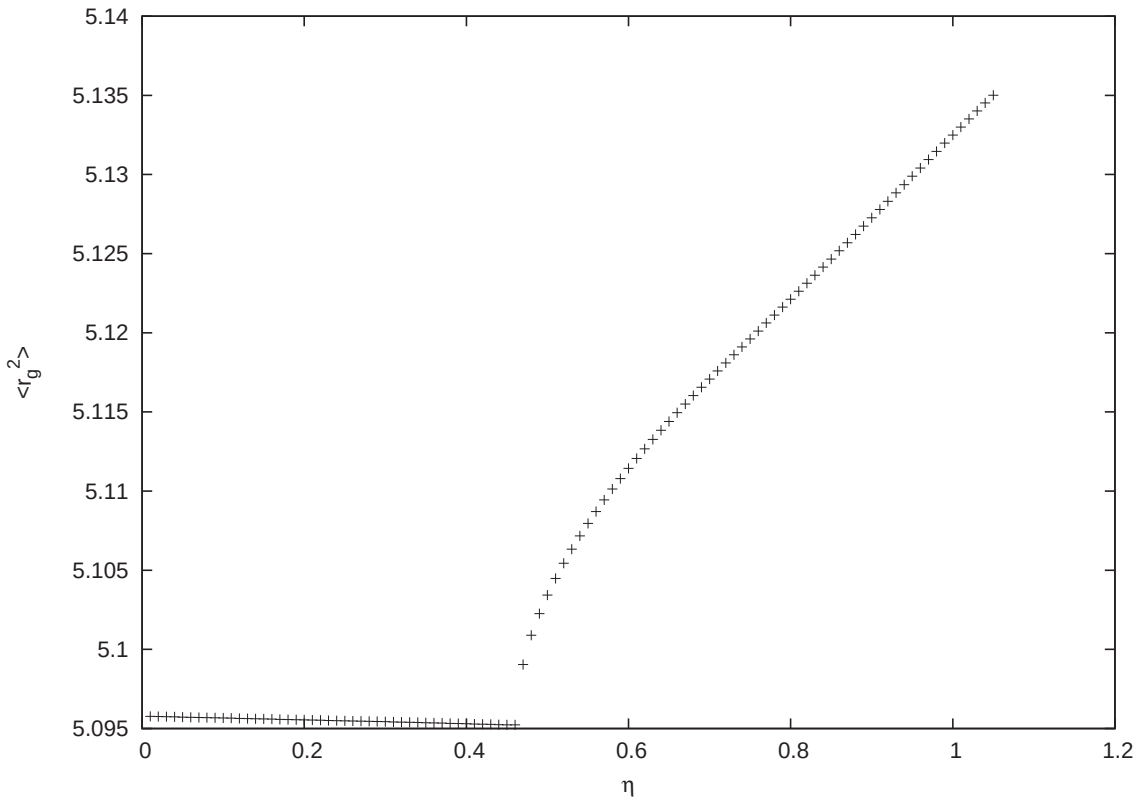

Figure 4.19: $\langle \vec{r_g}^{\,2} \rangle$ vs. η for 8000 chains

which neglects any effects of chain self-avoidance. The probability of finding $\cos\theta$ in the area lower than $-1 + D^2/2 = -1/2$ is much lower than finding the $\cos\theta$ around 1 :

$$\frac{P\big(\cos(-\frac{1}{2})\big)}{P\big(\cos(1)\big)} = \frac{\exp(50 \times \frac{-1}{2})}{\exp(50)} = \exp(-75) \approx 0,$$

therefore we can change the lower limit in the integral to $-\infty$. So Eq. (4.10) can be written as

$$\langle \cos\theta \rangle = \frac{\int_{-\infty}^{1} \exp\left(50 cos\theta\right) \cos\theta \; d\cos\theta}{\int_{-\infty}^{1} \exp\left(50 cos\theta\right) \; d\cos\theta} = 0.98. \tag{4.11}$$

Now we can write Eq. (2.5) as follows:

$$\langle \vec{r}_e{}^{\,2} \rangle = \sum_{i=1}^{N_c-1} \langle \vec{b}_i{}^{\,2} \rangle + 2 \sum_{i<j} \langle \vec{b}_i . \vec{b}_j \rangle = (N_c-1)b^2 + 2 \sum_{i<j} \langle \vec{b}_i . \vec{b}_j \rangle = (N_c-1) + 2 \sum_{i=1}^{N_c-2} (N_c-1-i)(x)^i \tag{4.12}$$

where x is the average of $\cos\theta$. After inserting $N_c = 8$ and $x = 0.98$, $\langle \vec{r}_e{}^{\,2} \rangle$ is found to be 46.8151, which is very close to the value of 46.82 which was mentioned in Section 4.1. As one can see in Figure 4.18, the $\langle \vec{r}_e{}^{\,2} \rangle$ for the isotropic phase is nearly the same as what was found above.

4.6 Distribution of the Probability Distribution Function

To supplement these calculations with some diagnostics, we tried to understand the distribution of the probability density of the chains in the nematic and isotropic phases. The goal is to find how many of the chains have a major effect in generating these phases. For example, we want to investigate how many of the chains contribute to half of the total probability density distribution in the nematic phase. It is clear

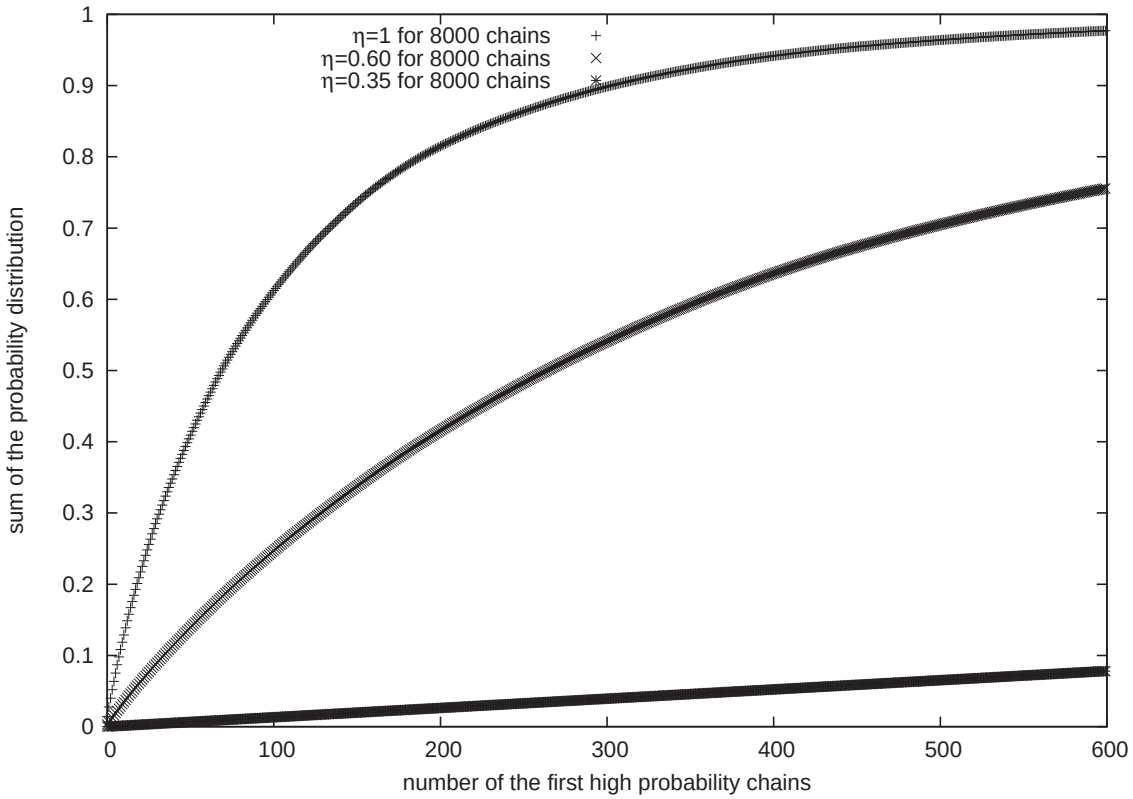

Figure 4.20: The probability distribution for 600 high probability distribution chains of the 8000 chain system at different η.

that some chains with special values of θ have a main role in generating the nematic phase while in the isotropic phase it can be guessed that almost all the chains play nearly an equal role.

For this purpose, first the probability distributions of the chains are sorted from maximum to minimum values. Therefore, define $y(1) = f(\vec{\omega}'_1)$, where ω'_1 is the chain with the largest probability distribution (Eq. (3.17)). Then define $y(i) = \sum_{j=1}^{i} f(\vec{\omega}'_j)$. This means that if $y(i) = 0.5$, just the i chains give half of the total probability distribution.

For example, in Figure 4.20, one can see the graph for just 600 chains of 8000 chains at different η. One can see that by decreasing η, the graph is shifted to the

right and a larger number of chains are involved in the nematic phase. By looking precisely at Figure 4.20, you can see that almost all of the chains are involved in the isotropic phase ($\eta = 0.35$) and the probability density is shared almost equally between them.

4.7 Discussion About Obtaining Different Results for Specific Number of Chains

In Figure 4.21, we compare different results for 8000 chains with different seeds and nearly the same sampling techniques. The difference between the results can be interpreted as randomness effects (since there are not enough chains) or possibly different solutions of Eq. (3.23). Different solutions may represent different minima of the Helmholtz free energy or different directions of system in the nematic phase. However, all solutions are consistent in predicting nearly the same onset density of the nematic phase (near $\eta = 0.49$).

To investigate more about these different results we plotted the Helmholtz free energy F vs. η for some different solutions of 8000 chains to check which one has the lowest free energy. We want to find the result which represents the actual minimum of the Helmholtz free energy.

Figure 4.22 shows several graphs of S_2 vs. η which are different from the graphs of Figure 4.21 and have very different features from each other. Figure 4.23 shows the free energy per molecule graphs of these results which is nearly the same for all of them and just one of them has a little higher free energy. We were looking for the minimum free energy among all these graphs, while we found that all of the graphs have nearly the same value of the Helmholtz free energy for each value of η. The

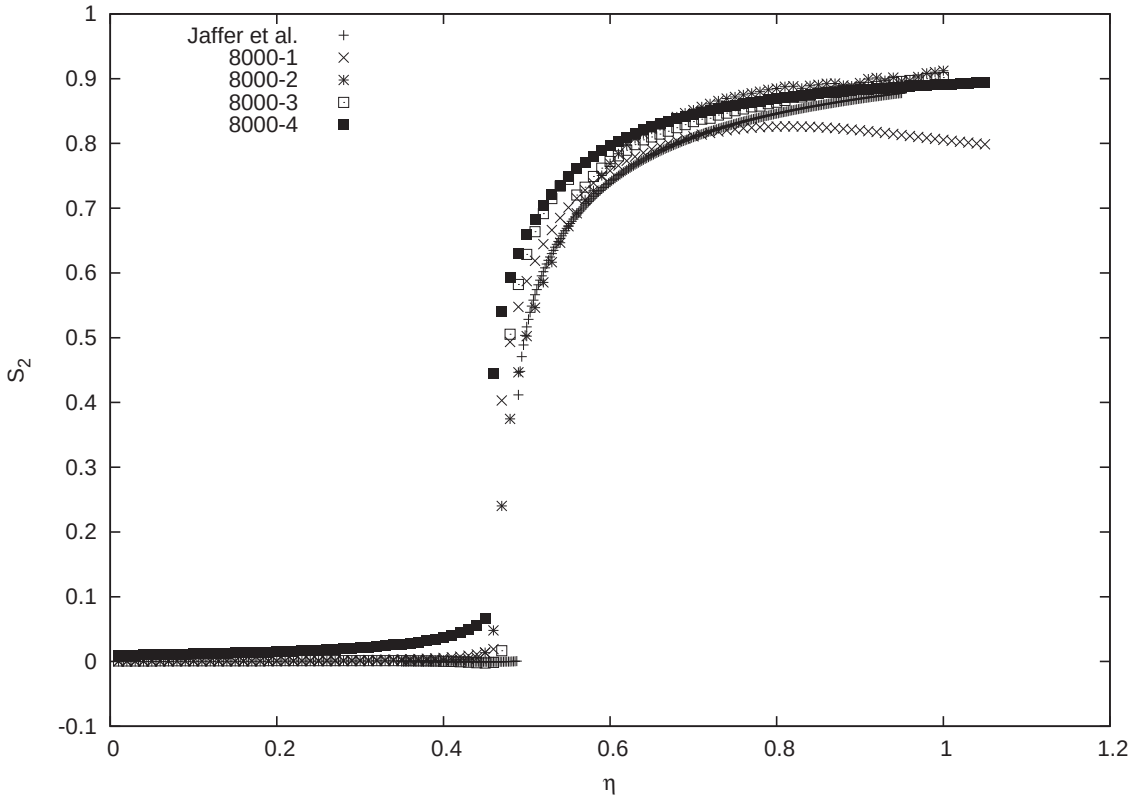

Figure 4.21: Different $S_2 - \eta$ graphs for 8000 chains are compared with Jaffer et al.

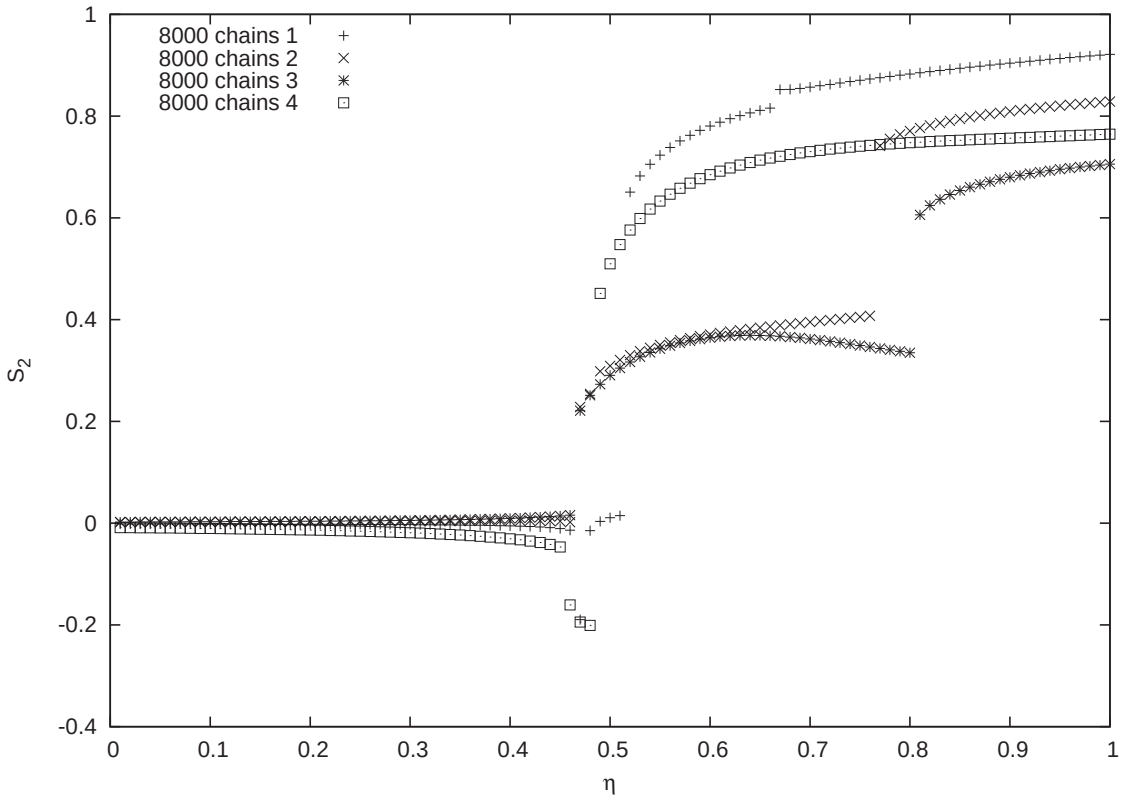

Figure 4.22: Different $S_2 - \eta$ graphs for 8000 chains

free energy for Figure 4.23 is calculated according to Eq. (2.39) after reducing the constant parts as

$$\frac{\beta F}{N} = \sum_{i=1}^{N} f(\vec{\omega}_i)\Big[\ln\big(\rho f(\vec{\omega}_i)\big)\Big] + \frac{1}{2}\sum_{i=1}^{N}\sum_{j=1}^{N}\rho f(\vec{\omega}_i) f(\vec{\omega}_j) V_{ex}(\vec{\omega}_i, \vec{\omega}_j). \tag{4.13}$$

Since the chains were generated using the Monte Carlo method by a probability proportional to their bond bending energy, the bond bending energy does not appear itself in the above equation.

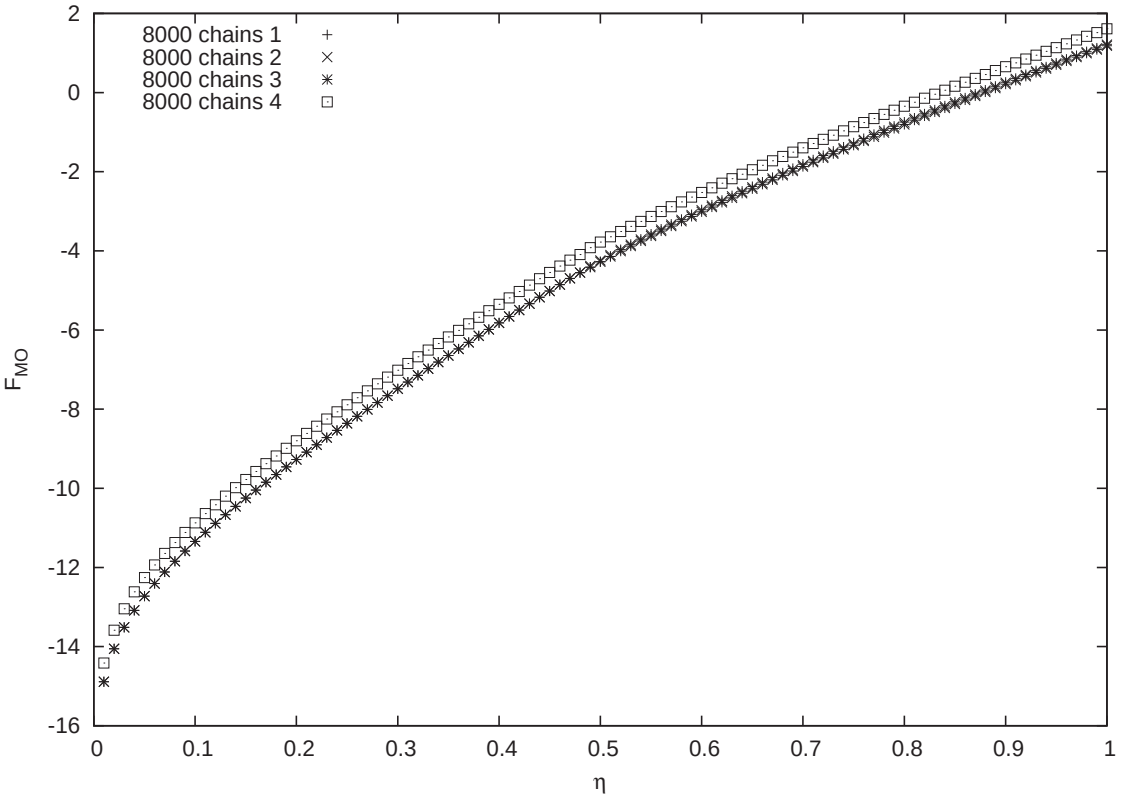

Figure 4.23: $F_{MO} - \eta$ graphs for 8000 chains corresponding to the results in Figure 4.22, where $F_{MO} = \beta F/N$

4.7.1 Matrix Definition of S_2

Since we guessed that the main reason in having different graphs of $S_2 - \eta$ is due to changing the direction of the director, we tried the matrix approach [20] to find the S_2 value by using the largest eigenvalue of the ordering matrix or using the twice the negative of second largest eigenvalue. In this way, if the director of the system of chains is modefied, the S_2 is calculated along that direction and not the original z direction. By using this method, if the system chooses another direction instead of the initial z direction, the $S2 - \eta$ graph will be continuous and will have a consistent value for each η. However small fluctuations in the phase transition area always occur.

The ordering matrix for finding S_2 is as follows:

$$\begin{pmatrix} \langle \frac{1}{2}(3\sin^2\theta\cos^2\phi - 1)\rangle & \langle \frac{3}{2}\sin^2\theta\cos\phi\sin\phi\rangle & \langle \frac{3}{2}\sin\theta\cos\theta\cos\phi\rangle \\ \langle \frac{3}{2}\sin^2\theta\cos\phi\sin\phi\rangle & \langle \frac{1}{2}(3\sin^2\theta\sin^2\phi - 1)\rangle & \langle \frac{3}{2}\sin\theta\cos\theta\sin\phi\rangle \\ \langle \frac{3}{2}\sin\theta\cos\theta\cos\phi\rangle & \langle \frac{3}{2}\sin\theta\cos\theta\sin\phi\rangle & \langle \frac{1}{2}(3\cos^2\theta - 1)\rangle \end{pmatrix}$$

the largest eigenvalue (λ_1 or I_1) of this matrix represents S_2. The eigenvector of the largest eigenvalue represents the orientation of the director in the chain set.

By looking at Figures 4.24 and 4.25, one can find that the two graphs which represent the $S_2 = \lambda_1 = I_1$ and $S_2 = -2\lambda_2 = -2I_2$ have nearly the same values of S_2 for each η and they are continuous. By looking at Figure 4.26, one sees the graphs of $S_2 = \lambda_1$ for three different sets of chains. The results are very close to each other in the nematic phase and the variance between the results is very small.

After calculating the matrix definition of S_2 for different sets of chains and obtaining continuous and consistent graphs, we tried to generate one set of chain but using different initial weights to orientate this set in different orientations to check whether the results are the same for different orientations or not. We used Eq. (4.3)

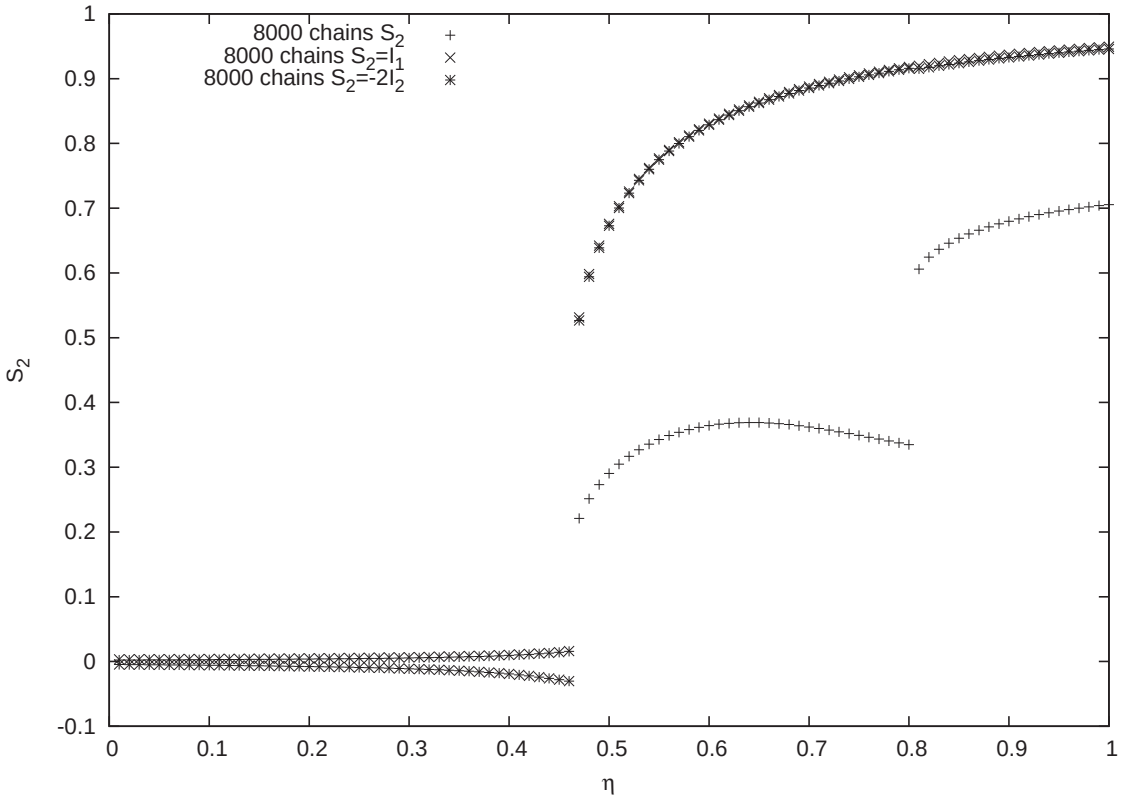

Figure 4.24: $S_2 - \eta$ graphs for different definitions of S_2 for one set of chains

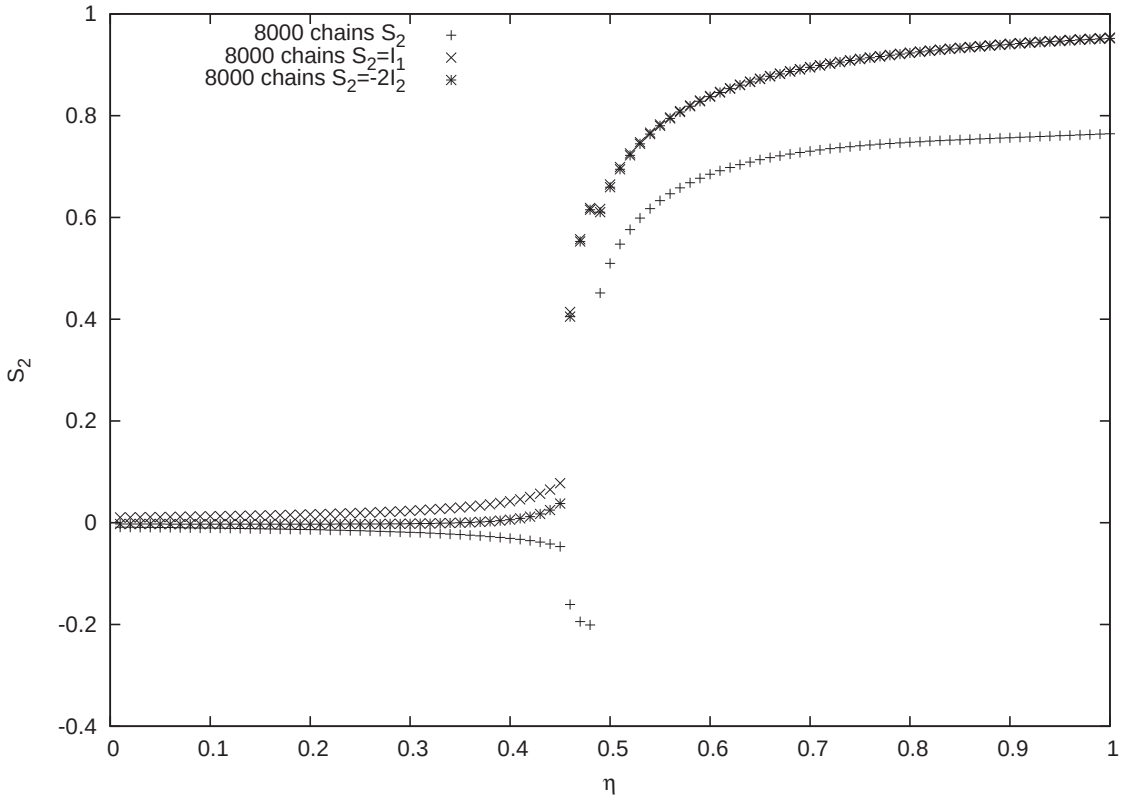

Figure 4.25: $S_2 - \eta$ graphs for different definitions of S_2 for another set of chains

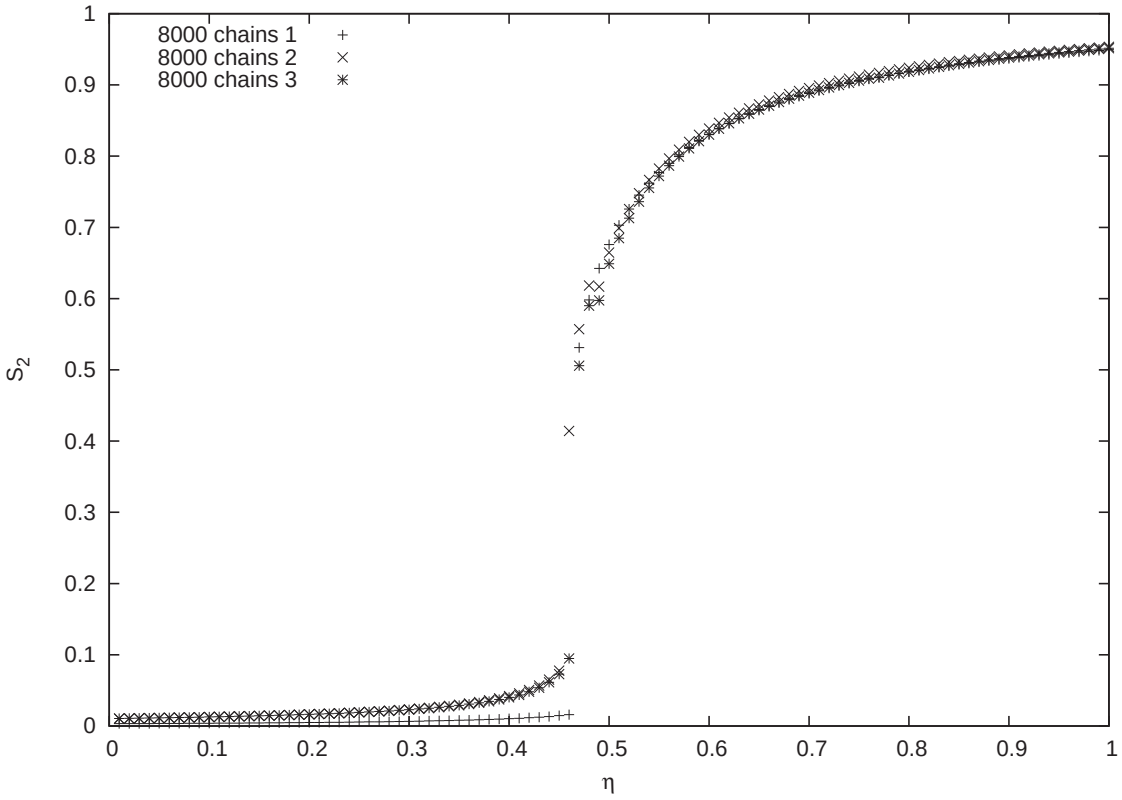

Figure 4.26: $S_2 - \eta$ graphs for different sets of chains (different seeds) using the matrix definition

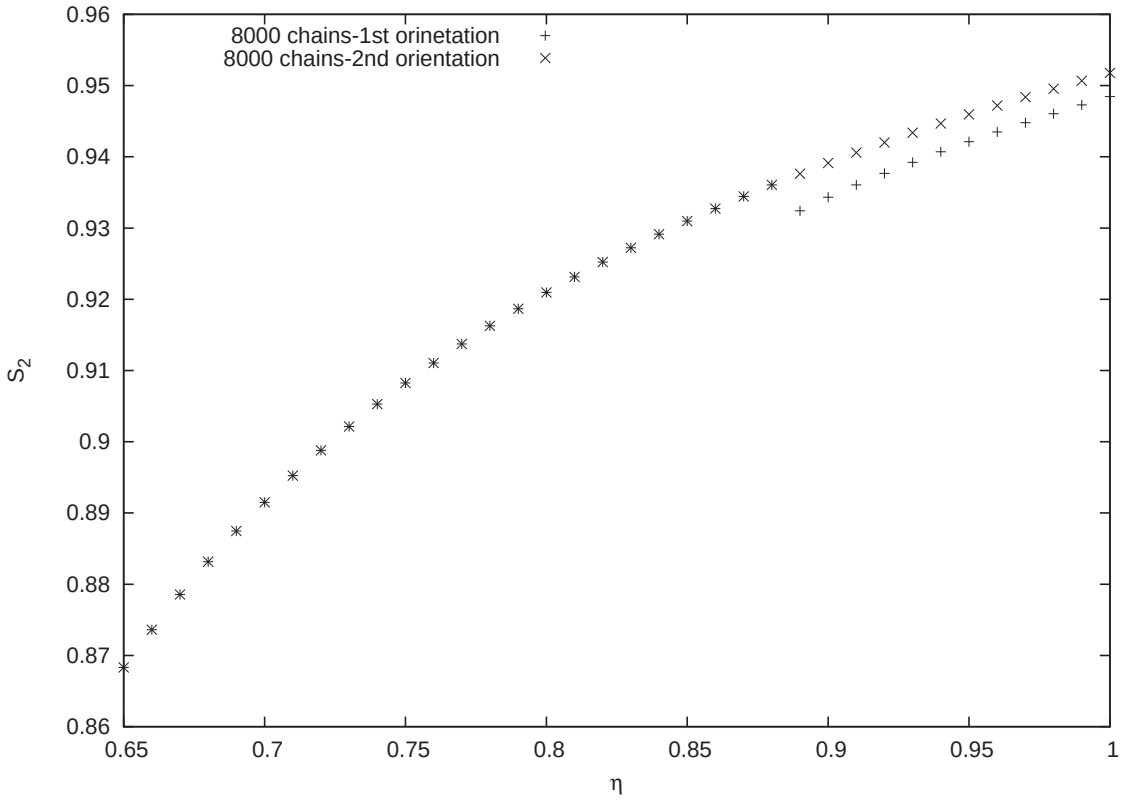

Figure 4.27: $S_2 - \eta$ graph for one one set of 8000 chains initialized in different orientations

for initialization of the weights but we calculated the $\cos\theta$ in relative to other directions and not the initial z direction. As we found in the previous graphs, the variance of results for different sets of chains (different seeds) is very small. By looking at Figure 4.27 one can see that the variation is very small for one set of chains which is orientated in different directions.

Chapter 5

Extension of theory to the Smectic-A Phase

5.1 Definition and Representation

Again, we remind the reader of the basic equation (2.45), which is a "self-consistent" equation for the probability distribution function:

$$\rho(\vec{R_1}) = c\ \exp[-\beta u_1(\vec{R_1}) + \int d\vec{R_2}\ f_M(\vec{R_1}, \vec{R_2})\rho(\vec{R_2})], \tag{5.1}$$

where $\vec{R}$ represents the set of variables $\vec{r_m}, \omega_1....\omega_{N_c-1}$, and $\vec{r_m}$ stands for the position of any one of the beads in the chain while $\omega_1....\omega_{N_c-1}$ stand for the orientations of the $N_c - 1$ bonds in the chain.

Since $\rho(\vec{R})$ does not depend on the the position of the chain in the isotropic and nematic phases, in the previous chapters it was assumed that $\rho(\vec{R}) = \rho(\vec{\omega})$. However in the case of the smectic phase, $\rho(\vec{R})$ depends also on the position of the chain. As explained in Section 1.2.3, in the smectic-A phase the molecules are positionally

ordered in one direction and disordered in the other two directions. This means that it can be assumed that the probability distribution function varies in the z-direction:

$$\rho(\vec{R}) = \rho(z, \vec{\omega}), \tag{5.2}$$

where $\vec{\omega}$ is the set of bond orientations and z is the z-coordinate of the mid point of a chain. For example, if the chain has 8 beads, z represents the average between the z coordinates of beads number four and five. If the chain has nine beads (odd number), z represents the z-coordinate of bead number 5. Therefore Eq. 5.1 becomes

$$\rho(z_1, \vec{\omega_1}) = c\ \exp[-\beta u_1(\vec{\omega_1}) - \int dz_2\, d\vec{\omega_2}\, A(z_1\, \vec{\omega_1}, z_2\, \vec{\omega_2})\rho(z_2, \vec{\omega_2})], \tag{5.3}$$

where $A(z_1\, \vec{\omega_1}, z_2\, \vec{\omega_2})$ is the excluded area between chain 1 and 2, defined in (Eq. 5.5) below.

According to Section 1.2.3, the probability density has a periodic nature in the smectic phase:

$$\rho(z + nd, \vec{\omega}) = \rho(z, \vec{\omega}), \tag{5.4}$$

where n can be any positive or negative integer and d is the period of the system.

5.1.1 Excluded Area

The excluded area between chains 1 and 2 is defined as follows:

$$A(z_1\, \vec{\omega_1}, z_2\, \vec{\omega_2}) = -\int\ dx_2\, dy_2\, f_M(\vec{R}_1, \vec{R}_2). \tag{5.5}$$

Due to translational invariance, we can choose $x_1 = y_1 = z_1 = 0$ while the function $A(z_1\vec{\omega_1}, z_2\vec{\omega_2})$ just depends on $z_{21} \equiv (z_2 - z_1)$ and not on z_1 and z_2 separately. Because

of the symmetry characteristic, the excluded area also satisfies

$$A(z_1\,\vec{\omega_1}, z_2\,\vec{\omega_2}) = A(z_2\,\vec{\omega_2}, z_1\,\vec{\omega_1}). \tag{5.6}$$

As mentioned above, $A(z_1, \vec{\omega}_1; z_2, \vec{\omega}_2) = A(0, \vec{\omega}_1; z_{21}, \vec{\omega}_2)$. By looking at Figure 5.1,

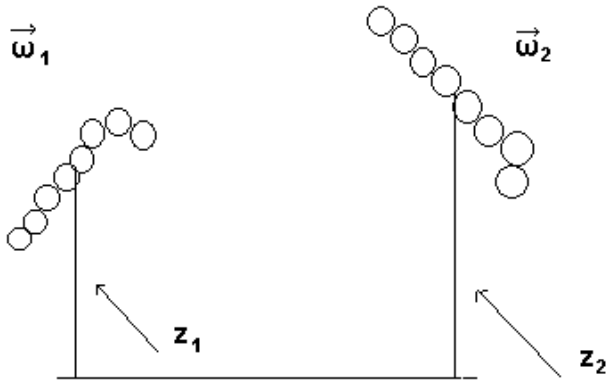

Figure 5.1: Excluded area between chains

"deep thought" indicates that

$$A(z_1, \vec{\omega}_1; z_2, \vec{\omega}_2) = A(z_2, -\vec{\omega}_1; z_1, -\vec{\omega}_2). \tag{5.7}$$

$$\therefore A(0, \vec{\omega}_1; z_{21}, \vec{\omega}_2) = A(0, -\vec{\omega}_1; -z_{21}, -\vec{\omega}_2), \tag{5.8}$$

which means that under inversion of both molecules' orientation, the molecules have the same excluded area when the z coordinates are interchanged. To make it clear, assume that the observer is rotated by π degrees. In this way, while the excluded area is constant, the orientations and z-direction change as in the right side of the above equation.

5.1.2 Barrett's Algorithm for Calculation of the Excluded Area

This section is similar to Section 3.2.1. The same Mayer function ($f_M(12) = e^{-\beta u_2(12)} - 1$) can be defined such that $f_M(12) = -1$ if there is any overlap of two chains ($u_2(12) \rightarrow \infty$), and $f_M(12) = 0$ if there is no overlap ($u_2(12)$=0). According to the Eq. (5.5), the excluded area is

$$A(z_1\,\vec{\omega_1}, z_2\,\vec{\omega_2}) = -\int dx_2\,dy_2\,f_M(\vec{R}_1, \vec{R}_2).$$

As in Section 3.2.1, we can express

$$f_M(12) = \frac{1}{n_{overlap}} \sum_{i,j}^{N_c} f_M(r_{ij}), \tag{5.9}$$

where $n_{overlap}$ is the number of monomer overlaps between chains 1 and 2, and N_c is the number of monomers in each chain. The above equation is valid when $n_{overlap}$ is not zero, otherwise, when there is no overlap, $f_M(12) = 0$. Therefore

$$A(z_1\,\vec{\omega}_1, z_2\,\vec{\omega}_2) = -\int_{overlap} dx_{12}\,dy_{12}\,f_M(12) = -\sum_{i,j}^{N_c} \int_{overlap} dx_{12}\,dy_{12}\,\frac{1}{n_{overlap}} f_M(r_{ij}). \tag{5.10}$$

Since $f_M(r_{ij}) = 0$ unless monomers i and j overlap with each other, the above equation can be written as

$$A(z_1\vec{\omega}_1, z_2\vec{\omega}_2) = -\sum_{i,j}^{N_c} \int_{overlap} dx_{12}\,dy_{12} \frac{1}{n_{overlap}} f_M(r_{ij}) = \sum_{i,j}^{N_c} \int_{overlap(i,j)} d\vec{r}_{ij}^{\,(2)} \frac{1}{n_{overlap}}, \tag{5.11}$$

where $d\vec{r}_{ij}^{\ (2)}$ is the vector in the two dimensional area and is calculated by the Monte Carlo method as

$$\int d\vec{r}_{ij}^{\ (2)} = \int_0^{D'} r_{ij}\, dr_{ij} \int_0^{2\pi} d\theta_{ij} = \pi D'^{\ 2} \int_0^1 d\upsilon_1 \int_0^1 d\upsilon_2, \tag{5.12}$$

where $\upsilon_1 \equiv r_{ij}^2/D'^{\ 2}$, $\upsilon_2 \equiv \theta_{ij}/2\pi$ and $D'^{\ 2}$ is:

$$D'^2 = D^2 - (z_i - z_j)^2. \tag{5.13}$$

In practice, two random numbers between zero and one are generated for υ_1, υ_2. By using the two last equations, $A(z_1\vec{\omega}_1, z_2\vec{\omega}_2)$ is numerically approximated by

$$A(z_1\vec{\omega}_1, z_2\vec{\omega}_2) = \sum_{i,j}^{N_c} \int_{overlap(i,j)} d\vec{r}_{ij}^{\ (2)} \frac{1}{n_{overlap}} \approx \sum_{i,j}^{N_c} \frac{1}{N_B} \pi D'^{\ 2} \sum_{k=1}^{N_B} \frac{1}{n_{overlap}}, \tag{5.14}$$

where N_B is the number of random "Barrett" points generated by the program. It is clear that the excluded area is non-zero in specified ranges of z_{21} and will be zero for other values. For example if $|z_{21}| > 8$ for 8 bead chains, it is clear that the excluded area will be zero.

5.1.3 Probability Density

By using the normalization equation (Eq. 2.17) we get

$$\int d\vec{r}\, d\vec{\omega} \rho(\vec{r}, \vec{\omega}) = \int dz dx dy\, d\vec{\omega}\, \rho(z, \vec{\omega}) = N. \tag{5.15}$$

The integral of $dxdy$ produces a factor of the system area, A, in the above integral. If it is assumed that L_z is the length of the system in the z direction then

$$\int_0^{L_z} dz = \frac{L_z}{d} \int_0^d dz. \tag{5.16}$$

It is clear that, at the end, A and L_z can go to infinity. Denoting the system volume $V = AL_z$, then Eq. (5.15) becomes

$$\frac{1}{d} \int_0^d dz\, d\vec{\omega}\, \rho(z, \vec{\omega}) = \frac{N}{V} \equiv \rho. \tag{5.17}$$

Similar to Section 3.2.2, it is useful to define

$$f(z, \vec{\omega}) = \frac{\rho(z, \vec{\omega})}{\rho}. \tag{5.18}$$

By using $f(z, \vec{\omega})$, Eq. (5.17) can be written as

$$\frac{1}{d} \int_0^d dz d\vec{\omega}\, f(z, \vec{\omega}) = 1. \tag{5.19}$$

From Eq. (5.3), $f(z, \vec{\omega})$ should satisfy

$$f(z_1, \vec{\omega}_1) = c'\, e^{-\beta\, u_1(\vec{\omega}_1)}\, e^{I(z_1, \vec{\omega}_1)}, \tag{5.20}$$

and from Eq. (5.19), c' is

$$c' = \left(\frac{1}{d} \int_0^d dz_1 d\vec{\omega}_1\, e^{-\beta\, u_1(\vec{\omega}_1)}\, e^{I(z_1, \vec{\omega}_1)} \right)^{-1} \tag{5.21}$$

Here $I(z_1, \vec{\omega}_1)$ is given by

$$I(z_1, \vec{\omega}_1) = -\int dz_2 \, d\vec{\omega}_2 \, A(z_1 \, \vec{\omega_1}, z_2 \, \vec{\omega_2}) \rho(z_2, \vec{\omega_2}), \tag{5.22}$$

As in Chapters three and four, the last three equations provide a *self consistent equation* for $f(z, \vec{\omega})$. However, when compared with the isotropic-nematic self consistent equation (Eq. (3.17)), the new self consistent equation has an additional feature that $f(z, \vec{\omega})$ and $I(z, \vec{\omega})$ both vary along the z axis.

5.2 Bifurcation Analysis

Following the analysis of Van Roij et al. [36] for perfectly rigid molecules, we assume that the solution for $f(z, \vec{\omega})$ is a small perturbation around the nematic solution in the previous chapters, i.e.

$$f(z, \vec{\omega}) = f_{nem}(\vec{\omega}) + \epsilon \, \Delta f(z, \vec{\omega}). \tag{5.23}$$

The second term in the right side of the above equation represents the perturbation around the nematic solution, where ϵ is a control parameter, assumed to be $|\epsilon| \ll 1$. By considering Eq. (5.18), $I(z_1, \vec{\omega}_1)$ can be written as

$$I(z_1, \vec{\omega}_1) = -\int dz_2 \, d\vec{\omega}_2 \, A(z_1 \, \vec{\omega_1}, z_2 \, \vec{\omega_2}) \rho f(z_2, \vec{\omega_2}), \tag{5.24}$$

Then we see that

$$I(z_1, \vec{\omega}_1) = I_{nem}(\vec{\omega}_1) + \epsilon \, \Delta I(z_1, \vec{\omega}_1). \tag{5.25}$$

By considering the last two equations, we find

$$\Delta I(z_1, \vec{\omega}_1) = -\rho \int dz_2 \, d\vec{\omega_2} \, A(z_1 \, \vec{\omega_1}, z_2 \, \vec{\omega_2}) \, \Delta f(z_2, \vec{\omega}_2). \tag{5.26}$$

Substituting Eqs. (5.25) and (5.23) into Eq. (5.20) gives

$$f_{nem}(\vec{\omega}) + \epsilon \, \Delta f(z, \vec{\omega}) = \frac{e^{-\beta u_1(\vec{\omega})} \, e^{I_{nem}(\vec{\omega})} \, e^{\epsilon \Delta I(z,\vec{\omega})}}{\frac{1}{d} \int_0^d \, dz d\vec{\omega} \, e^{-\beta \, u_1(\vec{\omega})} \, e^{I_{nem}(\vec{\omega})} \, e^{\epsilon \Delta I(z,\vec{\omega})}}. \tag{5.27}$$

By expanding $e^{\epsilon \Delta I(z,\vec{\omega})}$ on the right-hand-side of the above equation and keeping only terms up to linear order in ϵ, we get:

$$f_{nem}(\vec{\omega}) + \epsilon \, \Delta f(z, \vec{\omega}) \approx \frac{e^{-\beta u_1(\vec{\omega})} \, e^{I_{nem}(\vec{\omega})} \, (1 + \epsilon \Delta I(z, \vec{\omega}))}{\frac{1}{d} \int_0^d \, dz d\vec{\omega} \, e^{-\beta \, u_1(\vec{\omega})} \, e^{I_{nem}(\vec{\omega})} \, (1 + \epsilon \Delta I(z, \vec{\omega}))} \tag{5.28}$$

$$\approx f_{nem}(\vec{\omega})(1 + \epsilon \Delta I(z, \vec{\omega})) \left(1 - \frac{\frac{1}{d} \int_0^d \, dz d\vec{\omega} \, e^{-\beta \, u_1(\vec{\omega})} \, e^{I_{nem}(\vec{\omega})} \, \epsilon \Delta I(z, \vec{\omega})}{\int \, d\vec{\omega} \, e^{-\beta \, u_1(\vec{\omega})} \, e^{I_{nem}(\vec{\omega})}}\right).$$

By equating terms which have ϵ in both sides, we get

$$\Delta f(z, \vec{\omega}) \approx f_{nem}(\vec{\omega}) \Big[\Delta I(z, \vec{\omega}) - \frac{\frac{1}{d} \int_0^d \, dz d\vec{\omega} \, e^{-\beta \, u_1(\vec{\omega})} \, e^{I_{nem}(\vec{\omega})} \, \Delta I(z, \vec{\omega})}{\int \, d\vec{\omega} \, e^{-\beta \, u_1(\vec{\omega})} \, e^{I_{nem}(\vec{\omega})}} \Big], \tag{5.29}$$

where $f_{nem}(\vec{\omega})$ satisfies

$$f_{nem}(\vec{\omega}) = \frac{e^{-\beta \, u_1(\vec{\omega})} \, e^{I_{nem}(\vec{\omega})}}{\int \, d\vec{\omega} \, e^{-\beta \, u_1(\vec{\omega})} \, e^{I_{nem}(\vec{\omega})}} \tag{5.30}$$

Because of the normalization condition Eq. (5.19), which also applies to the nematic limit ($f_{nem}(\vec{\omega})$), the integral of $\Delta f(z, \vec{\omega})$ over a period should be zero:

$$\frac{1}{d} \int_0^d dz \, d\vec{\omega} \, \Delta f(z, \vec{\omega}) = 0. \tag{5.31}$$

One can easily show that this is satisfied by Eq. (5.29).

5.2.1 Fourier Series Representation

As mentioned, $\Delta f(z,\vec{\omega})$ should be a periodic function in the z-direction for all chain configurations $\vec{\omega}$ with period of d. Unfortunately, in the general case $\Delta f(z,\vec{\omega})$ is not necessarily an even or odd function of z. Therefore both cosine and sine terms should appear in the Fourier series representation of $\Delta f(z,\vec{\omega})$. In the lowest order Fourier representation , $\Delta f(z,\vec{\omega})$ is approximated by

$$\Delta f(z,\vec{\omega}) = \phi_e(\vec{\omega})\ \cos(qz) + \phi_o(\vec{\omega})\ \sin(qz), \tag{5.32}$$

where $q = 2\pi/d$ is the smectic "wave-number". A first "guess" for d is a value near $\langle|\vec{r_e}|\rangle$.

It is clear that if the orientation of a molecule is completely inverted, i.e., $\vec{\omega} \longrightarrow -\vec{\omega}$, the structure should be physically equivalent to the case in which z also inverted, i.e., $z \longrightarrow -z$. By using this characteristic of $\Delta f(z,\vec{\omega})$ and considering Eq. (5.32), we get

$$\phi_e(-\vec{\omega}) = \phi_e(\vec{\omega})\ \text{ and }\ \phi_o(-\vec{\omega}) = -\phi_o(\vec{\omega}). \tag{5.33}$$

Eq. (5.29) implies the fact that the same symmetry in z and $\vec{\omega}$ (as in Eqs. (5.32), (5.33)) applies to the function $\Delta I(z,\vec{\omega})$. Then, by integration over z, the second term on the right side of Eq. (5.29), i.e.,

$$\frac{1}{d}\int_0^d dz d\vec{\omega}\, e^{-\beta\, u_1(\vec{\omega})}\, e^{I_{nem}(\vec{\omega})}\, \Delta I(z,\vec{\omega})$$

vanishes. Hence Eq. (5.29) simplifies to

$$\Delta f(z,\vec{\omega}) \approx f_{nem}(\vec{\omega})\,\Delta I(z,\vec{\omega}). \tag{5.34}$$

5.3 Solution for $\Delta f(z,\vec{\omega})$

In the linearized bifurcation analysis, a self-consistent equation for $\Delta f(z,\vec{\omega})$ is obtained by combining Eqs. (5.26), (5.34) as well as the Fourier-series representation Eq. (5.32). As mentioned in Section 5.1.1, the excluded area in Eq. (5.26) depends only on the difference between z_2 and z_1 and not on z_1 and z_2 separately. Hence we can express:

$$A(z_1,\vec{\omega}_1;z_2,\vec{\omega}_2) = A(0,\vec{\omega}_1;z_{21},\vec{\omega}_2), \tag{5.35}$$

where $z_{21} = z_2 - z_1$. Writing $z_2 = z_{21} + z_1$ in Eq. (5.32), and using the sine and cosine rules, we find

$$\Delta f(z_2,\vec{\omega}_2) = \phi_e(\vec{\omega}_2)\left[\cos(qz_{21})\cos(qz_1) - \sin(qz_{21})\sin(qz_1)\right]$$

$$+\,\phi_o(\vec{\omega}_2)\left[\sin(qz_{21})\cos(qz_1) + \cos(qz_{21})\sin(qz_1)\right]. \tag{5.36}$$

Substituting Eq. (5.36) into Eq. (5.26), the latter gives:

$$\Delta I(z_1,\vec{\omega}) = \Delta I_e(\vec{\omega})cos(qz_1) + \Delta I_o(\vec{\omega})sin(qz_1), \tag{5.37}$$

where:

$$\Delta I_e(\vec{\omega}_1) = -\rho\int dz_{21}\,d\vec{\omega}_2\,A(0,\vec{\omega}_1;z_{21},\vec{\omega}_2)\left[\phi_e(\vec{\omega}_2)\cos(qz_{21}) + \phi_o(\vec{\omega}_2)\sin(qz_{21})\right], \tag{5.38}$$

$$\Delta I_o(\vec{\omega}_1) = -\rho \int dz_{21}\, d\vec{\omega}_2\, A(0,\vec{\omega}_1; z_{21}, \vec{\omega}_2) \Big[\phi_o(\vec{\omega}_2)\cos(qz_{21}) - \phi_e(\vec{\omega}_2)\sin(qz_{21})\Big]. \quad (5.39)$$

Comparing Eqs (5.32), (5.34) and (5.37), the functions $\Delta I_e(\vec{\omega})$ and $\Delta I_o(\vec{\omega})$ should have the same symmetry under inversion of $\vec{\omega}$ as $\phi_e(\vec{\omega})$ and $\phi_o(\vec{\omega})$ in Eq. (5.33), namely:

$$\Delta I_e(-\vec{\omega}) = \Delta I_e(\vec{\omega}) \text{ and } \Delta I_o(-\vec{\omega}) = -\Delta I_o(\vec{\omega}). \quad (5.40)$$

This uses the fact that the nematic distribution function is symmetric under inversion of $\vec{\omega}$, i.e., $f_{nem}(-\vec{\omega}) = f_{nem}(\vec{\omega})$. To verify the relations (5.40), we replace $\vec{\omega}_1$ by $-\vec{\omega}_1$ both Eqs. (5.38) and (5.39). Then, by using the condition (5.7) and those of Eq. (5.33), the parity conditions (5.40) are verified.

5.3.1 Final Equations

From Eqs. (5.32), (5.34) and (5.37) the final two coupled equations for the functions $\phi_e(\vec{\omega}_1)$ and $\phi_o(\vec{\omega}_1)$ are:

$$\phi_e(\vec{\omega}_1) = f_{nem}(\vec{\omega}_1)\, \Delta I_e(\vec{\omega}_1), \quad (5.41)$$

$$\phi_o(\vec{\omega}_1) = f_{nem}(\vec{\omega}_1)\, \Delta I_o(\vec{\omega}_1). \quad (5.42)$$

Using Eqs. (5.38) and (5.39), these become:

$$\phi_e(\vec{\omega}_1) = -\rho f_{nem}(\vec{\omega}_1)\Big[\int d\vec{\omega}_2 A_c(\vec{\omega}_1,\vec{\omega}_2;q)\phi_e(\vec{\omega}_2) + \int d\vec{\omega}_2 A_s(\vec{\omega}_1,\vec{\omega}_2;q)\phi_o(\vec{\omega}_2)\Big], \quad (5.43)$$

$$\phi_o(\vec{\omega}_1) = -\rho f_{nem}(\vec{\omega}_1)\Big[\int d\vec{\omega}_2 A_c(\vec{\omega}_1,\vec{\omega}_2;q)\phi_o(\vec{\omega}_2) - \int d\vec{\omega}_2 A_s(\vec{\omega}_1,\vec{\omega}_2;q)\phi_e(\vec{\omega}_2)\Big], \quad (5.44)$$

where

$$A_c(\vec{\omega}_1,\vec{\omega}_2;q) \equiv \int dz_{21}\, A(0,\vec{\omega}_1; z_{21},\vec{\omega}_2)\, \cos(qz_{21}), \quad (5.45)$$

$$A_s(\vec{\omega}_1, \vec{\omega}_2; q) \equiv \int dz_{21}\, A(0, \vec{\omega}_1; z_{21}, \vec{\omega}_2)\, \sin(q z_{21}). \tag{5.46}$$

It is clear that the above equations are *homogeneous* equations and always have a trivial solution of

$$\phi_e(\vec{\omega}) = \phi_o(\vec{\omega}) = 0.$$

The object of solving those equations is to find the smallest values of ρ and q which give non-trivial solutions.

To do the integrations $d\vec{\omega}_2$ in Eqs. (5.43), (5.44), we should replace the integrals by summation over Monte Carlo generated chains. To do this, we note from Eqs. (3.17), (3.18) that $f_{nem}(\vec{\omega})$ has the form

$$f_{nem}(\vec{\omega}) = f_0(\vec{\omega}) \hat{f}_{nem}(\vec{\omega}), \tag{5.47}$$

where

$$\hat{f}_{nem}(\vec{\omega}) = \frac{e^{I(\vec{\omega})}}{\int d\vec{\omega} f_0(\vec{\omega})\, e^{I(\vec{\omega})}}. \tag{5.48}$$

Hence, from Eqs. (5.43), (5.44) we can express

$$\phi_e(\vec{\omega}) = f_0(\vec{\omega}) \hat{\phi}_e(\vec{\omega}), \tag{5.49}$$

$$\phi_o(\vec{\omega}) = f_0(\vec{\omega}) \hat{\phi}_o(\vec{\omega}), \tag{5.50}$$

Recalling from Eqs. (3.19), (3.20) that:

$$\int d\vec{\omega}\, f_0(\vec{\omega})\, g(z, \vec{\omega}) = \langle\, g(z, \vec{\omega})\, \rangle_{(0)} = \frac{1}{N} \sum_{i=1}^{N} g(z, \vec{\omega}_i),$$

then the "summation " form of Eqs. (5.43), (5.44) is

$$\hat{\phi}_e(\vec{\omega}_1) = \frac{-\rho \hat{f}_{nem}(\vec{\omega}_1)}{N} \sum_{i=1}^{N} \Big[A_c(\vec{\omega}_1, \vec{\omega}_i; q)\, \hat{\phi}_e(\vec{\omega}_i) + A_s(\vec{\omega}_1, \vec{\omega}_i; q)\, \hat{\phi}_o(\vec{\omega}_i) \Big], \tag{5.51}$$

$$\hat{\phi}_o(\vec{\omega}_1) = \frac{-\rho \hat{f}_{nem}(\vec{\omega}_1)}{N} \sum_{i=1}^{N} \Big[A_c(\vec{\omega}_1, \vec{\omega}_i; q)\, \hat{\phi}_o(\vec{\omega}_i) - A_s(\vec{\omega}_1, \vec{\omega}_i; q)\, \hat{\phi}_e(\vec{\omega}_i) \Big], \tag{5.52}$$

where the sums are over all N generated MC chain configurations.

Chapter 6

Results for the Nematic-Smectic-A Transition

6.1 Introduction

The main goal of solving the final equations (Eqs. (5.51) and (5.52)) of the previous chapter, is to find the minimum values of q and ρ which yield non-trivial solution of these equations. To find the minimum value for ρ, the dimensionless volume fraction $\eta = \rho V_{mol}$ was used, where V_{mol} is constant for a fixed number of beads and fixed b and D. This minimum value of η should describe the phase transition point between the nematic and smectic phases.

As was defined in Section 5.2.1, q is equal to $2\pi/d$, which is the smectic "wave-number". The initial guess for d is a value near $\langle|\vec{r}_e|\rangle$ although it is clear that d may not have exactly this value.

6.1.1 Problems

With some exceptions, most problems encountered in this part of the work are similar to those faced previously in studying the isotropic-nematic phase transition.

The main difficulty in this work is related to the number of unknown variables. Unlike in the isotropic-nematic part, we have no specific ideas for the initial guesses of $\phi_e(\vec{\omega})$ and $\phi_o(\vec{\omega})$. Since we should calculate the excluded area between two chains for different values of z_{21}, it is important to chose the appropriate value of dz, which gives the change step in the value of z. The precision to use for dz, for the $A_s(\vec{\omega}_1, \vec{\omega}_2; q)$ and $A_c(\vec{\omega}_1, \vec{\omega}_2; q)$ integrals, was not clear. The precision and range of d (period) also was not clear.

Reaching equilibrium with the smectic-A self consistent equations is a significantly harder process compared to studying the isotropic-nematic equations. Unfortunately, most of the time, the final self consistent equations for the smectic-A reached the trivial equilibrium solution of zero. This means that instead of converging to a non-zero constant solution, they approach the trivial solution of zero for nearly all values of $\vec{\omega}$. But we need to reach the equilibrium in which, for most of the chains, $\phi_e(\vec{\omega})$ and $\phi_o(\vec{\omega})$ reach non-zero constant values. This was one of the most problematic issues faced in this part. It was very difficult to find initial parameters which help us to reach non-trivial equilibrium of the self consistent equations.

Calculation of the excluded area is a significantly more time consuming process than the calculation of excluded volume. The excluded area $A(0, \vec{\omega}_1; z_{21}, \vec{\omega}_2)$ between two chains and for different values of z_{21} is a three-dimensional matrix, having a z dimension beside the two other dimensions (two chains from the set of generated chains) of the excluded volume. In this work, a precision of $dz = 0.05$ (in units of bond-length) was considered satisfactory. For eight-monomer chains, the maximum

range of z_{21} giving a non-zero excluded area is from -8 to 8, when the chains are fully extended and parallel to the z-axis. This requires storing a maximum of 320 (i.e., $16/dz$) values of $A(0, \vec{\omega}_1; z_{21}, \vec{\omega}_2)$ for each pair of chains. It is clear that to save the excluded area matrix of just 1500 chains, more than one Gigabyte of memory is needed:

$$1500 \times \frac{1500}{2} \times 320 \times 8\text{Byte} = 2.9 \text{ Giga Byte}. \tag{6.1}$$

The factor 1/2 comes from the symmetry condition Eq. (5.6). Hence, the RAM memory cannot be relied upon to save the excluded area matrix. Also, the A_s and A_c matrices require a large amount of memory.

6.2 Initial Guesses and Techniques Used

6.2.1 Initial Guesses

6.2.1.1 Initial guess for q

To find an initial guess for q, the final equations of the previous chapter were first solved for a much simpler case. This was done by considering the perfectly aligned hard-rod fluid (completely cylindrical molecules). The symmetry of completely aligned hard-rod molecules allows the assumption that the fourier series of $\Delta f(z, \vec{\omega})$ is an even function of $\vec{\omega}$. In this case $\phi_o(\vec{\omega})$ is zero, which causes one of the final equations (Eq. (5.44)) to vanish. Since there is now just one configuration $\vec{\omega}$ in the system corresponding to alignment of all rods in the same direction, the integral over $\vec{\omega}$ simplifies significantly.

After considering the above facts, Eq. (5.43) becomes

$$\phi_e(\vec{\omega}) = -\rho\, A_c(\vec{\omega}, \vec{\omega}; q)\, \phi_e(\vec{\omega}). \tag{6.2}$$

This equation yields a non-trivial solution if and only if

$$-\rho\, A_c(\vec{\omega}; q) = 1. \tag{6.3}$$

The excluded area for aligned hard-rod molecules of diameter D and length L has the simple form of a step function with values of πD^2 (if $|z_{21}| < L$) and zero (if $|z_{21}| > L$). Hence A_c is given by

$$A_c(\vec{\omega}; q) = \int_{-L}^{L} dz_{21}\, A(0, \vec{\omega}, z_{21}, \vec{\omega})\, \cos(qz_{21}) = 2\int_{0}^{L} dz_{21}\ \pi D^2\ \cos(qz_{21})$$

$$= 2\pi D^2 \int_{0}^{L} dz_{21}\ \cos(qz_{21}) = 2\pi D^2\, \frac{\sin(qL)}{q}. \tag{6.4}$$

Substituting the last equation into Eq. (6.3) and using the definition of η, we get

$$\frac{-\rho\ 2\pi D^2\ sin(qL)}{q} = 1 \Rightarrow \frac{-\eta\ 2\pi D^2\ sin(qL)}{q\, V_{mol}} = 1. \tag{6.5}$$

The molecular volume V_{mol} for cylindrical molecules is

$$V_{mol} = \frac{\pi D^2\, L}{4}. \tag{6.6}$$

Therefore, by considering the two last equations, we get

$$-8\eta j_0(qL) = 1, \tag{6.7}$$

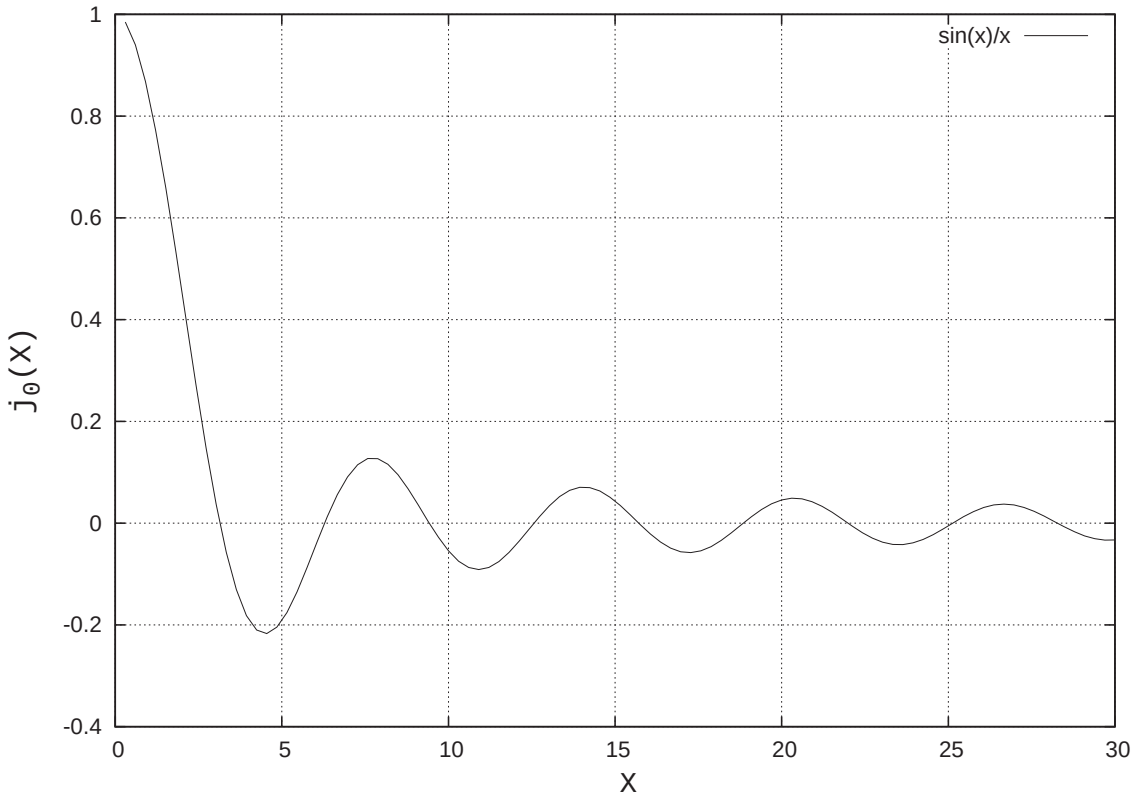

Figure 6.1: Plot of the function $j_0(X) = \sin(X)/X$ vs. X, for finding the solution of the perfectly aligned limit, Eq. (6.7)

where $j_0(X) = \sin X/X$. This result was first derived by Mulder [37]. It is instructive to plot the function $j_0(X)$, shown in Figure 6.1. This shows that Eq. (6.7) only has solutions when $j_0(X)$ is negative. As mentioned earlier, the bifurcation analysis seeks the minimum value of the volume fraction η for which a non-trivial smectic solution exists. As seen from Figure 6.1, the smallest value of η which satisfies Eq. (6.7) is that corresponding to the first and deepest minimum of the function $j_0(X)$ (where $X = qL$), which occurs at a value $X_b = 4.493$. The resulting "bifurcation" value of η, denoted η_b is

$$\eta_b = \frac{-1}{8 j_0(X_b)} = 0.575. \tag{6.8}$$

The associated "bifurcation" wavenumber is found from $X_b = q_b L = 4.493$. The

resulting smectic period $d_b = 2\pi/q_b$ has the value $d_b/L = 2\pi/X_b = 1.40$. These results provide guidelines for seeking the appropriate wavenumber and volume fraction in our more general studies, where we use the mean end-to-end distance R_{mean}

$$R_{mean} = \langle |\vec{r}_e| \rangle = \int d\vec{R}\, \rho(\vec{R})\, |\vec{r}_e|. \tag{6.9}$$

in place of the molecular length L.

6.2.1.2 Initial guess for ϕ_e and ϕ_o

As discussed in Section 5.2.1, generally $\Delta f(z, \vec{\omega})$ of a specific chain is not an even or odd function of z and is the combination of both $\sin(qz)$ and $\cos(qz)$. Even so, since the z coordinate of each chain is calculated from the middle point of that chain, the function may be an even function for some chain configurations $\vec{\omega}$. Experience showed that for many of the chains, $\Delta f(z, \vec{\omega})$ is a combination of both sine and cosine with the same order of magnitude for ϕ_e and ϕ_o. However, for many other chains, $\phi_o(\vec{\omega})$ is zero or much smaller than $\phi_e(\vec{\omega})$ and $\Delta f(z, \vec{\omega})$ is nearly an even function of z for those chains.

For these reasons, either the same value was used for the initial guesses of both $\phi_e(\vec{\omega})$ and $\phi_o(\vec{\omega})$ or a larger value was used for $\phi_e(\vec{\omega})$. The later was the most common situation for most of the results. For example, in most of the our results, we used initial guesses $\phi_e(\vec{\omega}_i) = 200\ f_{nem}(\vec{\omega}_i)$ and $\phi_o(\vec{\omega}_i) = 2\ f_{nem}(\vec{\omega}_i)$, where $f_{nem}(\vec{\omega}_i)$ is the full nematic probability density function of configuration $\vec{\omega}_i$, Eqs. (3.17) and (3.18).

6.2.2 Mixing Method [35]

As introduced in Section 4.3.2, instead of using $\phi_o^{(m)}(\vec{\omega})$ and $\phi_e^{(m)}(\vec{\omega})$ for the next $(m+1)$ iteration, the combination of previous $\phi_o^{(i)}(\vec{\omega})$ and $\phi_e^{(i)}(\vec{\omega})$, where $i < m+1$, can be used as input for the next iteration.

As in Section 4.3.2, we use the following equation as a mixing method algorithm:

$$\phi_{o,in}^{(n+1)} = \alpha\, \phi_{o,in}^{(n)} + (1-\alpha)\, \phi_{o,out}^{(n)}, \tag{6.10}$$

where $\phi_{o,in}^{(n)}$ is the input for the n^{th} iteration of ϕ_o and $\phi_{o,out}^{(n)}$ is the output of that iteration. The same algorithm is applied to ϕ_e

Unlike the previous study of the isotropic-nematic transition, the output values of ϕ_e and ϕ_o could not be used as input for the next iteration (iteration method). Using the output ϕ_e and ϕ_o for the next iteration is the same as using the mixing method with $\alpha = 0$. Unlike in the isotropic-nematic study, where we used $\alpha = 0.15$, the proper α for the present study is a value near $\alpha = 0.85$, which was found by trial and error.

6.2.3 Speed of the Program

More than a month was spent on finding methods to increase the speed of the program. This was done by reducing some of the time-consuming parts of the program and saving some of the time-consuming calculations in the RAM memory. By improving many sections of the program with time-saving techniques, a speed increase of more than 100% was obtained .

As discussed in Section 6.1.1, it is nearly impossible to save the excluded area matrix $A(0, \vec{\omega}_1; z_{21}, \vec{\omega}_2)$ in the RAM memory, so there are two options for treating

this matrix. The first option is to calculate the $A_s(\vec{\omega}_i, \vec{\omega}_j, q)$ and $A_c(\vec{\omega}_i, \vec{\omega}_j, q)$ integrals of each pair of chains immediately after the calculation of the excluded areas $A(0, \vec{\omega}_1; z_{21}, \vec{\omega}_2)$ of the associated chains and save the $A_s(\vec{\omega}_i, \vec{\omega}_j, q)$ and $A_c(\vec{\omega}_i, \vec{\omega}_j, q)$ matrices in RAM. In this technique, just $A_s(\vec{\omega}_i, \vec{\omega}_j, q)$ and $A_c(\vec{\omega}_i, \vec{\omega}_j, q)$ are stored in RAM memory. In this technique the excluded area matrix should be recalculated every time that q is changed. The second option is to save the excluded areas on the Hard Disk Drive (HDD) and only call it when q is changed . Actually the first option is used in the second technique also. This means that after reading all excluded areas from HDD, the $A_s(\vec{\omega}_i, \vec{\omega}_j, q)$ and $A_c(\vec{\omega}_i, \vec{\omega}_j, q)$ are calculated and stored in the RAM memory.

The second method is faster for a series of different q, because we avoid calculating excluded areas several times, but we need a few Gigabytes memory of HDD and read this huge amount of memory every time q is changed. It should be mentioned that according to experience, most of the time it is necessary to vary q for different values of η and it is not possible to work just with one value of q.

6.2.4 Problem of Reaching Equilibrium

As mentioned in the first part of this chapter (Section. 6.1.1), reaching equilibrium for the smectic-A phase is more difficult than in the isotropic-nematic case. There are two types of equilibrium for the smectic-A equations. First, the values of ϕ_e and ϕ_o may converge to the trivial solution $\phi_e = \phi_o = 0$. In the second case, ϕ_e and ϕ_o reach some non-zero constant values. Obviously, the second case is our wanted equilibrium for most chain conformations $\vec{\omega}$. However, besides this kind of equilibrium for most $\vec{\omega}$, the first type of equilibrium is found for a limited number of conformations $\vec{\omega}$. This means that it is acceptable if ϕ_e and ϕ_o reach a zero value for a few of the chains,

while reach non-zero constant values for all the rest.

The key is to choose proper initial values of ϕ_e, ϕ_o and q that help the equations to reach the second kind of equilibrium. Otherwise, in most of the cases, instead of converging to non-zero constant solutions, they converge to trivial solutions of zero for nearly all of the chains.

After months of trying different values for the variables, such as the initial values of ϕ_e and ϕ_o, and trying different degrees of precision, the second kind of equilibrium was finally obtained in the systems. But we did not always reach 100% equilibrium for all $2N$ variables (for each chain there are two different variables, ϕ_e and ϕ_o).

In our definition, if for example 98% of the variables reach a non-zero constant equilibrium, 1% reach a zero value and the other 1% keep changing (they do not reach equilibrium), this equilibrium is accepted as reasonable, while we obtained a few 100% equilibria in our studies. The latter is defined as a kind of equilibrium in which if 99.5% of the variables reach non-zero constant equilibrium, while the rest of the variables converge to zero. It is clear that the number of variables which reach a non-zero constant value should be significantly higher than those which approach zero.

6.3 Range of Smectic-A Solutions

For a specific value of q, η was varied in the range of $[0.4-1.15]$ or some similar range. This was done for numerous different values of q. The first technique (calculate the excluded area matrix every time that the q is changed) has been used up to now but to do the calculations for a larger number of chains we are trying to use the second technique of saving the excluded areas on the HDD.

In this part we found the range that the final self consistent equations of the

previous chapter (Eqs. (5.43) and (5.44)) have a non-trivial solution. By referring to Figure 6.2, one can see that all the points which show a non-trivial equilibrium are in the range $\eta \geq 0.68$. It indicates that a smectic phase in the range of η lower than 0.68 is not obtained. However the exact location of the phase transition is not clear.

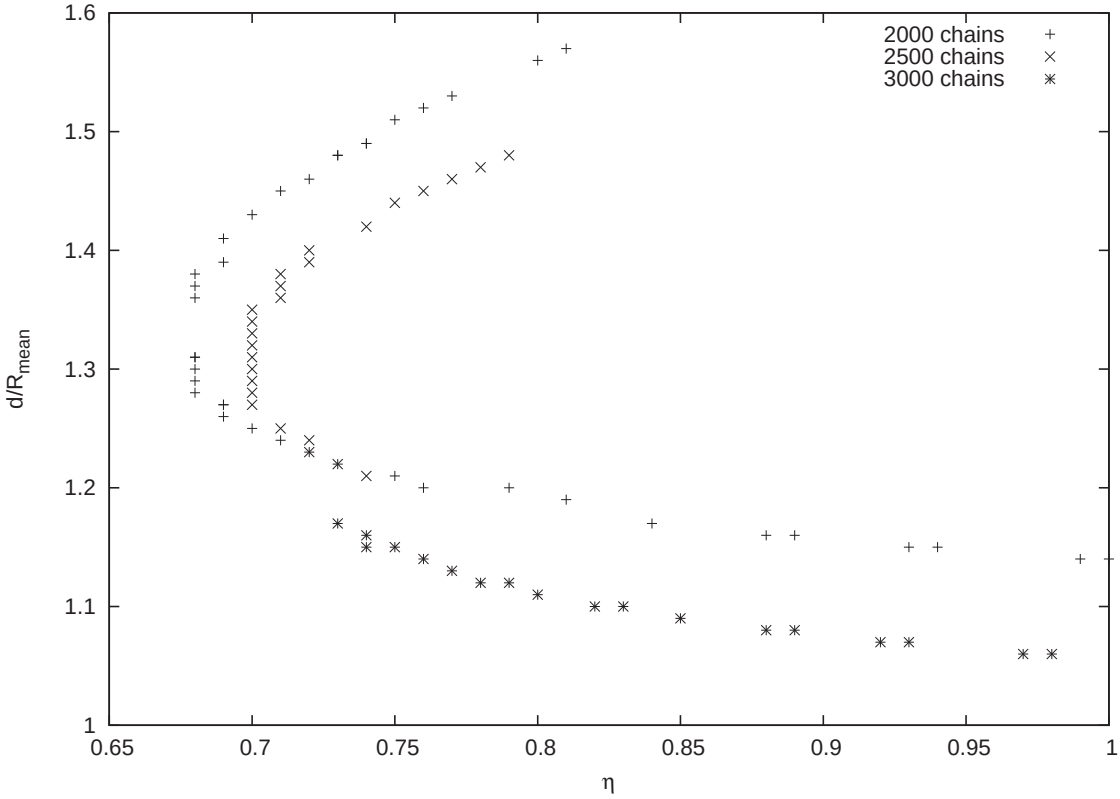

Figure 6.2: Range of volume fraction η vs. period d in which a non-trivial solution for the smectic-A phase is obtained.

Different η ranges were used, which typically started from $\eta > 1$ and continued down to $\eta = 0.4$. All of the studied d/R_{mean} are greater than one, which is similar to the aligned limit result (Section 6.2.1.1). Typically, when one specific $q = 2\pi/d$ value is used, just one or none of the examined η values will give a non-trivial solution for that q. It means that for a specific used period d, just for a few η does the system reach equilibrium. Two of the cases shown in Figures 6.2 (for 2000 and 2500 chains)

show features similar to Figure 6.1 and Eq. (6.7), in that for a given value of η there can be two different solutions for q. We are expecting a similar feature for 3000 chains after doing calculation for higher d/R_{mean}.

6.3.1 Table of Data

Some of the data from the previous figures is contained in the following table. The table has seven columns. The first and second columns are η and the ratio of period d to R_{mean}. The third and forth columns represent the number of iterations used and the number of chains. In the fifth column, the ratio between the initial guesses for ϕ_e and ϕ_o can be found, denoted by LIe and LIo, respectively. The second to last column contains the percentage of the total variables which reached both kinds of equilibrium, while the last column contains the percentage of the total variables which reached only a non-zero equilibrium (second defined equilibrium). Obviously the first number should be larger than the second one, since the first number includes both kinds of equilibrium.

η	$\frac{d}{<\vec{r}_e^2>^{\frac{1}{2}}}$	Iteration No.	Chains No.	$\frac{LIe}{LIo}$	Total Equi. %	Non-Zero Equi. %
0.74	1.13	83	1500	100	100	99.9667
0.74	1.15	500	1500	100	99.0333	98.9667
0.80	1.13	500	1500	100	96.4667	94.8667
0.84	1.115	600	1500	100	99.8333	99.6667
0.84	1.125	600	1500	100	98.6000	97.9333
0.84	1.11	500	1500	100	99.6667	99.1333
0.84	1.11	500	1500	1	99.8667	98.9000
0.92	1.086	500	1500	100	99.9667	99.7333
0.92	1.086	500	1500	1	99.9667	99.7667
0.93	1.15	500	2000	100	99.8250	96.5250
0.99	1.14	47	2000	100	100	99.875
1.00	1.062	500	1500	1	99.2333	96.8667
1.00	1.14	50	2000	100	100	99.975
1.08	1.046	500	1500	100	98.2667	92.1333

For example, in the eighth row (corresponding to $\eta = 0.92$) the first and second numbers for equilibrium percentages are 99.9667 and 99.7333. Since there were 1500 chains, there were 3000 variables. So the percentages indicate that 2999 of the variables reached equilibrium, 2992 of them reached non-zero constant values, seven went to zero, and one variable did not reach any kind of equilibrium.

Chapter 7

Summary and Conclusions

7.1 Summary

In this thesis, liquid crystal phase transitions of semi-flexible hard-sphere chains were studied by using Onsager theory. The first part of thesis studied the isotropic-nematic phase transition and the second part was concerned with the nematic-smectic phase transition.

In chapter one the fundamental concepts of this project, such as the different phases in liquid crystals, were described. In addition, this chapter gave an overview of the model used in this thesis and a brief comparison with previous related studies. In the next three chapters (2-4), we focused on the isotropic-nematic phase transition. Chapter two described the details of the hard-sphere semiflexible chain model employed and the Helmholtz free energy functional based on keeping just the second viral coefficient correction to the ideal-gas free energy (i.e. Onsager theory). In this chapter we also described our Monte Carlo chain generation method based on Prof. B. G. Nickel's algorithm. In chapter three we discussed the solution of the probability density equation by using an iteration method, and how this is combined

with Monte Carlo methods for evaluating the excluded volume (Barrett's algorithm) as well as phase-space integrals. Chapter four contained the results we obtained for variation of order parameter S_2 and reduced pressure P^* with volume fraction η for different numbers of generated chains. The phase transitions between the isotropic and nematic phase were distinguished by specific behavior such as jumps in those graphs. We compared our results with those of Jaffer et al, which were based on an approximate analytical evaluation of the excluded volume for semiflexible hard sphere chains [10]. These should give nearly the same results as we obtained in the high bending-stiffness case, and our results do agree with those of Jaffer et al. We explored using the mixing method to obtain improved results. We also investigated the behavior of the mean square end-to-end distance and square radius of gyration versus η. The isotropic-nematic phase transition is clearly indicated by the break in these curves.

In chapters five and six, we investigated the smectic-A -nematic phase transition. The theory for the this part was slightly different from the first part, since in the first part it was assumed that the probability density of each molecular configuration depends only on the set of bond orientations and does not depend on the positions of the chains. Chapter five explained the theoretical extension to the smectic-A phase. In this chapter we obtained the probability density function for the smectic-A phase by using a bifurcation analysis about the nematic phase and using lowest order Fourier series expansion of the probability density. The mathematical steps which led us to two coupled self-consistent equations were described. In chapter six, the results of our studies of the smectic-A phase were gathered in a graph of period d vs. η which represents the range in which the smectic phase is allowed. The phase transition point should be near the lowest volume fraction for η for which the equations reach

equilibrium for nearly all the chains. For the eight-bead chains studied, this is roughly estimated to be at $\eta \approx 0.68$, but there remain significant numerical uncertainties in this finding.

7.2 Future Work

The present work was successful in showing the existence of liquid-crystal phase transitions (isotropic-nematic and nematic-smectic) in a system of semiflexible hard-sphere chains using the Onsager theory. Our studies were limited, however, to considering only eight-bead chains and weak flexibility (i.e., high bending energy, $\kappa = 50$). It is of interest to extend the studies both to longer chains and to more flexible molecules. As a check on our results for the isotropic-nematic transition, we compared them with those of Jaffer et al. [10], which employed the same model but used an approximate analytical evaluation of the excluded volume. For more flexible molecules, it is likely that the approximations made by Jaffer et al. [10] (as well as those in related work by Fynewever and Yethiraj [13], [38]) become less valid, and the results of the present theory should show greater differences from those works.

One important point of the present work is that it extended the theory to the smectic-A phase, which was not considered in previous related studies [10], [11], [13], [38]. In this phase, the probability density varies periodically in space. However, our studies were limited to a bifurcation treatment about the nematic phase and use of a lowest-order Fourier series representation of the probability density, which should only be valid close to the assumed second-order nematic-smectic transition. To extend the study "deeper" into the smectic phase, and to calculate the variation of properties such as the order parameter S_2, reduced pressure P^*, and various mean-square radii as functions of the volume fraction η farther from the transition point, require a more

detailed theory. In particular, we need to solve the full non-linear theory for the smectic-A phase described in Section 5.1, as well as keep higher-order terms in the Fourier series representation of the probability density.

Bibliography

[1] Rene Van Roij, *Simple Theories of Complex Fluids.* FOM-Institute for Atomic and Molecular Physics, Amsterdam, 1996.

[2] Internet web page by D. Lundström and J. Yilbar, *http://www.kth.se/fakulteter/tfy/kmf/lcd/lcd 1.htm* Royal Institute of Technology, Stokholm.

[3] P. G. de Gennes and J. Prost *The Physics of Liquid Crystals* Clarendon, Oxford, 1993.

[4] Internet web page by Stefan Agamanolis, *http://web.media.mit.edu/ stefan/liquid-crystals/node2.html* MIT Media Lab.

[5] Internet webpage by Prof. Charles Rosenblatt, *http://liq-xtal.cwru.edu/lcdemo.htm* Department of Physics, Case Western Reserve University, Cleveland, Ohio.

[6] L Onsager *The effects of shape on the interaction of colloidal particles*, Ann. NY Acad. Sci. 51, 627 (1949).

[7] P. Bolhuis and D. Frenkel, *Tracing the phase-boundaries of hard spherocylinders*, J. Chem. Phys. 106, 666-687(1997).

[8] M.P. Allen, G.T. Evans, D. Frenkel and B.M. Mulder, *Hard convex body fluids*, Adv. Chem. Phys. 86:1-166(1993).

[9] S. Fraden, *Observation, Prediction, and Simulation of PhaseTransitions in Complex Fluids*, NATO ASI series C, Vol. 460, edited by M. Baus, L. F. Rull,and J. P. Ryckaert (Kluwer Academic, Dordrecht, 1995).

[10] K. M. Jaffer, S. B. Opps, D. E. Sullivan, B. G. Nickel and L. Mederos *The Nematic-Isotropic Phase Transition In Smiflexible Fused Hard-Sphere Chain Fluids*, J. Chem. Phys., 114, 3314 (2001).

[11] R. Diplock, D. E. Sullivan, K. M. Jaffer and S. B. Opps *Nematic-isotropic phase transition in diblock fused-sphere chain fluids*, Phys. Rev. E 69, 062701 (2004).

[12] C. McBride and C. Vega, *A Monte Carlo study of the influence of molecular flexibility on the phase diagram of a fused hard sphere model*, J. Chem. Phys. 117, 10370-10379 (2002).

[13] H. Fynewever and A. Yethiraj, *Phase Behavior of Semiflexible Tangent Hard Sphere Chains*, J. Chem. Phys. 108, 1636-1644, (1998).

[14] C. McBride, C. Vega and L.G. MacDowell, *Isotropic-nematic phase transition: Influence of intramolecular flexibility using a fused hard sphere model*, Phys. Rev. E 64, 011703 (2001).

[15] P. Bladon and D. Frenkel, *Simulating Polymer Liquid Crystals*, J. Phys. Condensed Matter 47, 9445-9449(1996).

[16] A. R. Khokhlov, and A. N. Semenov, *Liquid-crystalline ordering in solutions of partially flexible macromolecules*, Physica A 112, 605-614 (1982).

[17] S. M. Cui, O. Akcakir and J. Z. Y. Chen, *Isotropic-nematic interface of liquid-crystalline polymers*, Phys. Rev. E 51, 4548-4557 (1995).

[18] R. C. Hidalgo, D. E. Sullivan and J. Z. Y. Chen, *Smectic ordering of homogeneous semiflexible polymers*, Phys. Rev. E 71, 041804 (2005).

[19] M. Whittle and A. J. Masters, Mol. Phys. 72, 247 (1991).

[20] M. R. Wilson and M. P. Allen, Mol. Phys. 80, 277 (1993).

[21] M. R. Wilson, Mol. Phys. 81, 675 (1994).

[22] J. D. Parsons, Phys. Rev. A 19, 1225 (1979).

[23] S.-D. Lee, J. Chem. Phys. 87, 4972 (1987).

[24] E. Velasco, L. Mederos and D. E. Sullivan, *Density-functional study of the nematic-isotropic interface of hard spherocylinders*, Phys. Rev. E 66, 021708 (2002).

[25] P. van der Schoot J. Phys. II France 6, 1557 (1996).

[26] J. D. Weinhold , S. K. Kumar and I. Szleifer, *The effects of chain conformations on the thermodynamics of polymeric systems: A mean-field theory*, Europhys. Lett. 35, 695-700 (1996) .

[27] P. G. de Gennes, *Scaling Concepts in Polymer Chemistry*, Cornell University Press, London 1979 .

[28] Michel Daune, *Molecular Biophysics, Structure in Motion.* (Oxford University Press, 1999).

[29] T. Boublik, C. Vega, and M. Diaz-Pena, (J. Chem. Phys. 93, 730 (1990)).

[30] B. J. Alder and T. E. Wainwright *Phase Transition for a Hard Sphere System*, J. Chem. Phys. 27, 1208-1209 (1957).

[31] G Stell, in *The Equilibrium Theory of Classical Fluids*, eds. H. L. Frisch and J. L. Lebowitz, (Benjamin, New York, 1964), p.II-171.

[32] Biochemistry 9, 3471 (1970).

[33] A. J. Barrett *Second Osmotic Virial Coeficient for Linear Excluded Volume Polymers in the Domb-Joyce Model*, Macromolecules, 18, 196 (1985) .

[34] W. H. Press, S. A. Teukolsky, W. T. Vetterling and B. P. Flannery, *Numerical Recipes in C++ 2002* (Cambridge University Press).

[35] A. A. Broyles, *Radial Distribution Function from the Born-Green Integral Equation* (J. Chem. Phys. 33, 456-458 (1960)).

[36] R. van Roij, P. Bolhuis, B. Mulder and D. Frenkel, *Transverse interlayer order in lyotropic smectic liquid crystals*, Phys. Rev. E 52, R1277-R1280 (1995).

[37] Bela Mulder *Density-functional approach to smectic order in an aligned hard-rod fluid*, Phys. Rev. A 35, 3095-3101 (1987).

[38] H. Fynewever and A. Yethiraj, *Isotropic to nematic transition in semiflexible polymer melts,* Mol. Phys. 93, 693 (1998).

[39] Karim M. Jaffer, *The Nematic-Isotropic Phase Transition In Rigid Linear Fused Hard-Sphere Chain Fluids*, M. Sc. Thesis, University of Guelph, Guelph, 1999.

[40] Fatkullin, V. Slastikov, *A Note on the Onsager Model of Nematic Phase Transitions.*, Commun. Math. Sci. 3, 1, 21-26 (2005),

[41] Kerson Huang, *Statistical Mechanics*, (John Wiley, New York, 1987).